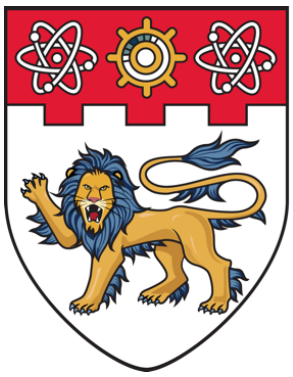

NANYANG TECHNOLOGICAL UNIVERSITY
SINGAPORE

ADSORPTION-BASED FLUOROCARBON SEPARATION IN ZEOLITES AND METAL ORGANIC FRAMEWORKS

JUWAN ARACHCHILLAGE DARSHIKA KUMARI WANIGARATHNA

Interdisciplinary Graduate School
Nanyang Environment & Water Research Institute

2018

ADSORPTION-BASED FLUOROCARBON SEPARATION IN ZEOLITES AND METAL ORGANIC FRAMEWORKS

JUWAN ARACHCHILLAGE DARSHIKA KUMARI WANIGARATHNA

Interdisciplinary Graduate School
Nanyang Environment & Water Research Institute

A thesis submitted to the Nanyang Technological University in partial fulfillment of the requirement for the degree of
Doctor of Philosophy

2018

Acknowledgements

First, I would like to express my utmost gratitude to my supervisor Associate Professor Liu Bin, for his guidance, encouragement and support. He always tries his best to answer any of my queries, and gladly allows his time for discussions whenever necessary. His creative and constructive ideas and wisdom has motivated me throughout this project.

I am also grateful to my co-supervisor Associate Professor Zhang Qichun and to my mentor Assistant Professor Ni Ran for the valuable suggestions provided. Sincerest thanks shall be extended to Dr.Gao Jiajian for his unlimited knowledge sharing with me in every aspects. His patient guidance and kind support throughout my study is highly appreciated. Appreciation is also given to all the team members and friends for their kind help and support over the years. Also, I am really thankful to Dr. Wang Xiujuan, Dr. Yu Shucong and the technical staff of the School of Chemical and Biomedical Engineering(SCBE) for the guidance and assistance provided during the use of SCBE common research facilities.

I would like to thank Nanyang Environment & Water Research Institute and Interdisciplinary Graduate School for providing me the opportunity and scholarship to pursue the PhD degree.

Finally, I wish to express my most heartfelt gratitude to my parents and my husband for their everlasting love and support throughout my life.

Table of Contents

List of Figures

List of Tables

Abstract

Fluorocompounds have important applications in industry, but is environmentally unfriendly, which can cause ozone depletion and contribute to the global warming with long atmospheric lifetime and high global warming potential. Therefore, reclamation of used fluorocompounds via energy efficient adsorption-based capture and separation shall greatly contribute to control their environmental release while reducing the impact on the environment.

R32 (difluoromethane), R22 (chlorodifluoromethane), R125 (Pentafluoroethane), R134a (1,1,1,2-Tetrafluoroethane) and R143a (1,1,1-Trifluoroethane) are important fluorocarbons that are widely being used in different types of air conditioning and refrigeration systems either as single components or as blends of two or more fluorocarbons. In this study, the choices of porous materials for the separation of blends of these fluorocarbons were systematically studied.

During this study, absolute separation of R32, R22 and R125 fluorocarbon blend was achieved using 4A molecular sieve zeolite under ambient conditions. Steric effects were responsible for the separation of R32 and R22 from R125 while both steric and kinetics effects (due to the larger molecular size of R22 compared to R32) facilitated the successful separation of R22 from R32. The regular pore structure, excellent match of pore size of 4A zeolite with the molecular sizes of the fluorocarbon make the product gases very pure, to the extent of direct industrial applications.

Further, a facile method for the adsorption separation of fluorocarbon blends containing R134a, R125 and R143a refrigerants into their pure components using commercial zeolite 13X and pore size modified 5A zeolite was introduced. The mixed gas breakthrough experiments reveal that zeolite 13X selectively adsorbs R134a over R125 and R143a. By running two adsorption cycles, it is possible to obtain R134a with ultrahigh purity. Through chemical modification of tetraethyl orthosilicate (TEOS), the pore size of 5A zeolite could be successfully narrowed to the extent to just adsorb R125 while excluding R143a. The modified 5A zeolite was utilized to separate refrigerant mixtures containing R125 and R143a into their pure components.

Among the various types of adsorbents, emerging Metal Organic Frameworks (MOFs) displays excellent gas capture and separation performances thanks to the designability and adjustability of their structures and thereby the functions. The metal-organic frameworks UiO-66(Zr) and HKUST-1 are demonstrated to have excellent performance characteristics to separate fluorocarbon mixtures at room temperature. Breakthrough data obtained for binary R22/R32 and R32/R125 mixtures reveal high selectivities and capacities of UiO-66(Zr) and HKUST-1 for the separation and recycling of these fluorocarbon mixtures. Furthermore, the UiO-66(Zr) and HKUST-1 saturated with R22 and R125 can be regenerated at temperatures as low as 120 ^{o}C with excellent desorption-adsorption cycling stabilities.

Chapter 1

Introduction

Chlorofluorocarbons (CFCs), Hydrochlorofluorocarbons (HCFCs), Hydrofluorocarbons (HFCs), Perfluorocompounds (PFCs) and other fluorinated compounds are mostly recognized as useful compounds because of their variety of application as refrigerants, solvents, fluoropolymers and etc (Table 1-1). However, according to the U.S. Environmental Protection Agency (EPA), most of the fluorocompounds depletes the ozone layer, contributes to global warming (Table 1-2) and can present health hazards to those who are exposed to it. Therefore, fluorocompound is strictly regulated by EPA.

Currently the refrigerant and air conditioning industry consume largest amount of fluorocarbons compared to other industries such as foam, aerosol etc (Figure 1-1). However, with the implementation of Montreal and Kyoto protocols, the refrigerant and air conditioning industry undergo major transition from the use of CFCs, HCFCs to use of HFCs and other non-global warming potential refrigerants. For an example CFC12 that has been used in domestic refrigerators and mobile air conditioning systems are now replaced with HFC134a because of its high ozone layer deletion potential. Also, R410A which is blended from R32 and R125 now widely being used in residential air conditioning systems as a replacement for ozone depleting HCFC22. With this step-wise phase out, high demand for HCFCs and HFCs is expected.

The semiconductor industry uses perfluorocompounds (PFCs) such as CHF_3 (HFC23), CF_4, C_2F_6, C_3F_8, SF_6, and NF_3 in two important production processes – plasma etching thin films and plasma cleaning chemical vapor deposition (CVD) tool champers. PFCs are critical to current semiconductor manufacturing methods because they possess unique characteristics when used in a plasma that currently cannot be duplicated by alternatives. Under normal operating conditions, anywhere from 10 to 80 percent of the PFC gases pass through the manufacturing tool chambers unreacted and are released into the atmosphere. But, they are also potent greenhouse gases with very high global warming potential.

The recent reports indicate increasing trend of the emissions of greenhouse gases globally, which include the increased emissions of aforementioned fluorocompounds as well(Figure 1-2).[1] In Singapore, since early 1990s, there has been more than 100-fold increase in fluorocompound emissions (Figure 1-3). Section 608 of the Clean Air Act of 1990 prohibits venting of fluorocompounds directly into the atmosphere. Therefore, recovery, recycling and reclamation of used fluorocompounds will contribute to the prevention of global warming and ozone depletion as well as to the reduction of their production.

Table 1-1 Common applications of HCFCs and HFCs

Type of Fluorocarbon	**Applications**
HCFC-22	Residential air conditioning and refrigeration
HFC-134a	Domestic and commercial refrigeration
	Mobile air conditioning(MACs)
	foam and MDIs
	Propellants and aerosols
HFC-32	Residential and Commercial air conditioning
HFC-125	Residential and Commercial air conditioning (to prepare refrigerant blends R410A, R407A, R407C, R404A etc)
	Fire extinguishers
HFC-143a	Commercial and industrial refrigeration (to prepare refrigerant blends eg. R404A)
HFC-23	Commercial and industrial refrigeration
R410A	Air conditioning applications
R407C	Air-conditioning applications
R404A	Low temperature refrigeration applications
HFC-152a	Industrial aerosol sector and extruded polystyrene foam
HFC-245fa	Blowing agents in PU foam

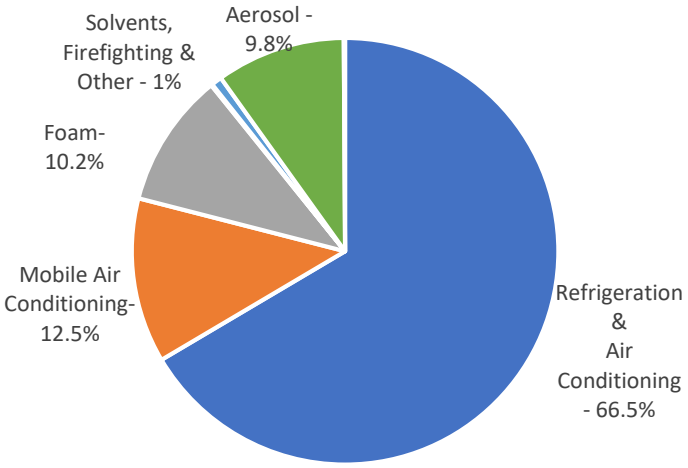

Figure 1-1 Global Consumption of HFCs by application in 2015(Data source: United Nations Environment Programme (UNEP)).

Table 1-2. PFCs, HCFCs and HFCs [2]

Chemical Formula	**Atmospheric Lifetime (years)**	**Global Warming Potential (100-year time horizon)**
CHF_3	264	11,700
CF_4	50,000	6,500
C_2F_6	10,000	9,200
C_3F_8	2,600	7,000
SF_6	3,200	23,900
NF_3	740	8,000
CCl_2F_2(R12)	100	10900
$CHClF_2$ (R22)	12	1810
CH_2F_2 (R32)	4.9	675
CHF_2CF_3 (R125)	29	3500
CH_2FCF_3 (R134a)	14	1430
CH_3CF_3 (R143a)	52	4470

Singapore shares worldwide concern in reducing consumption of ozone depleting substances (ODS) and help preserve the stratospheric ozone layer for a safe and healthy environment. To

signify her commitment to reduce consumption of ODS and protect the ozone layer, Singapore became a party to the Montreal protocol on 5 January 1989.

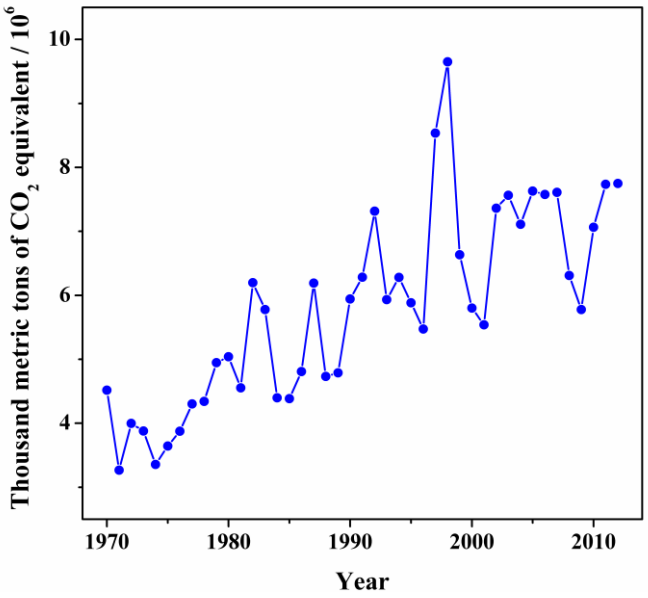

Figure 1-2 World HFC, PFC, and SF_6 emissions[3]

On 2 March 1993, Singapore also acceded to the 1990 London Amendment to the Montreal Protocol and subsequently to the Copenhagen Amendment and the Montreal Amendment on 22 Sep 2000.[4] With the need to reduce the fluorocarbon emissions as well as the high value of fluorocompounds, it is of key interest to develop a simple and economical method to recycle and reclaim used fluorocompounds for further commercial use.

The most frequently used method for the reclamation of used fluorocompounds in large scale is the cryogenic separation i.e., liquefaction followed by distillation. However, in many cases, the purity of fluorocompounds separated after distillation cannot immediately meet the industrial application standards. For example, the mixture of R32 and R125 (the boiling point of R32 and R125 are -51.7 ^{o}C and -48.1^{o}C, respectively, at atmospheric pressure) forms an azeotrope at the composition of 50 wt% of R32, making the complete separation of R32 from R125 extremely difficult.

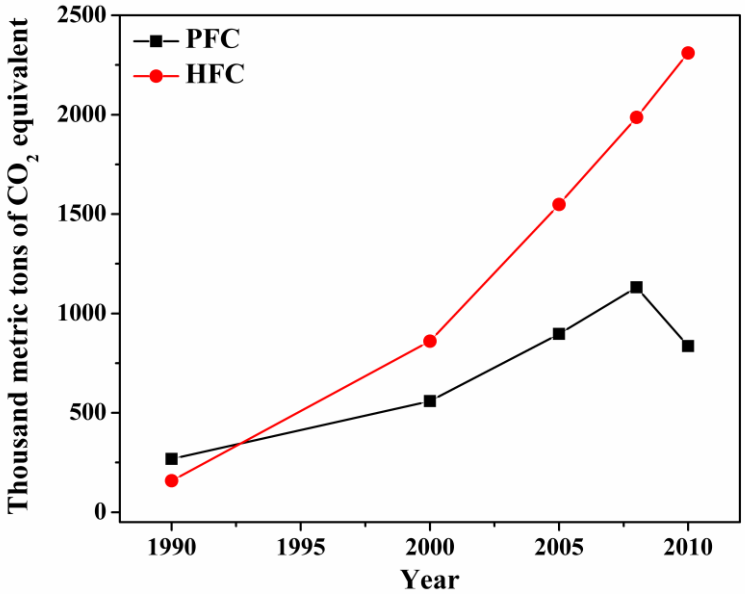

Figure 1-3. Hydrofluorocarbons (HFC) and Perfluorocompounds (PFC) emissions in Singapore[5]

Although the product purity is high in cryogenic gas separation processes, the economic range is still very low in the current economic feasibility level since it is an energy-intensive process. Considering all of these issues associated with the current fluorocarbon reclamation methods, there is an urgent need for exploring industrially applicable alternatives. Adsorption based gas separation is a well-established technology which is considered as a more energy efficient method though the proper selection of suitable adsorbent is crucial.[6] The operating principle of adsorption gas separation is the preferential adsorption of one or more gases from the feed mixture producing an effluent gas enriched with less selectively adsorb gases. In order to design an optimum gas adsorption process, productivity must be maximized while minimizing the product inventory at a specified product purity.[7]

Motivation

Currently, simple and economical methods to recycle and reclaim used fluorocompounds for further commercial use are scarce. Therefore, the key interest of this PhD programme was to develop industrially applicable adsorption-based fluorocompound reclamation process.

Objectives

The objective of this study was to select/ design & synthesis of suitable adsorbents for the adsorption-based separation of R32, R22, R125, R134a, R143a fluorocarbons blends with relevant industry purification standards for further commercial use.

Our specific goals at different stages are:

(a) To systematically study the choices of adsorbents and the adsorbent preparation parameters on the separation of fluorocompound mixtures.
(b) To optimize the operating conditions such as temperature, pressure, gas flow rate etc, for effective fluorocompound gas separation.
(c) To design/modify suitable adsorbents for enhanced adsorption capacity and selectivity.
(d) To study the potentials of novel Metal Organic Frameworks (MOFs) for the fluorocarbon separation.

Organization of the dissertation

Chapter 1 provides a general introduction of the topics to be covered in this dissertation, including the background and significance of reclamation of fluorocompounds, discusses the motivations as well as the primary objectives of this PhD research project.

Chapter 2 summarizes the up to-date literature on the adsorption-based fluorocarbon adsorption, separation in zeolites and metal organic frameworks. Also general principals of the adsorption-based gas separation have included.

Chapter 3 provides the information on the methods used for the characterizations and analysis.

Chapter 4 describes a facile method that can be used for the absolute separation of R32, R22 and R125 fluorocarbon blend over 4A molecular sieve zeolite.

Chapter 5 presents the separation of R125, R134a and R143a fluorocarbon blend in 13X and surface modified 5A zeolite.

Chapter 6 describes successful utilization of metal organic frameworks for the fluorocarbon separation.

Chapter 7 summarizes a general conclusion of this PhD project, and provides recommendation of directions for future research in adsorption-based fluorocarbon separation.

Chapter 2

Literature Review

2.1 Adsorption based gas separation

Adsorption based gas separation is a very common method that is being used for many industrial scale gas separation applications. For example, it is being widely used for the natural gas purification, pre-combustion capture and separation of CO_2/H_2 , separation of post combustion flue gas streams containing CO_2 and N_2 and etc. However, the published data for the separation of fluorocarbons using adsorption-based methods are scarce. When considering particular adsorbent for selective separation of gases, three major mechanisms 1) Steric gas separation (molecular sieving effect), 2) Thermodynamic equilibrium gas separation (preferential adsorption due to adsorbent surface – adsorbate interactions), 3) Kinetic gas separation (different diffusion rates) determine the selectivity and capacity of the adsorption. Adsorbents with uniform aperture size (ex: zeolites) are ideal for steric separations and the pore size of such materials needs to be precisely tailored to lie between the kinetic diameters of the two molecules that are to be separated in order to utilize them for kinetic separations.

2.2 Key considerations during material selection

Although the adsorption gas separation is a well-developed and industrialized technique, the selection of most suitable adsorbent is crucial and is unique from one gas separation process to another. The starting point of the adsorbent selection is the study of fundamental properties of the targeted gases such as molecular size, polarizability, dipole moment, magnetic susceptibility etc. For an example, if the potential adsorbent has highly polar surface (zeolites, activated alumina etc), gases with higher dipole moment will be attracted more to the surface.

Physical properties (kinetic diameter, boiling point, polarizability, dipole moment) of some of the common HFCs, HCFCs and PFCs are shown in table 2-1 and 2-2.[8] According to the reported literature the molecular size increase as R32<R22<R125. Although there are no data available

on the molecular sizes of R134a and R143a, considering their molecular structure, these gases may have molecular sizes closer to the R125. It should be noted that, not only the molecular size but also the polarizability and the dipole moment of the molecules are important parameters especially when designing thermodynamic equilibrium gas separations. In general, the boiling points of the gas molecules can be used to compare different adsorption affinities since the high boiling point of a particular gas indicates the stronger gas-gas interactions and can have stronger attractions to the adsorbent surface as well.[9] But this fact cannot be rationalized for all gases because of the various other factors involved.

Table 2-1 Physical properties of some of the HFCs and HCFCs [10, 11]

CFC/HCFC/HFC	Kinetic diameter/Å	Boiling point/K	Polarizability(α)/ cm^3/mol	Dipole moment/Debye
R12 (CCl_2F_2)	4.4	243.2	-	0.51
R13 ($CClF_3$)	4.5	191.5	-	0.50
R22 ($CHClF_2$)	4.2	232.1	-	1.42
R32 (CH_2F_2)	3.9	221.3	13.2	1.97
R125 (CHF_2CF_3)	4.4	224.9	14.3	1.54
R134a (CH_2FCF_3)	-	246.9	13.8	2.06
R143a (CH_3CF_3)	-	225.8	14.4	2.32

Table 2-2 Physical properties of some of the PFCs

PFC	Kinetic diameter	Boiling point	Polaizability	Dipole moment
CF_4	4.66	145.11	38.4	0
C_2F_6	5.10	195.21	68.2	0
SF_6	5.13	209.25	65.4	0
NF_3	3.62	144.11	36.2	0.235
N_2	3.64	77.35	17.4	0

2.3 Conventional adsorbents for the gas separation applications

The use of traditional adsorbents such as molecular sieve carbon, molecular sieve zeolites, silica gel, activated carbon and organic polymers for gas separation is already can be seen in industrial scale. Although not commercialized yet, the emerging porous materials such as metal organic frameworks(MOFs) with very high surface area, pore volume and high density of active sites have also shown excellent performances for different gas separation applications.

2.3.1 Zeolites

Zeolites are crystalline aluminosilicates of alkali or alkali earth elements in which primary units are formed by the tetrahedra of silicon and aluminum, SiO_4 and $A1O_4$. The chemical composition of zeolites can be represented by the chemical formula:

$$M_{x/n}[(A1O_2)_x(SiO_2)_y] \cdot zH_2O$$

where x and y are integers with y/x equal to or greater than 1, n is the valence of cation M, and z is the number of water molecules in each unit cell. The microporous zeolites, especially Type A zeolites, are often refer as molecular sieves due to their smaller apertures sizes which can facilitate molecular level separations. The zeolites with low Si/Al ratios contain charge balancing alkali or alkali earth metals that acts as strong active sites for gas adsorption. Since the variety of zeolite structures with pore sizes from small to larger sizes are now exist, the proper zeolite can be chosen based on their steric selectivity or thermodynamic selectivity. The physical properties of some of the widely studied zeolites for gas separation applications are listed in table 2-3 and figure 2-1.

Utilization of smaller pore zeolite (Linde Type A(LTA), 13X, ZSM-5 etc) for the steric separation of gas mixtures is extensively reported.[12, 13] For example, 3A zeolite is extensively use for drying or dehydration of gases or alcohols, which excludes all hydrocarbons, O_2 and N_2. Commercially, 5A zeolite is used in large-scale in processes for the separation of normal paraffins from branched-chain (e.g., iso-) paraffins and cyclic hydrocarbons. Further, silver-exchanged zeolite A has used for the absolute ethylene/ethane separation. This molecular

sieving type separation is attributed to the pore size of the adsorbent, which falls between ethylene and ethane kinetic diameters. In the case of LTA zeolites, through the ion exchange processes, the pore aperture size can be effectively controlled to obtain required molecular selectivity.[14] The surface of the zeolite is essentially oxygen and those oxygen atoms are more accessible and exposed to the guest molecules compared to the framework Al and Si atoms. Also, the anionic oxygen atoms are more abundant and are much more polarizable than the Al and Si cations. Therefore, the numerous anionic oxygen atoms dominate the van der Waals interactions with the sorbate molecules. Besides anionic oxygen, the charge balancing cations in the zeolite surface are also accessible for the adsorbate molecules. For adsorbate molecules with permanent dipoles and quadrupoles, the interactions with these exposed cations often dominate the overall interaction potential.

Table 2-3 Properties of some of the well-studied zeolites.

Name	Topology	Si/Al ratio	Pore diameter/aperture (Å)	Surface area (m^2/g)	References
Small pore aperture					
Type A	LTA	1	11/4.2	~ 475	[15]
Chabazite	CHA	2-5	7.37/3.72	~	
Intermediate pore aperture					
ZSM-5	MFI	10-15	6.4/4.7 6.4/4.46	~ 420	
Mordenite	MOR	2-5	Larger channel: (6.60 x 7.05) Smaller channel: (4.82 x 3.92)	~ 425	[16]
Large pore aperture					
Type X	FAU	1-1.5	11/7.4	~ 570	[17, 18, 19]
Type Y	FAU	1.5-3	11/7.4	~ 540	

2.3.2 Activated carbon

Activated carbon is produced from carbonaceous materials such as wood, coal, coconut shells etc. More pores starting from the existing pores in the raw materials are created through the activated process. After different activation processes, the product activated carbon is characterized by the BET surface area in the range of 300 – 4000 m^2/g.[20] Compared to molecular sieve adsorbents, activated carbon has pores in a wide range starting from micropore to macropore size. Pore volume and pore size distribution of various kinds of activated carbons are shown in figure 2-2. Because of its surface hydrophobicity, it is the only commercial adsorbent used to treat the aqueous compounds. The non-polar surface of the activated carbon creates weak van der Waals interaction with adsorbates generating low heat of adsorption compared to other commercial adsorbents which often promote energy efficient regeneration.

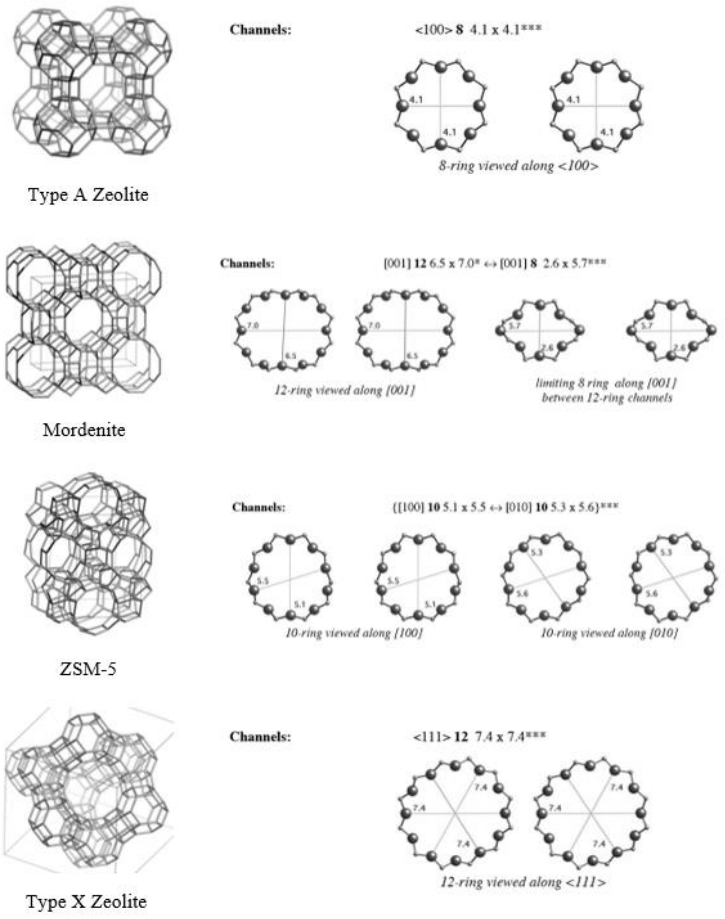

Figure 2-1 Pore sizes of some common zeolites.

Surface chemistry of activated carbon

Depending on the treatment or modification conditions, the surface of the activated carbon can be either acidic or basic. If the surface contains oxygen containing groups such as hydroxyls, lactones, carboxyl the surface become acidic. The acidic properties on the surface can be created through an oxidation process with the presence of oxygen at elevated temperatures. The basic characters can be created by degas at high temperature under vacuum or inert atmosphere and subsequent oxidation at room temperature after cooling.[20]

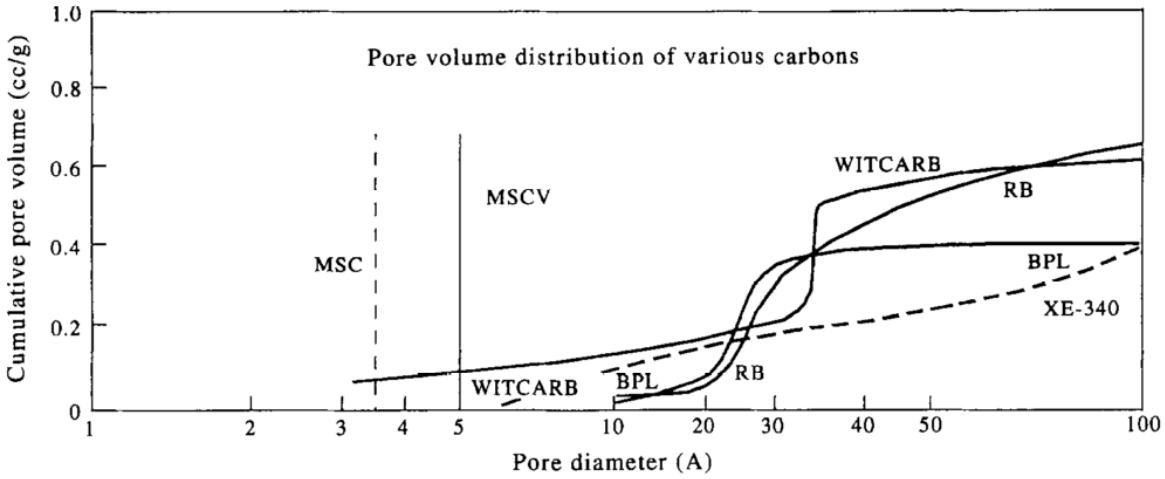

Figure 2-2 Pore volume distribution of different types of activated carbons[21]

2.3.3 Fluorocarbon adsorption in conventional zeolites, activated carbons and silicas

Several previous literatures report the adsorption separation of fluorocompounds in traditional adsorbents (Table 2-4), especially for the separation of different by-products during the productions of useful fluorocompounds. Adsorption of R23 (Trifluoromethane) on three zeolites, Na-Y, K,H-Y, Rb,Na-Y have been investigated since the removal of unwanted R23 during the production of R22 is an important industrial requirement.[22] The R23 adsorption capacities of Na-Y, K,H-Y, Rb,Na-Y measured at 1 bar and 298 K are 3.8, 4.4 and 3.8 mmol/g respectively.

Very high R32 and R134a adsorption capacities are reported in several types of activated carbons (activated carbon powder (ACP), activated carbon fiber (ACF), Maxsorb III) thanks to their exceptionally high surface areas and pore volumes. ACP exhibit highest R32 adsorption capacity of 8.8 mmol/g (measured at 297.2 K and 2 bar) among various traditional adsorbents (Figure 2-3).[23, 24]Further, Maxsorb III which possess extremely high surface area and pore volume (surface area and pore volume are 3150 m^2/g and 1.7 cm^3/g respectively) display highest R134a adsorption capacity (12.7 mmol/g) reported so far.[25]

Adsorption and adsorption based separation of HFC125 and CFC115 on activated carbon is reported.[26] Adsorption capacity of vruf carbon with BET surface area 1330m^2/g was measured in the pressure range of 0.01 to 120 kPa. According to the results at low pressures CFC115 adsorbed preferentially to the vruf carbon but at high pressures the selectivity of HFC125 increases due to the entropic effects. HFC125 has smaller molecular size compared to CFC115 which promote the efficient packing within the pores of vruf carbon. Hence the selectivity of CFC 115 decreases with the increase of pressure.

Silica gel is a mesoporous material, that is, with pores mostly larger than 20 ˚Å. It is widely used as a desiccant because of the large water adsorption capacity and ease of regeneration. The weak hydrogen bonding interaction of water with surface silanol groups of silica gel is the main reason for its easy regeneration. The pore surface of silica gel contains abundant surface silanol groups. Therefore, surface of silica gel can be readily modified by grafting monomolecular layer of organic ligands. Frere et al reported R12, R22 and R125 adsorption in silica gel. At 1 bar and 303 K, the adsorption capacities of R12, R22 and R125 are 2.0, 2.0, 2.4 mmol/g respectively. Compared to the activated carbon, the low fluorocarbon adsorption capacity in silica gel can be attributed to their low surface area (750 m^2/g) and pore volume (0.35 cm^3/g).

Table 2-4 Adsorption of fluorocarbons in Zeolites, Silicas and Activated Carbons

Adsorbent	BET surface area (m^2/g)	Total Pore volume (cm^3/g)	Adsorption amount (mmol/g)					Ref
			R32	R22	R134a	R125	R12	
Activated Carbon (BPL)	1180	0.55		4.6[b]			4.2[b]	27
Vruf Carbon	1330	0.81				3.0		26
Activated Carbon Powder(ACP)	3200	1.7	8.8[c]					24
Activated Carbon Fiber (ACF)	2200	1.0	6.9[c]					24
Fluka charcoal	1143	-			3.25[a]			28
Maxsorb III	3150	1.7			12.7			25
Silica gel	750	0.35		2.0	2.4		2.0	29

[a] at 293 [b] at 303 K [c] at 2 bar

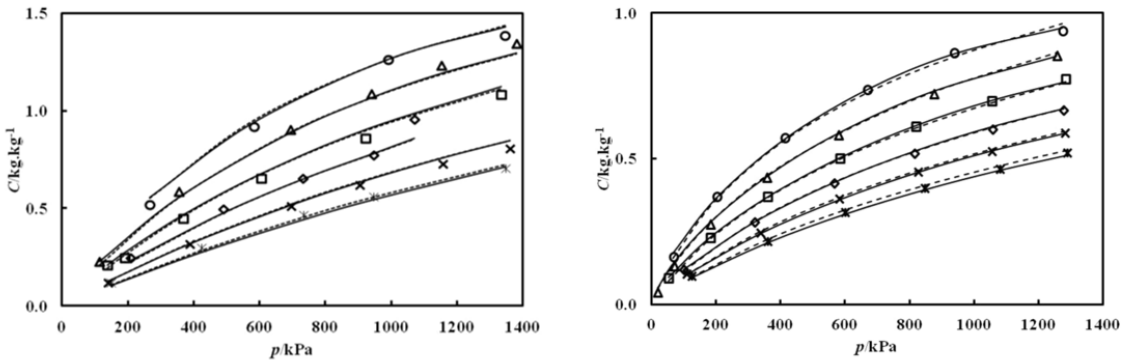

Figure 2-3 Experimental R32 adsorption isotherms in (a) Activated carbon powder (ACP) and (b) Activated carbon fiber (ACF), Legend: O, 24.8°C; ∆, 34.8 °C; □, 44.7 °C; ◊, 54.3 °C; ×, 64.4 °C; ∗, 74.3 °C.

2.3.4 Pore size engineering of Zeolites for the selective gas adsorption

Pore size engineering of zeolites is an attractive method to improve the selectivity. Pore size of the zeolites can be modified by mainly using three methods.

1. Cation exchange process

If consider zeolite 4A, by exchanging the extra framework Na^+ cation with larger K^+ cations the pore size of the 4A zeolite can be reduced. By ion exchange with divalent Ca^+ cations, the two Na^+ cations exchange with single Ca^{2+} cations hence the larger pore size can be achieved.

2. Pre-adsorption of polar molecules

Molecular sieving effect of zeolites can be regulated by pre-adsorption of polar molecules. The strong interaction of cations in the zeolite surface and the polar molecules create diffusion barrier by clustering them around the cations in the zeolite pore channels.

3. Modification of zeolite framework

The crystallographic changes of the zeolite framework can be formed by thermal treatment, implantation of new atom groups either internal or external surface and by using coating methods. It has identified that treatment of zeolite crystals in contact with water vapor at elevated temperatures can change the molecular sieve behaviour. But the pore size change will be depending on the amount of water vapor, treatment temperature, treatment time etc.

The internal and external modification of zeolites can be performed by allowing the reaction between silanol groups in zeolite surfaces and suitable chemicals.

One method is reaction with silane;

$$Si - OH + SiH_4 \longrightarrow Si - O\text{-}SiH_3 + H_2$$

$$Si - O - SiH_3 + Si - OH \longrightarrow Si - O - SiH_2 - O\text{-}Si + H_2$$

Hydrolysis reaction (SiH_2, SiH_3 groups hydrolysed with water to give $-Si(OH)_2$- and $-Si(OH)_3$ groups)

$$Si - O - SiH_2 - O\text{-}Si + H_2O \longrightarrow Si - O - Si(OH)_2 - O\text{-}Si + H_2$$

Second method is reaction with diborane; (its electron deficient character reactive towards the oxygen bridges Si – O – Si)

Primary reaction

$$2(Si - OH) + B_2H_6 \longrightarrow 2(Si - O - BH_2) + H_2$$

Secondary reaction

$$Si - O - BH_2 + HO - Si \longrightarrow Si - O - BH - O - Si + H_2$$

Hydrolysis reaction can occur not only with water but also with molecules such as CH_3OH because of the reactivity of chemisorbed groups.

$$Si - O - BH_2 + H_2O \longrightarrow Si - O - B(OH)_2 + H_2$$

$$Si - O - BH - O - Si + H_2O \longrightarrow Si - O - B(OH) - O - Si$$

Similar reactions can occur with agents X_nR_m where X = Si, B, Ge and R = H, Cl

Further, the pore size of the zeolites can be controlled by various boron – nitrogen compounds.

External surface modification of the zeolite crystals

One accepted method to modify the external surface of the Zeolite without affecting the internal pore structure is irreversible deposition of $Si(OCH_3)_4$ on the external Zeolite surface.[13] Later hydrocarbon residue can be removed by calcinations with oxygen, forming a silica coated zeolite. This process regenerate silanol groups. $Si(OCH_3)_4$ is a bigger molecule so that it cannot penetrate in to the internal pore structure. For this process optimization of contact time of the modifier, the temperature, the zeolite acidity and the amount of reaction cycles are required. Depending on the deposit amount of SiO_2 on the zeolite surface pore size can be controlled. Methyl-chlorosilane also can be used to modify the zeolite external surface.

A recent study indicate that after deposition of 1 mmol of silane and successful oxidation, the pore size of the original modenite (0.62 nm) can be reduced to 0.35 – 0.4 nm. [30] Further through this process, due to the decreased polarity of the zeolite surface, the adsorption characteristics of the zeolite can be tailored. It was revealed that reaction temperature and pressure have greater effect on this silanation process. Modification at low temperature (273 K) resulted in homogeneous coating of silica through pore channels reducing available pore volume. But high temperature modification (373 K) only cover the external surface and no significant reduction of internal pore volume was observed.

Modification of natural zeolite by ion exchange with NH_3 and treatment with NaOH is reported.[31]During this study dried natural zeolite overnight at 120 ˚C with particle size 0.25 – 0.5 mm was added to 0.5 M NH_4NO_3 solution to perform the ion exchange. After washing several times with deionized water, the sample was calcined at 500 ˚C for 2h to recover the final product.

In a recent research it is reported the change of pore structure of natural zeolite after treating with NaOH aqueous solution. During his research MFI zeolite with (Si/Al = 37) was used. This NaOH treatment increases the external surface area and total surface area of the MFI zeolite. This increase of surface area is due to the formation of supermicropores with 1.8 nm in diameter. These were formed by the dissolution of amorphous phase at the boundary of the MFI zeolite. It was further revealed that the size and volume of the ultramicropores remains unchanged. The rate determining step for the dissolution of MFI zeolite would be the diffusion process of NaOH aqueous solution in to the newly formed supermicropores.

According to the reported literature, the use of NaOH concentration greater than 0.5 M results in significant destruction of zeolite forming protonic sites (not Si-OH-Al) with weak acid strength.[32] It demonstrates that desilication at mild conditions such as 0.1, 0.2 M NaOH does not disturb the crystallinity of resulting materials.

The use of acid washing for the modification of large pore zeolite Y was reported.[33] In this work acid solutions were prepared in various concentrations from citric acid and nitric acid/ammonium nitrate by dissolving in deionized water. In typical treatment 0.5g of NH_4Y zeolite added in to 10 ml of citric acid or 6 ml of HNO_3/NH_4NO_3. Mixture was heated and stirred (500 rpm) for some time and then filtered, washed with deionized water and dried at 110 ºC and calcined at 500 ºC in air for 3 h.

Recently functionalization of pure–silica MFI zeolite with aliphatic alcohols also reported.[34] There are different methods available for the functionalization of mesoporous materials.

1. Direct synthesis via the sol gel process involving the co-condensation of organotrialkoxysilanes ($R - Si(OR')_3$) or organochlorosilanes $R - SiCl_3$ with the tetraalkoxysilanes ($Si-(OR)_4$) that are the primary silica sources for mesoporous material formation

2. Post synthesis modification via grafting the mesoporous material with silane coupling agents such as NH-(SiR)2, Cl-SiR3 or RO-SiR'3

It was reported that etherification reaction of alcohol with silica particles can convert their hydrophilic external surface in to hydrophobic surface. It was noted that hydrophobicity increased with the increase of length of the alkyl group.

Another recent study reports the functionalization of pure silica MFI zeolite with higher aliphatic alcohols with larger organic groups (1-butanol, 1-hexanol). Zeolite nano particles of different sizes were subjected to functionalization in order to investigate the effect of particle size of the zeolite functionalization. During this study TGA was used to measure the alcohol content of the functionalized materials. According to the results functionalization of surface due to alcohol loading is more significant when the particle size decreases. This was confirmed by treatment of different size MFI particles with 1-butanol. The micropore volume measured was negligible may be due to the TPA cations in the pore structure. Therefore, the modification can be done only in the external surface silanol groups. Finally, it was concluded that TPA and alcohol content of as made and butanol functionalized MFI particles match with the internal silanol surface defects.

2.4 Metal Organic Frameworks for the Adsorption Separation of Fluorocompounds

Metal Organic Frameworks are the novel class of hybrid material, which are composed of metal oxides units attached together covalently by organic linkers to form architecturally stable structures with permeant porosity. So far, they have shown enormous potential applications in different technological fields including gas storage,[35, 36] separation,[37, 38, 39, 40, 41, 42]catalysis,[43, 44,

[45, 46] sensing,[47] drug delivery and etc. Figure 2-4 shows the striking increase of all type of MOF structures (1D, 2D, 3D) reported during the past decade, mainly because of the designability and adjustability in their structures and functions as suitable for various types of applications.[48]

2.4.1 Advantages of MOFs over other conventional adsorbents for the separation of fluorocompounds.

When considering MOFs for the adsorption based separation of fluorocompounds, several specific attributes such as stability and reusability, adsorption capacity and selectivity for the target molecules, energy requirement for regeneration need to be carefully evaluated. Though numerous literatures are available on the adsorption based separations of CO_2/N_2, CO_2/CH_4, SF_6/N_2 and etc using metal organic frameworks, limited number of literatures are available on the adsorption based capture and separation of fluorocompounds.

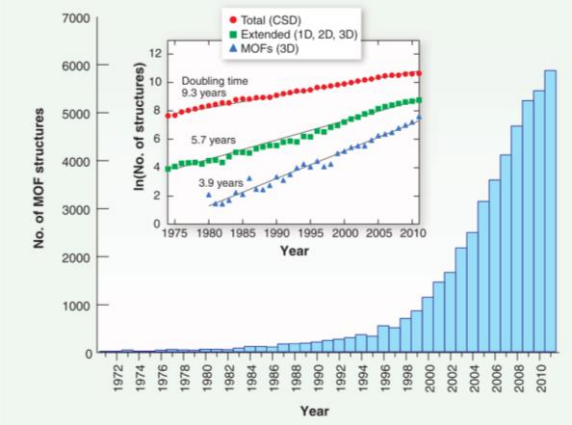

Figure 2-4 Metal organic framework structures (1D, 2D, 3D) reported in the Cambridge Structural Database (CSD) from 1971 to 201148. Reprinted with permission from ref 48. Copyright (2013) The American Association for the Advancement of Science.

The advantages of MOFs over other conventional porous adsorbents for the adsorption based fluorocarbon separations can be presented under below categories: (i) Higher adsorption capacity due to larger surface area and pore volume (ii) Tunability of pore size for the shape-selective separation and possible pore surface functionalization for the selective gas adsorption

(iii) High stability (iv) Several possible synthesis routes as suitable for industrial scale production (v) Moderate energy requirement for regeneration.

(i) Higher adsorption capacity due to large surface area and pore volume

Design and synthesis of porous materials with exceptionally high surface area and pore volume is a challenging task. But such materials are especially important for the gas storage and separation applications. Carbon, Zeolite and Silicas were claimed for highest surface areas before the introduction of MOFs. As shown in figure 2-5, within very short period of time, MOFs with surface areas as high as 7000 m^2/g are reported.[48]

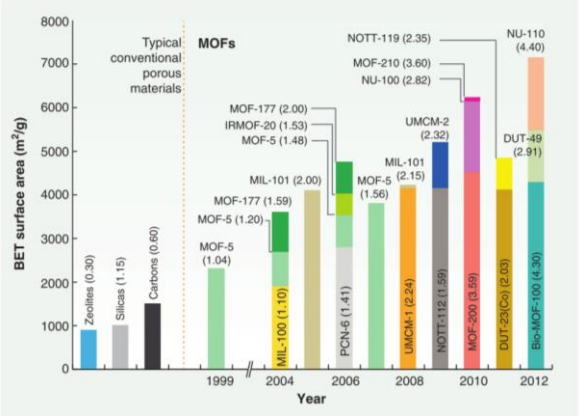

Figure 2-5 Progress in the synthesis of ultrahigh-porosity MOFs: A comparison with typical conventional materials. Values in parentheses represent the pore volume (cm3/g) of these materials.[48] Reprinted with permission from ref 48. Copyright (2013) The American Association for the Advancement of Science.

Table 2-5 summarizes the some of the well-studied MOF with extremely high surface areas and pore volume. The designability of organic linkers from smaller size to larger sizes, together with different metal nodes have led the synthesis of different MOF structures with high surface area and high permanent porosity.[49] It is well known that higher the surface area and porosity then higher the number of adsorption sites available for the physisorption of gas molecules.

Table 2-5 BET surface area and pore volume for highly porous MOFs [50]

MOF	BET surface area (m^2g^{-1})	Pore volume (cm^3g^{-1})
MFU-4 L	2750	1.26
NOTT-102	2940	1.14
PCN-61	3000	1.36
SNU-77	3670	1.52
MOF-5	3800	1.55
UMCM-1-NH2	3920	-
PCN-66	4000	1.36
UMCM-1	4160	-
MIL-101	4230	2.15
Bio-MOF-100	4300	4.30
UMCM-2	5200	2.32
NU-100	6140	2.82
MOF-210	6240	3.6

(ii) Tunability of pore size for the shape-selective separation and possible pore surface functionalization for the selective gas adsorption

The separation processes of gaseous mixtures using microporous adsorbents can be designed either based on shape-selectivity of adsorbent or the different chemical and physical interaction of gases in the mixture with the pore surface of the adsorbent.

One of the recent advance for the tunability of MOF pore size has been the development of a class of MOFs known as zeolitic imidazole frameworks (ZIFs), in which metal atoms such as Zn are linked through N atoms by ditopic imidazolate ($C_3N_2H_3$-) Im) or functionalized Im links to form neutral frameworks. In this case, desired topologies can be achieved by design and, in particular, isoreticular series of compounds with the same topology but different sizes and functionalities of cavities (-Cl, -CN, -Me, -Br, and -NO_2) can be prepared (Figure 2-6).[51]

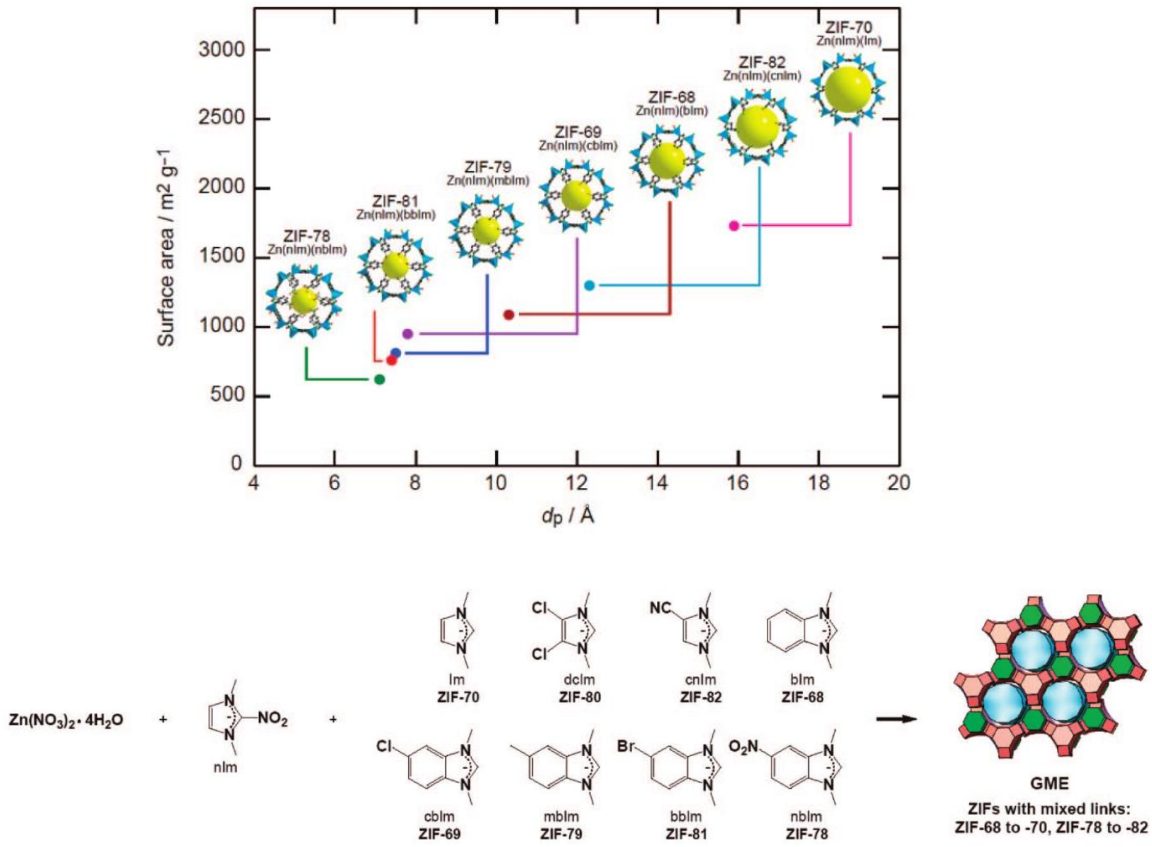

Figure 2-6 Plot of pore diameter (dp) vs surface area for the GME ZIFs, indicating a nearly linear relationship (To illustrate the variation of the pore size and functionality)

The design of IRMOF series based on MOF-5 also demonstrate the possibility of tuning pore size and functionality(-Br, -NH_2, -OC_3H_7, -OC_5H_{11}, -C_2H_4, -C_4H_4) while maintaining the original topology.[52] Other than these isoreticular series of ZIFs and MOF-5, many other types of MOFs have successfully synthesized with functionalized organic linkers (MIL-101, UiO-66, UiO-67 and etc). Apart from predesigned ligands and thereby pores, post synthetic modification of MOFs by introducing bulky groups, not only anchored on ligands (through covalent bonds)

but on open metal sites (through coordination), can also be used to tune the pore size and shape, thereby achieving the selective adsorption and separation of guest molecules.

MOFs with open active metal sites (HKUST-1, M-MOF-74: M = Ni, Co, Zn, Fe or Mg, MIL-100(Fe)) have already proved their suitability for the selective separation of different gaseous mixtures based on thermodynamic equilibrium effect. A recent study has revealed the selective capture of chlorodifluoromethane(R22) from air using open metal site containing LIFM-26 metal organic framework. LIFM-26 has abundant open Fe II/III sites generated by desolvation and Cl atoms with strong electronegativity which can facilitate synergistic interactions with fluorocarbons over N_2, resulting in good separation ability.[53]

The major drawback of polar zeolite for the separation of fluorocarbons is that, irrespective of the differences in polarizability, dipole moment and molecular sizes of fluorocarbons, due to the strong interaction of fluorine with the extra framework cations in the zeolite, in most of the cases they show poor thermodynamics based equilibrium separation. In cases like this, the advantage of MOFs is that the interaction between fluorine and metal sites or hydrogen bonding characteristics are more predictable.

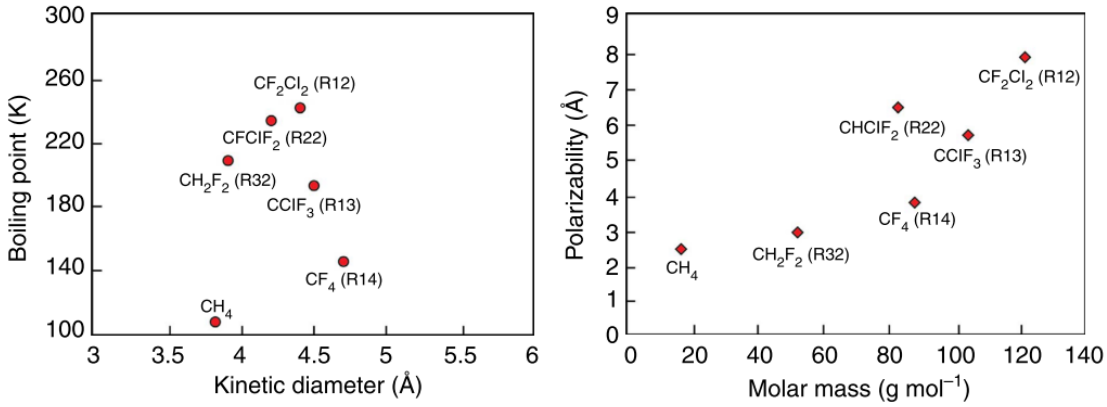

Figure 2-7 Polarizability and kinetic diameter of some of the fluorocarbons[40].

Figure 2-7 shows the kinetic diameter and polarizability of some of the fluorocarbon refrigerants. For the capture and separation of these listed fluorocarbons, design of proper adsorption surface with suitable functional groups is more desirable due to their almost similar

molecular sizes but different atomic composition which may show different interactions with different surface functional groups.

(iii) Chemical, thermal and mechanical stabilities of MOFs

The chemical, thermal and mechanical stability of MOFs have been considered as problematic, especially compared to conventional zeolites. However, with the growth of diverse MOFs structures, chemically and thermally stables MOFs are now available. Chemical stability of some of the well-studied MOFs in aqueous solutions with different pH values are shown in figure 2-8.[54] However not all examples have been tested from pH 0 to 14, and some have shown stability extending below pH 0 or above pH 14.

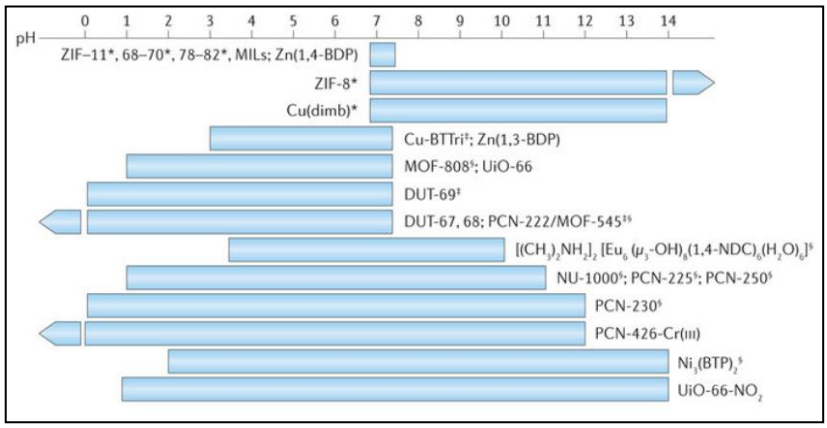

Figure 2-8 The Chemical (acid-base) stability of some representative MOFs[54].

When comparing hydrothermal stability of MOF with conventional zeolite, indeed, zeolite shows excellent stability over wide temperature range. This is not surprising because zeolites are purely inorganic materials and should display better stability than the inorganic–organic MOF structures. The vulnerability of MOFs typically lies in the lability of ligand-metal bonds. In most cases, MOF structure collapse due to the exchange of ligand with the water or other nucleophiles in excessive amounts. Increase chemical and water stability is reported in MOFs which contained high valence metal ions, such as $Cr^{3+,}$ $Fe^{3+,}$ and Zr^{4+}.The enhanced chemical stability in these MOFs are mainly due to the enhanced electrostatic interaction between the

metal ions and the ligands. For an example UiO-66 MOFs based on Zr^{4+} /Hf^{4+} are water stable with good resistance to moderately acidic or basic solutions.

The thermal stability of the MOFs mainly depends on the node-linker bond breakage followed by the thermal combustion of the linker. Therefore, the thermal stability of MOFs generally related to the node-linker bond strength and number of linkers connected to the metal node.

The thermal stability of MOF is more important than their chemical stability, when considering them for gas separation applications. Because, during adsorption based gas separation processes, the MOFs will be subjected to cyclic heating and cooling operations in order to recover the adsorbate and to regenerate.

Usually the activation of MOFs is accomplished by heating them at temperatures below 150º C. Because in most of the cases, the solvents present in the pores can be removed at that temperature. It may not be necessary to use much higher temperatures for the MOFs regeneration during adsorption cycles due to the probable moderate interaction of fluorocarbons with MOF pore surfaces. Several types of MOFs with sufficient thermal stability for the gas separation applications are now available (Table 2-6).

Table 2-6 Representative MOFs with high thermal stabilities.

MOF	Stable Temperature ºC	Ref
HKUST-1	340	55, 56, 57
MIL-101(Cr)	290	58, 59, 60
UiO-66, UiO-66-Br, UiO-66-NH2, UiO-66-NO2	350-500	61, 62
NU100	325	63
NU110	325	50
ZIF-8	300	64, 65
Fe-BTC	300	66

(iv) Several possible synthesis routes as suitable for industrial scale production

Almost 50 years ago, with the introduction of organic structure directing agents for the synthesis of microporous zeolites, despite the extensive efforts that scientists have devoted, only less than 200 different zeolite structures are known to date. In contrast, especially during last decade, thousands of new MOF structures are reported. At the same time, investigations on different synthesis methods has led the synthesis of MOF in large scale with the potential of industrial scale production. For an example, several synthesis routes have developed for HKUST-1 bulk production without using hazardous organic solvents, oxidizing precursors,[57] or high temperature.[56, 67] Besides the conventional solvothermal method for the MOF synthesis, BASF has developed electrochemical method to avoid the large amount of precursor salts and the safety issues accompanied.[68] Table 2-7 shows some of the MOFs which are already commercially available. For the comparison of Space-Time-Yield (STY), Zeolite is also included in the table.

Table 2-7 MOFs that have been synthesized in large amounts [69, 70]

MOF	Comment	STY (Kg m^{-3} d^{-1})
HKUST-1	Commercially available as Basolite C 300	225
Fe-BTC	Commercially available as Basolite F 300	20
ZIF-8	Commercially available as Basolite Z1200	100
MIL-53	Commercially available as Basolite A100	160
$[Mg(O_2CH)_2]$	Commercially available as Basolite M050	> 300
Zeolite	-	50-150

Synthesis cost is a critical issue, when considering the potential of MOFs for the industrial scale fluorocarbon separations. Both synthetic zeolite and MOFs are synthesized using hydrothermal

or solvothermal reactions. Therefore, compared to the synthetic zeolites, the cost of reactors and the cost of utilities to synthesize MOFs can be assumed to be comparable.

Table 2-8 Cost of starting materials to produce some representative MOFs [71]

MOF	Cost /US$ kg^{-1}
CuBTC (HKUST-1)	20.08
CoCo (Co3[Co(CN)6]2)	35.14
MOF-5 (IRMOF-1)	2.93
Zn/DOBDC (Zn-MOF-74)	1.90
Co/DOBDC (Co-MOF-74)	6.48
Ni/DOBDC (Ni-MOF-74)	13.3
Mg/DOBDC (Mg-MOF-74)	1.19
MIL-100	15.64
MIL-101	4.57
Silica gel	1.00

Moreover, to prepare MOFs does not need additional capital investment into a totally new technology. However, the organic linkers and solvents used for MOFs synthesis create considerable difference in production cost when compared to zeolite. Besides using fine chemical regents, if some new technologies can make use of petroleum raw materials that contain abundant aromatic compounds, for the synthesis of aromatic organic linkers, the overall production cost can be significantly lowered. Without using large amount of solvents for the activation of MOFs, use of supercritical drying technique can further used to reduce the production cost significantly. Cost of some representative MOFs based on the cost of their starting materials are shown in table 2-8.

(v) Moderate energy requirement for adsorbent regeneration

The energy requirement for the regeneration of adsorbents is a crucial factor which practically decide the economic feasibility of the process in industrial scale applications. So far, zeolites are widely being used as industrial gas separation processes, but in our case, strong adsorption of fluorocarbons to the zeolite makes the regeneration process less economical. Figure 2-9 shows the R12, R22, R32, R13, and R14 adsorption in MIL-101.[40] By observing the nature of adsorption isotherms, it was noticed that the gases were adsorbed by MIL-101 preferentially through van-der Waals interactions rather than electrostatic interactions. This was concluded by comparing their adsorption and desorption curves which matched perfectly without any hysteresis (Figure 2-10). Such adsorbents have moderate sorbate-sorbent interactions so that they can be easily regenerate using PSA.[72]

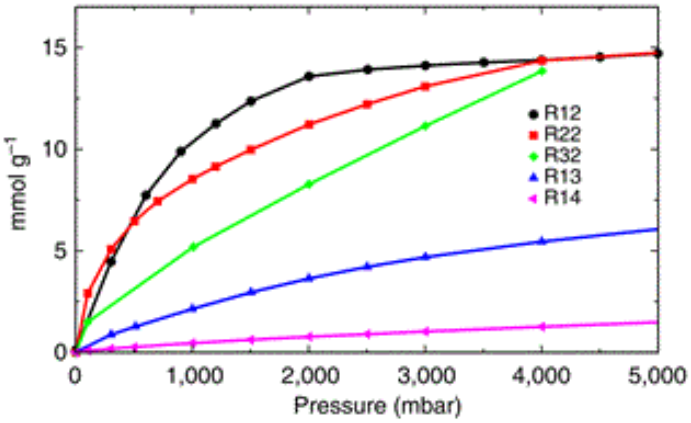

Figure 2-9 R12, R22, R32, R13, R14 adsorption isotherms on MIL-101[40]

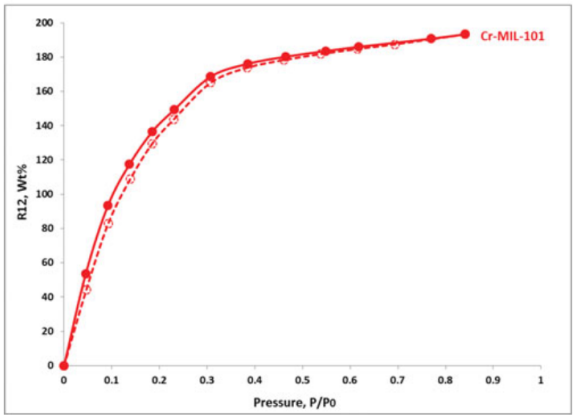

Figure 2-10 Fully reversible R12 desorption isotherm on MIL-101(Cr)[72]

Separation of mixtures of fluorocarbons with the aim of reuse is much more challenging compared to other gas separation processes (CO_2/CH_4, CO_2/N_2, SF_6/N_2 etc). Because of the existence of highly electronegative fluorine in these fluorocarbons, in most of the cases, they are equally attracted to adsorbent surfaces, making it difficult to separate them only based on thermodynamic selectivity. However, due to the design flexibility of MOFs, there is a possibility to optimize all steric, kinetic and thermodynamic selectivity such a way that target fluorocarbon mixtures can be successfully separated with desired purity. Considering all these aspects, exploration of MOFs for the capture and separation of fluorocarbons is very important.

2.4.2 Fluorocarbon capture and separation in metal organic frameworks

Although the gas adsorption and separation potentials of MOFs has comprehensively studied, fluorocompound adsorption and separation has been mostly limited to conventional porous adsorbents such as activated carbons, zeolites and silicas. So far, the reported adsorption and adsorption based separations of fluorocompounds on porous adsorbents are aimed at the removal of byproducts during the production of different fluorocompounds, using in adsorption based heating and cooling systems and rarely on recycling of used fluorocompounds. However, review of reported literature on adsorption/adsorption separation of different fluorocompounds on metal organic framework is important to design efficient fluorocarbon recycling process.

2.4.2.1 Adsorption and adsorption-based separation of PFCs (CF_4, C_2F_6, NF_3, SF_6 etc.)

PFCs are critical to current semiconductor manufacturing methods because they possess unique characteristics when used in a plasma that currently cannot be duplicated by alternatives. The semiconductor industry uses perfluorocompounds (PFCs) such as CF_4, C_2F_6, C_3F_8, SF_6, CHF_3 (HFC-23) and NF_3 in two important production processes – plasma etching thin films and plasma cleaning chemical vapor deposition (CVD) tool champers. The vent gas from semiconductor plasma etching process often contains unreacted CF_4 and/or C_2F_6, and other perfluorocompounds (PFCs) such as SF_6, NF_3, and CHF_3 as well as N_2. Other than in the

semiconductor industry, SF_6 and SF_6/N_2 mixtures are being widely used in medium and high voltage switchgears and in gas insulated transmission lines thanks to their dielectric strength and excellent insulating properties. However, these PFCs are among the most potent and long-lasting type of greenhouse gases (Table 2-9).

Table 2-9 Semiconductor Process Gases

Chemical Formula	**Atmospheric Lifetime (years)**	**Global Warming Potential (100-year time horizon)**
CHF_3	264	11,700
CF_4	50,000	6,500
C_2F_6	10,000	9,200
C_3F_8	2,600	7,000
SF_6	3,200	23,900
NF_3	740	8,000

The major abatement technologies of these compounds can be divided into four general categories: thermal destruction, chemical conversion, plasma destruction, and recovery/reclaim systems.[73] Though these compounds have excellent chemical stability, the major issue associated with the recovery/recycling and reuse them, especially in semiconductor manufacturing processes, is that the recycled substances should have ultrahigh purity to avoid any unwanted contamination to intrinsic silicon.[74] Several researchers have studied the potential of metal organic frameworks for the adsorption based recycling of these compounds.

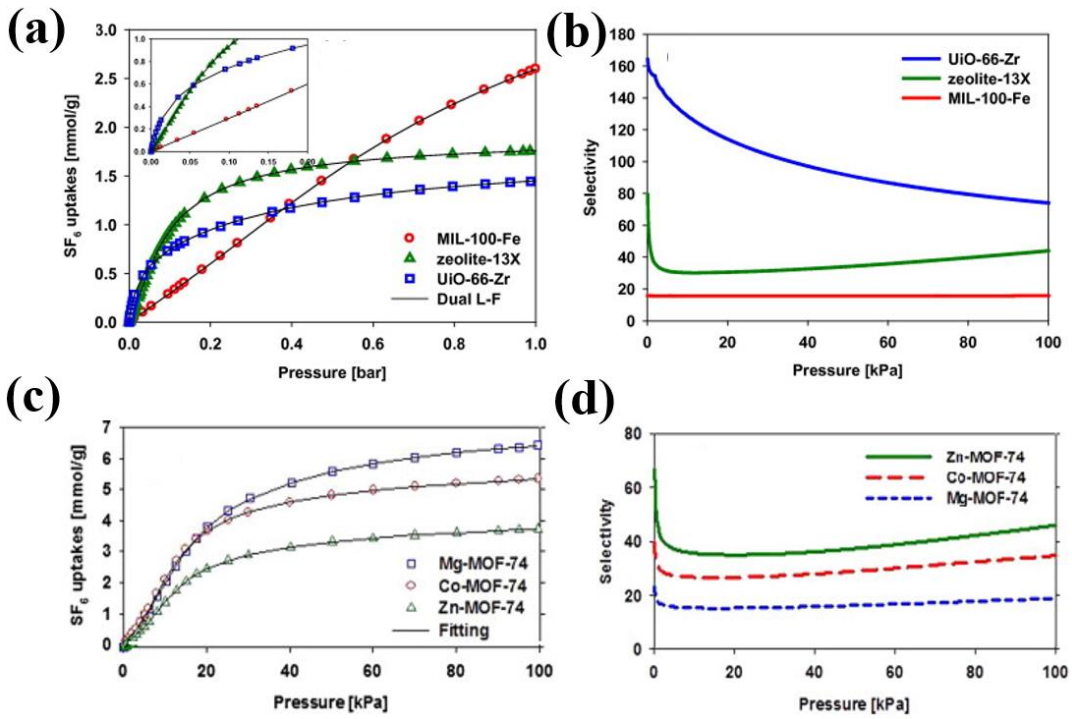

Figure 2-11 SF_6 pure gas adsorption isotherms and selectivity calculated using IAST theory (a), (b) on MIL-100-Fe, Zeolite 13X, UiO-66-Zr at 293 K (c),(d) on M-MOF-74 (M= Mg, Co, Zn) at 298 K respectively.[75, 76] Reproduced with permission from ref 75 & 76.

Table 2-10 lists the reported adsorption capacities (at 1bar and 298 K) of SF_6, CF_4 and C_2F_6 in several types of metal organic frameworks and other conventional adsorbents. So far, the highest adsorption capacity of SF_6 is reported in Mg-MOF-74 (6 mmol/g) followed by Co-MOF-74 (5.2 mmol/g), $Cu_3(BTC)_2$(4.78 mmol/g) and Zn-MOF-74(3.8 mmol/g). It is interesting to note that all these MOFs can be categorized under single group that has coordinatively unsaturated metal sites(CUS). The unsaturated metal centers in one dimensional hexagonal channels (11 Å dia) of isostructural Mg-MOF-74, Co-MOF-74 and Zn-MOF-74 are responsible for their high SF_6 adsorption capacity. Though the highest SF_6 adsorption capacity in Mg-MOF-74 is consistent with the order of their surface areas (Mg-MOF-74 > Co-MOF-74 > Zn-MOF-74), Co-MOF-74 exhibits higher binding affinity to SF_6 as verified using their isosteric heat of adsorption. The adsorption capacities of mesoporous MOFs (MIL-101 and DUT-9) under atmospheric conditions (2.01 mmol/g for MIL-101 and 2.32 mmol/g for DUT-9) are not as high as on MOFs with CUS, but at high pressure (18 bar), they exhibit highest SF_6 uptake of 12.3 mmol/g, which

is characteristic to the MOFs with larger surface areas and pore volumes (pore volumes are 1.5, 1.8 cm^3/g respectively). Other than the ones mentioned above, several other MOFs (Co_2(1,4-bdc)$_2$(dabco) (3.39 mmol/g), Zn_4O(btb) (3.12 mmol/g), MIL-100(Fe)(2.94 mmol/g), $Zn_4O(dmcpz)_3$ (2.54 mmol/g)) are reported for their high SF_6 adsorption capacities.

Table 2-10 Adsorption capacities of different PFCs and N_2 in MOFs at 1 bar and 298 K

Adsorbent	**BET surface area (m^2/g)**	**Total Pore volume (cm^3/g)**	**Adsorption amount (mmol/g)**				**Ref**
			SF_6	**CF_4**	**C_2F_6**	**N_2**	
Mg-MOF-74	1631	-	6.3			1.05	[75]
Co-MOF-74	1219	-	5.2			0.63	[75]
$Cu_3(btc)_2$	-	0.8	4.78	1.16			[77, 78]
Zn-MOF-74	992	-	3.8			0.32	[75]
Co_2(1,4-bdc)$_2$(dabco)	-	0.8	3.39	0.71			[77]
Zn_4O(btb)	-	0.9	3.12	0.49			[77]
MIL-100(Fe)	1619[a]	0.9/0.82[a]	2.95/1.6[a]	0.54		0.13	[77, 79]
$Zn_4O(dmcpz)_3$	-	0.5	2.54	1.87			[77]
DUT-8(Ni)	-	0.9	Very low	Very low			[77]
DUT-9	-	1.8	2.32	0.45			[77]
MIL-101	2674	1.5	2.01	0.54			[77, 80]
MOFF-5	2445	-	1.74	0.09			[81]
UiO-66(Zr)	1333	-	1.45			0.21	[76, 79]
Zeolite 13X[b]	721	-	1.75	0.76	1.55	0.24	[76, 82, 83]
Zeolite 5A[c]	552	0.2	Very low	0.55	-	0.26	[82, 84]
Activated Carbon [c]	633	0.23		0.72	1.26	0.25	[82]
Silica gel [c]	584	0.21			0.5	0.04	[82]

[a] on granular MIL-100(Fe) [b] at 293 K [c] at 303 K

The main feature of SF_6 adsorption isotherms in zeolite 13X compared to those in MOFs is the sharp increase of uptake at low pressure region followed by saturation around 3 bar. Because of this, though zeolite 13X indicate higher SF_6 adsorption capacity than some MOFs, the working capacity between 0.1 and 1 bar become very low.

Interestingly, adsorption of CF_4 in both zeolites and MOFs are much lower compared to SF_6, that can be rationalized by their differences in polarizabilities (Table 2-3). The significant

difference of SF_6 and CF_4 in adsorption capacity in these MOFs, suggest their possible equilibrium separation. However, to the best of our knowledge separation of SF_6/CF_4 mixture in MOFs or in Zeolite is not reported in literature.

Because of the important applications of SF_6/N_2 mixtures as insulators for electrical cable/equipment, SF_6/N_2 separation is an industrially important goal. Figure 2-11 demonstrates the adsorption capacity and SF_6/N_2 selectivity of several MOFs and zeolites. As shown in figure 2-11(b) and (d) among various MOFs and zeolites, UiO-66(Zr) own the highest reported SF_6/N_2 (10:90 mixture) selectivity of 74 (calculated using the Ideal Adsorption Solution Theory (IAST) at 1 bar and 293 K) exceeding the selectivities of Zn-MOF-74 (46), Zeolite-13X (44), Co-MOF-74 (35), Ca-A zeolite (28), MIL-100(Fe) granule (25) and Mg-MOF-74 (19). The higher selectivity of UiO-66(Zr) can be explained by the strong SF_6 adsorption originating from the pore confinement effects of small pores (8, 11 Å) compared to M-MOF-74, Zeolite 13X and MIL-100(Fe). Relevant to the conditions in plasma etching processes of the semiconductor industry, UiO-66-Zr presents even higher selectivities (172) for diluted SF_6 concentrations (0.2%). Besides the calculated IAST selectivities, the experimental breakthrough data also proves the high selectivity of UiO-66(Zr) for SF_6/N_2 separation. However, it should be noted that adsorption capacity of UiO-66(Zr) (1.45 mmol/g) is much lower than in other reported MOFs whereas both adsorption capacity and selectivity are equally important criteria to achieve efficient gas separation. Among the isostructural M-MOF-74(M= Mg, Co, Zn) series, the IAST-derived SF_6/N_2 separation selectivity is highest for Zn-MOF-74, contrary to their order of BET surface areas and SF_6 adsorption capacities. The higher selectivity exhibited by the Zn-MOF-74 may have occur due to the relatively small adsorption amount of N_2. Further, Zn-MOF-74 outperform benchmark zeolite 13X in both adsorption capacity and selectivity. However, by analyzing all working capacity, selectivity and regeneration performances of these MOFs, Co-MOF-74 seems more suitable for the aforementioned separation as it exhibits high working capacity (1.96 mmol/g), high selectivity (35) and high regenerablity (>80%) via vacuum swing adsorption.

2.4.2.2 Adsorption and adsorption-based separation of CFCs, HCFCs and HFCs (R13, R12, R22, R32, R125, R134a etc.)

CFCs, HCFCs and HFCs are industrially important compounds because of their useful applications in different technological fields, especially in the air conditioning and refrigeration industry. However, driven by their zero-ozone layer depletion potential and the low global warming potential, the major fraction of current refrigerant demand is fulfilled by the HFCs succeeding the CFCs and HCFCs which have high ozone layer depleting potential and high GWP. For an example R12 that has been used in domestic refrigerators and mobile air conditioning systems are now replaced with R134a because of the zero-ozone layer deletion potential. Also, R410A which is blended from R32 and R125 now widely being used in residential air conditioning systems as a replacement for R22.

Recovery and Reclamation of used fluorocarbons positively contribute to the environmental sustainability while providing an alternative to fulfill their increasing demand. Therefore, planning and design of energy efficient adsorption-based fluorocarbon reclamation processes is an urgent requirement. However, as an emerging adsorbent, utilization of metal organic frameworks for the fluorocarbon separation requires comprehensive study on various fluorocarbon-MOFs interactions.

Table 2-11 lists the reported adsorption capacities of R32, R22, R125, R134a and R12 fluorocarbon refrigerant in several adsorbents including MOFs, Zeolites, Activated Carbons and Silicas. It is clear to note the extremely high fluorocarbon adsorption capacities in MOFs compared to the conventional zeolites and silicas.

R22 is a common fluorocarbon refrigerant that is being widely used in residential air conditioning and refrigeration systems and many researchers have studied their adsorption in different types of MOFs which include MAF-X10 [$Zn_4O(bpz)_2(bdc)$], MAF-X12 [$Zn_4O(bpz)_2(ndc)$], MAF-X13 [$Zn_4O(bpz)_2(bpdc)$], MIL-101(Cr) and LIFM-26. Since R22 molecular size (≈ 4.2 Å)[40] is smaller than the pore aperture sizes of all these adsorbents, the R22 adsorption capacities of these materials can be fairly compared without considering any

diffusional limitations. Among these materials MAF-X13 exhibits highest R22 adsorption capacity followed by MAF-X10, MAF-X12, MIL-101(Cr) and LIFM-26. At 1 bar and 298 K, isoreticular MAF-X10, MAF-X12 and MAF-X13 possess R22 adsorption capacities of 10.5, 9.5, 13.5 mmol/g respectively. MAF-X10 is isostructural with MOF-5[85] except that two thirds of bdc linkers are substitute by bpz linkers forming hydrophobic pore surface and more moisture tolerant structure which is beneficial for the adsorption of hydrophobic fluorocarbons.[86] Its isostructural analogue MAF-X13 has shown higher adsorption capacities than MAF-X10 mainly because of the differences in their cavity size and pore volume. Besides the high adsorption capacity, they possess high thermal stabilities (MAF-X10 is stable at 550 °C while MAF-X12 and MAF-X13 are stable at 450 °C), suggesting their applicability in real time fluorocarbon capture processes. Under similar operating conditions, high adsorption capacity of R22 (6.5 mmol/g)) in LIFM-26 (constructed using 2,3,5,6-tetrachloride terephthalic acid and $Fe_3O(H_2O)_3$) which is isostructural to MOF-235 and $Fe_3(F_4BDC)_3(H_2O)_3$ is also reported.[53] The material consists of one type of tetrahedral cage (7Å dia) constructed from five Fe_3O clusters and six tcdc ligands and two types of channels each with the different shape (round and elliptic) and different size (9 Å dia, 11.5 x 6.5 $Å^2$ respectively, Figure 2-12). Similar to MAF-X10 and MAF-X12, LIFM-26 also exhibits type I R22 adsorption and this steep gas uptake at low pressure region is characteristic to the adsorbent-adsorbate pair with strong adsorption affinity, in this case probably due to the existence of open metal sites and polar functional groups. Importantly, the adsorption enthalpy of LIFM-26 (25 kJ/mol) is much lower than MAF-X series (31.4 – 32.9 kJ/mol) suggesting the moderate adsorption affinity of R22 to LIFM-26 and it is beneficial for the energy efficient regeneration. But, though this material shown to be have good water/chemical stability, it has only moderate thermal stability as observed during thermogravimetric (TGA) analysis which indicate collapse of structure at temperatures above 200 °C.

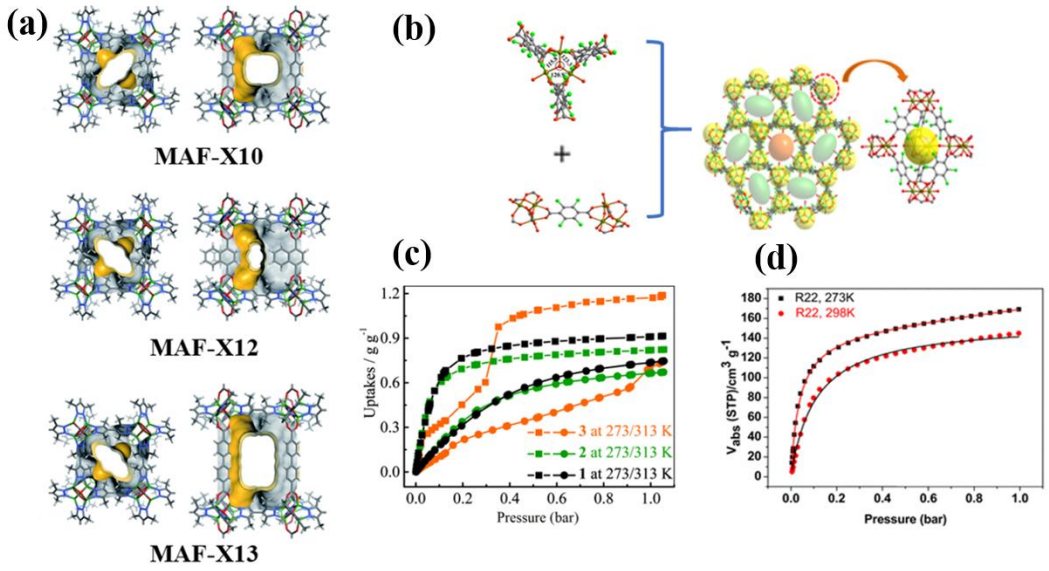

Figure 2-12 (a) The pore structure of MAF-X10, MAF-X12 and MAF-X13 viewed along two characteristic directions (b) The Trimeric Fe_3O cluster, $tcdc^{-2}$ coordination mode and packing diagram along the C axis of LIFM-26 (c), (d) R22 adsorption isotherms of MAF-X10, MAF-X12, MAF-X13 and LIFM-26 respectively.[53, 86] Reproduced with permission from reference 53 & 86. Copyright (2017) John Wiley and Sons.

Recently Motkuri et al reported adsorption of several fluorocarbons including R22, R32, R12, R13 and R14 on MIL-101 which is known for its extremely high surface area and giant pore volume.[40, 87] At 1 bar and 298 K, MIL-101 indicate highest uptake of R12 (10.5 mmol/g) followed by R22(8.5 mmol/g), R32 (5 mmol/g), R13(2.4 mmol/g) and R14 (< 1 mmol/g). Besides MIL-101, they have studied the adsorption characteristics of R12 in MIL-100 (Fe), Co-MOF-74 and Ni-MOF-74. Both Co-MOF-74 and Ni-MOF-74 indicate higher adsorption capacities (4.5, 5 mmol/g respectively) at low pressure region (P/P_0=0.01) and reach saturation at P/P_0 =0.05 indicating strong interactions of R12 with the open metal sites in these MOFs. However, a recent work indicates even higher R12 adsorption capacity (6 mmol/g) in pore engineered Ni-BPP (BPP= 3,3′-dioxido-4,4′-biphenyldicarboxylate, biphenyl with para-COOH). Ni-BPP is analogues to Ni-MOF-74[88] and with the substitution of $dobdc^{-2}$ linker with BPP, the pore expanded Ni-BPP has achieved higher surface area and pore volume than Ni-MOF-74 resulting higher adsorption capacities than its' parent material(Figure 2-13). Figure 2-

13b shows the increase of pore volume and average pore width with the change of ligand from $dobdc^{-2}$ to BPP and TPP (TPP = 3,3′-dioxido-4,4′-triphenyldicarboxylate, triphenyl with para-COOH, Figure 2.13a). The same study reports high R134a adsorption capacity in Ni-MOF-74 and even higher capacities in its pore expanded analogues: Ni-BPP and N-TPP All these materials show type I R134a adsorption suggesting the strong interaction of R134a with their pore surface. Though Ni-TPP exhibit highest saturation capacity (0.77 g/g) than its' analogues Ni-BPP (0.75 g/g) and Ni-MOF-74 (0.58 g/g), capacity difference of Ni-BPP and Ni-TPP is only 0.02 g/g due to the smaller surface area but higher pore volume of Ni-TPP.

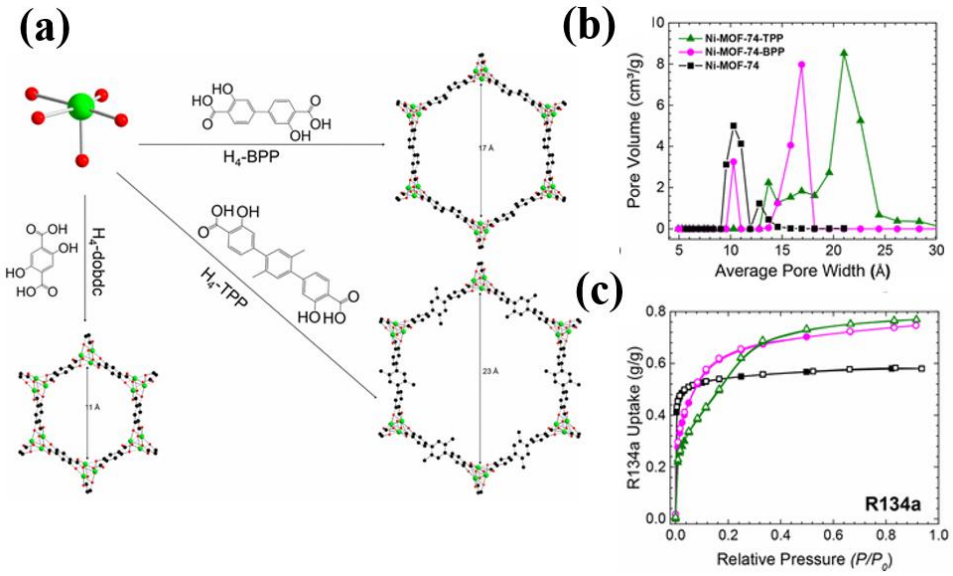

Figure 2-13 Schematic representation of the Ni2+ node, organic bridging ligands, and the corresponding structures (as viewed along the c-axis) of the pore-expanded Ni-MOF-74 analogues (a) Pore size distributions (b) R134a pure gas adsorption isotherms (c).[88] Reproduced with permission from ref 88.

Chen et al[81] recently revealed second highest R12 (6.6 mmol/g) and R134a (5.4 mmol/g) adsorption capacities in MOFF-5 than MIL-101 and Ni-BPP respectively. Reaction of fluorinated tritopic tetrazole ligand (figure 2-14a) with $CuCl_2$. $2H_2O$ in a mixture of N, N-diethylformamide (DEF), methanol and water formulate MOFF-5 with a three-dimensional network: $[Cu(H_2O)_6]_{1.5}[(Cu_4Cl)_3(\mathbf{2}\text{-}3H^+)_8(H_2O)_{12}]$. Other than for R12 and R134a, this material is shown to possess very high adsorption capacities for HFC-227ea, CFC-113, HCFC-225ca,

perfluorohexane and dichloromethane as well. However, it exhibited poor SF_6 and R14 adsorption capacities which authors tentatively rationalized using the low polarities of these guests and mismatched with the highly polarized environment inside the fluorinated cavities, though there is not overall correlation between the dipole moments and their adsorption capacities within MOFF-5. The poor stability to water and moist air appears to be the major disadvantages on its applicability in fluorocompounds capture and separation.

Table 2-11 Adsorption capacities of different types of metal organic frameworks, zeolites and activated carbons (At 1 bar and 298 K).

Adsorbent	BET surface area (m^2/g)	Total Pore volume (cm^3/g)	Adsorption amount (mmol/g)					Ref
			R32	R22	R134a	R125	R12	
MAF-X10	2032	0.798		10.5[a]				86
MAF-X12	1787	0.713		9.5[a]				86
MAF-X13	2742	1.014		13.5[a]				86
MIL-101(Cr)	-	-	5	8.5			10.5	40
LIFM-26	1513	0.59		6.5				53
MIL-100(Fe)	-	-					5.8	40
Co-MOF-74	-	-					4.5	40
Ni-MOF-74	1146	0.49			5.3		5.0	40, 88, 89
Ni-MOF-74 (BPP)	2039	0.83			5.8		6.0	88
Ni-MOF-74 (TPP)	1975	1.14			4.7			88
MOFF-5	2445	-			5.4		6.6	81
Zeolite 13X	588	0.306			2.7[b]	2.3[b]		90
Zeolite 5A	484	0.28	4.6[b]	2.8[b]		2.7[b]		91
Activated Carbon (BPL)	1180	0.55		4.6[c]			4.2[c]	27
Vruf Carbon	1330	0.81				3.0		26
Activated Carbon	3200	1.7	8.8[d]					24
Activated Carbon Fiber	2200	1.0	6.9[d]					24
Fluka Charcoal	1143	-			3.25[b]			28
Maxsorb III	3150	1.7			12.7			25
Silica gel	750	0.35		2.0	2.4		2.0	29

[a] at 273 K [b] at 293 [c] at 303 K [d] at 2 bar

To obtain efficient fluorocarbon separation, the MOFs can be selected based on their (1) molecular sieving effect, which is based upon size/shape exclusion of certain components of a gas mixture; (2) thermodynamic equilibrium effect, due to the differences in adsorption affinities to the MOF surface; and (3) the kinetic effect, due to differences in the diffusion rates of different components of a gas mixture. In this regard, information on molecular sizes, polarizabilities, dipole moments of the gases in the mixtures that are to be separated is extremely important. Table 2-1 lists these properties of selected HCFCs and HFCs.

Among the available literature on the fluorocarbon adsorption in metal organic frameworks only Motkuri et al detail the fluorocarbon separations. With the aid of experimental and simulated column breakthrough results, they have showed thermodynamic equilibrium separation of fluorocarbon blend containing R12, R14, R32, R22, and R12 in MIL-101 based on the differences of their polarizabilities

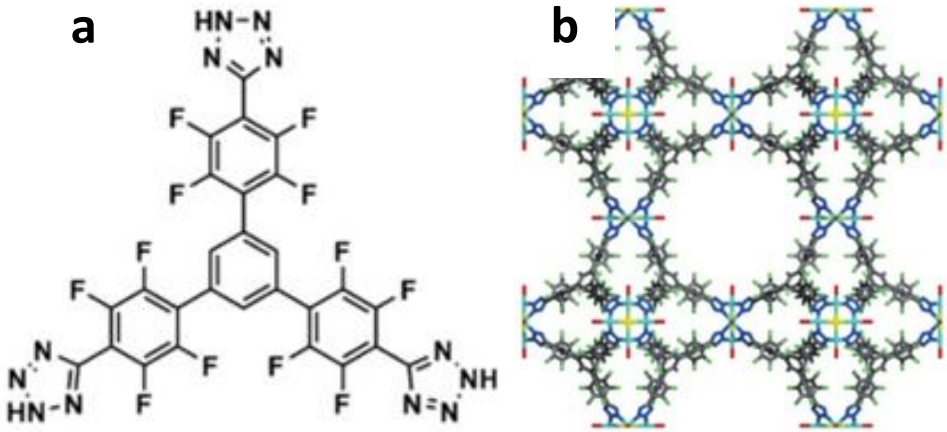

Figure 2-14 Extensively fluorinated tritopic MOF precursor (a) synchrotron X-ray crystal structure of MOFF-5.[81] Reprinted with permission from reference 81. Copyright (2015) John Wiley and Sons.

(Table 2-1). Generally, for selectivity based upon a physisorptive adsorption mechanism, the separation relies on the gas molecules having different physical properties, such as the polarizability or the quadrupole moment, resulting in a higher enthalpy of adsorption of certain molecules over others. The variation of polarizabilities of these fluorocarbons with the molar

mass is shown in figure 2-15b. The general trend is the polarizabilities increases with the incease of molar mass. Following the order of adsorption capacity, the simulated breakthrough results indicate early breakthrough of R14 through the column filled with MIL-101 followed by R13, R32, R12 and R22 respectively (Figure 2-15d). Though R13 and R14 have higher polarizability than R32, they indicate early breakthrough than R32. R32 has lower molar mass and molecular size compared to R13 and R14 which promote its' efficient packing within the pores of MIL-101 resulting higher adsorption capacity and eventually contributing to higher selectivity.

MOFs with open metal sites create strong electrostatic interactions with the gas molecules and substantial gas selectivity can be achieved based on the differences in polarizabilities and dipole moments of the gases in the mixture that is to be separated. However, in the case of fluorocarbon separation, irrespective of the differences of their polarizabilities, the possible formation of strong open metal site M·····F electrostatic interactions may adversely affect their degree of gas selectivity. For an example, open metal site containing LIFM-26 and M-MOF-74 indicate steep fluorocarbon uptakes at low pressure region and it is more pronounced compared to that on MIL-101 suggesting strong fluorocarbon affinity to open metal sites.[92] Such strong fluorocarbon interactions with the pore surfaces often result high adsorption capacities but at the same time they adversely effect on the adsorption selectivity which is not beneficial for gas separation especially when high product purity is required.

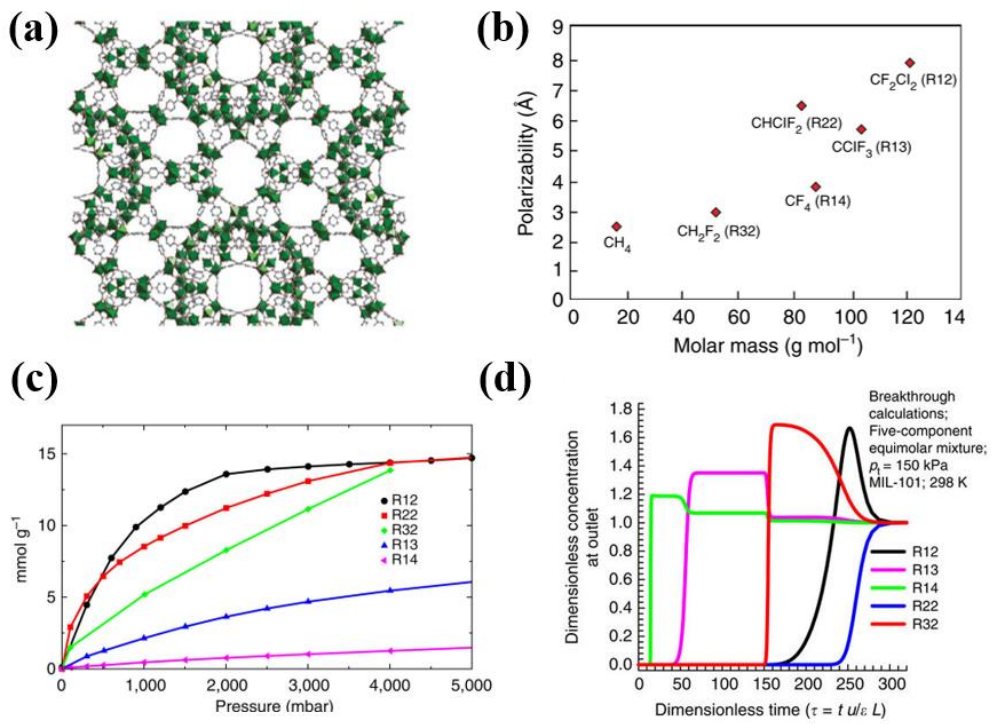

Figure 2-15 Crystal structure of MIL-101 (a) Physical parameters of fluorocarbons (b) Soption profiles of various fluorocarbon refrigerants in MIL-101 at 298 K (c) Simulated breakthrough characteristics of an adsorber packed with MIL-101 for a feed of equimolar R12, R13, R14, R22 and R32.[40] Reproduced with permission from ref 40.

Besides utilization of MOFs for the separation of fluorocarbons based on the thermodynamic equilibrium effects, the possible kinetic and steric separation based on the differences in their molecular sizes (Table 2-1) has not yet explored. However, there are numerous literature available on the separation of small molecules over molecular sieve MOFs. For example, $Mn(HCOO)_2$, a porous framework structure containing cages with a diameter of about 5.5 Å (Figure 2-16a) connected to each other via small windows of about 4.5 Å, has shown high selectivity for CO_2 over other larger molecules (N_2, O_2, Ar etc) because of the steric effects.[93] SIFSIX-3-Zn is another MOF constructed from short building blocks forming ultra-small pore diameter as suitable for steric separation of small gas molecules.[94] It is isostructural to SIFSIX-1-Cu except that the relatively long ligand 4,4′-bipyridine in SIFSIX-1-Cu is replaced by shorter pyrazine in SIFSIX-3-Zn, and Cu(II) is replaced with Zn(II). The reduction in ligand length

results contracted pore aperture of SIFSIX-3-Zn (3.84 Å) versus SIFSIX-1-Cu (9.54 Å). Also, doubly interpenetrated SIFSIX-2-Cu-i (isostructural to SIFSIX-2-Cu) constructed using $CuSiF_6$ and 4,4'-dipyridylacetylene possess smaller pore size of 5.15 Å compared to 13.05 Å in SIFSIX-2-Cu as suitable (Figure 2-16b) for small gas molecule separation. Though these types of MOFs are suitable for steric separation of fluorocarbons, their low surface area and pore volume significantly effect on the adsorption capacity. Therefore, design/selection of molecular sieve MOFs with high selectivity and adsorption capacity is highly a challenging task that need to be explored to a greater extend.

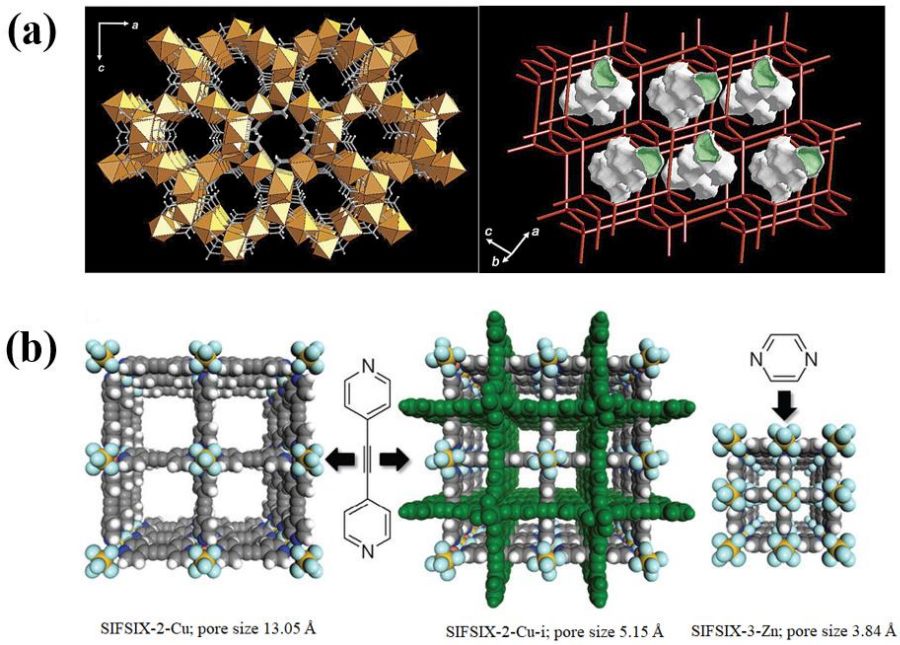

Figure 2-16 (a) X-ray crystal structure and crystal topology of $Mn(COO)_2$ (b) Structures of SIFSIX-Cu, interpenetrated SIFSIX-Cu-i and pore contracted SIFSIX-3-Zn[93, 95]. Reproduced with permission from ref 93 & 95.

2.5 Characterization of adsorbents

The adsorbents used for gas separation and purification processes can be broadly divided in to three categories based on their pore size distribution(PSD). Adsorbents with pores less than 2 nm are categorized as microporous adsorbents, between 2 -50 nm as mesoporus adsorbents and adsorbents with pores greater than 50 nm as macropore adsorbents. Physical gas adsorption is the most widely used technique for the adsorbent characterization.[96] According to the Brunauer

classification of isotherms, there are mainly five types of gas adsorption isotherms which are describe the adsorbents with wide range of PSD (figure 2-17). If the pore size of the adsorbent comparable with the gas molecule, type 1 isotherm can be expected i.e true microporous adsorbents.[14] These types of adsorbents reach their saturation limit soon after filling the micropores. Type II and type III adsorption isotherms can be expected for the adsorbent with different pore sizes, in which adsorption capacity increase with the increase of loading due to the multilayer formation and subsequent capillary condensation. Type IV isotherm indicate the formation of two layers either on the planner surface or pore walls which has higher pore diameter than the adsorbate diameter.[14]

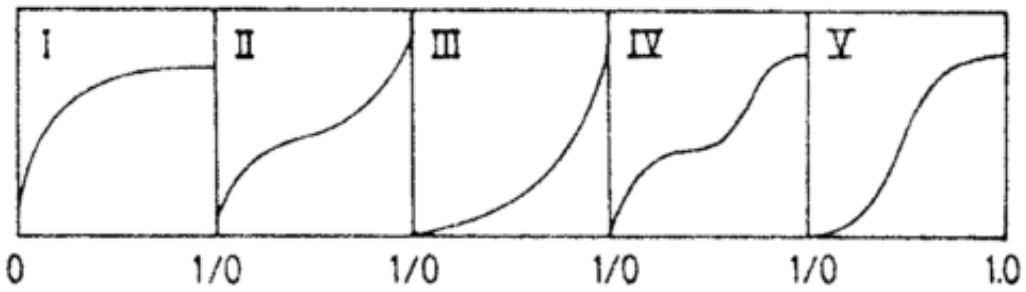

Figure 2-17 Brunauer classification of isotherms.

Different types of equipment are available for the characterization of porous adsorbents either based on volumetric adsorption measurements or gravimetric adsorption measurements.[97] Depending on the required information, different types of probe gases are used as adsorbates such as N_2, Ar, CO_2. Use of Nitrogen adsorption at liquid nitrogen temperature (77 K) up to atmospheric pressure enable to get the information on pore size distribution of micro-, meso- , macro- adsorbents approximately in the porosity range of 0.5 – 200 nm.[96] The inertness, almost spherical shape, the ability to use it at wide range (10-5 to 0.995) pressures is enable the N_2 to use as adsorbate for most of the adsorbent characterizations.

Measurement of microporosity

Molecular sieve adsorbents are widely used for the adsorption separation applications based on the molecular sieving effect. In very fine pores, the adorbate – adsorbent interactions increase

due to the close proximity of the pore walls. Therefore, gas adsorption experiments at very low pressure is required for the accurate determination of micropore size distribution less than 0.7 nm. When the size of adsorbate is comparable with pore size of the adsorbent, the molecular motion is hindered, and molecules need to overcome the energy barriers to enter in to the micropores. But at very low temperature(for an example at liquid nitrogen temperature 77K), the probability to overcome this energy barrier is low and it may take longer time to reach the equilibrium.[98]

Smaller molecules such as CO_2 at 273 K can be used to determine the micropore size distribution instead of using N_2. But the vapor pressure of CO_2 at 273K is around 35 bar. Hence high-pressure gas analysing equipments are required to determine the all range of pore size distributions.

The use of Argon as the adsorbate for the determination of pore size and surface area at 87 K is more suitable, because compared to nitrogen at 77 K, pore filing can be shifted to higher relative pressure at 87 K reducing kinetic restrictions associated with nitrogen at 77 K.[99]

2.6 Selectivity of adsorbents using Ideal Adsorption Solution Theory (IAST).

The selectivity is the most important fact in the adsorption gas separation process as it determines the efficiency of the process through the achievement of required purity. The selectivity of adsorption separation process can be expressed as mentioned below.[100]

$$\text{Selectivity} = \frac{q1/q2}{p1/p2}$$

Where q1 and q2 are the uptake of gas 1 and gas 2 respectively. P1 and P2 are the partial pressure of corresponding component. Use of column breakthrough apparatus along with the gas chromatography enable the measurement of selectivity of gases in the mixture.[101] But due to the difficulties associate with the experimental determination of gas selectivity, Ideal Adsorption Solution Theory (IAST) is being used to calculate selectivity from pure component gas isotherms in many of the studies. The accuracy of the IAST for the prediction of gas selectivity

in different types of adsorbents is already been established.[102, 103] In order to use it, first the adsorption isotherm should fit with an isotherm model and solving below set of equations, quantitative estimation can be done on the selectivity of the particular adsorbent (at different gas compositions and feed pressures).

For mixture of gas containing component 1,2

$$Py_1 = P_1^{o} X_1$$

$$Py_2 = P_2^{o} X_2$$

$$\int_0^{\frac{Py1}{x1}} F1(P)\left(\frac{1}{P}\right) lnP = \int_0^{\frac{Py2}{x2}} F2(P)\left(\frac{1}{P}\right) lnP$$

where $F_1(P)$ and $F_2(P)$ are the fitted functions.

Selectivity $=(X_1/Y_1)/(X_2/Y_2)$ where X, Y are mole fractions in adsorbed phase and bulk phase respectively.

Chapter 3

Methodology

3.1 Characterization of Materials

3.1.1 X - ray diffraction analysis

The synthesized materials were characterized using X-ray diffraction (XRD) on a D2 phaser X-ray diffractometer (Bruker) equipped with LynxEye detector.

3.1.2 Surface area and pore characteristics

Pore structure and surface area of the adsorbents were evaluated by performing N_2 adsorption isotherms at 77 K on Quantrachrom AS6 pore size and surface area analyzer. Prior to the isotherm measurements all the adsorbents were degassed under relevant activation temperatures under dynamic vacuum for a minimum period of 16 hrs. The isotherm points measured at the P/P_0 range of 0.05-0.3 was used to calculate the surface area using Brunauer−Emmett−Teller (BET) method. t-plot method and BJH methods were used to obtain the micropore volume and pore size distribution.

3.1.3 Particle size and Morphology

Morphological information of the synthesized adsorbents was studied by field-emission scanning electron microscope (JOEL, JSM6700).

3.1.4 FTIR analysis

Fourier transformed infrared spectroscopy (FTIR) spectra were collected on IR spectrometer (PerkinElmer) with a resolution of 4 cm^{-1} in the range from 4000 to 450 cm^{-1}.

3.1.5 TGA analysis

Thermogravimetric analysis (TGA) was performed on the adsorbents on a Pyris diamond TGA at a heating rate of 10 K/min up to 973 K with flow of air/nitrogen.

3.2 Single gas adsorption equilibrium measurements

Single gas equilibrium isotherm measurements can be used to obtain set of valuable information for screening of adsorbents for various applications. The adsorption isotherm provides the amounts of adsorbate adsorbed on the surface of adsorbent at different pressures under isothermal conditions. Besides, the measured isotherms at different temperatures can be used to calculate isosteric heat of adsorption. In our study, volumetric method was used to obtain the equilibrium adsorption isotherms. All the pure gas equilibrium adsorption isotherm measurements were measured using Isorb-HP high pressure gas adsorption analyzer (Qunatachrom instruments, USA). This instrument provides in-situ degas and isotherm measurements in the temperature range of and up to 200 bar. Typically, about 1 g of adsorbent was used for the isotherm measurement. Prior to each adsorption measurement, adsorbents loaded in the sample cell was activated by heating the cell at desired activation temperature under high vacuum for at least 8 h. At equilibrium pressures lower than 0.5 bar, it was considered as reaching the equilibrium if the sorption rate calculated using 6 equilibrium pressure points taken at 30 s intervals is less than 0.1 mbar/min. For equilibrium pressures greater than 0.5 bar, the sorption rate limit was set as 0.2 mbar/min. No time limit was assigned for the equilibrium adsorption. Heat of adsorption was calculated from the pure gas adsorption data collected at different temperatures using Clausius-Clapeyron equation (Eq. 1) in the software.

$$\Delta_{ad}H^{o} = R\left\{\frac{[\partial \ln p]}{[\partial\left(\frac{1}{T}\right)]}\right\}_{\theta} \qquad (1)$$

3.3 Dynamic column breakthrough experiments

Dynamic column breakthrough experiments can be used to obtain actual selectivities of the adsorbents under various operating conditions. During these experiments, the gas mixtures with different compositions are feed in to a column packed with adsorbents. By analysing the composition of gas breakthrough from the column, the selectivity can be determined. Also using this column breakthrough setup, the operating conditions such as feed flow rate, feed

composition, column length, operating temperature and pressure can be easily optimized to improve the selectivity.

Design of Adsorption reactor system

Schematic diagram of adsorption reactor system is shown in figure 1. This reactor system is consists of different components as mentioned below.

- Mass Flow Controllers(MFCs) and Mass Flow Meters(MFMs)

Four MFCs which are specially calibrated to control the flow rate of R32, R22, R125 and He was purchased from Alicat Scintific. One MFM was purchased from the same company to measure the mixed gas flow rates. All MFCs and MFM have the accuracy of +/- 1% at full scale. By using these MFCs, it is possible to mix the gas with different known compositions.

- Tube Furnace

New tube furnace with 3" internal diameter and 12" heated chamber length was purchased from Thermcraft, Inc., USA in order to use for the activation of adsorbents at elevated temperature. This tube furnace is capable of operating at temperature as high as 1100 ˚C and can be mounted either horizontally or vertically.

- Molecular Vacuum Pump

Molecular vaccum pump which can operate from intermediate vacuum (~10−2 Pa) up to ultra-high vacuum levels (~10−8 Pa) was installed inline with adsorption column.

- Gas Chromatography

GC 2014 provided by Shimadzu Cooperation, Japan was used inline with adsorption reactor system to measure the composition of effluent. The existing GC was upgraded to measure the composition of different Freon gases. The existing column was replaced with CP-SilicaPLOT capillary column purchased from Agilent Technologies. This is 30 m in length with 0.7 mm

outer diameter and is capable of operating at maximum temperature up to 120 ˚C to identify specially R32, R125, R22, R143a, R134a and C1-C4 isomers.

- Reactor column

Stainless steel tube with ½ inch internal diameter and 35 cm was used as the column to pack the adsorbents in large quantity. Set of smaller columns with ¼ inch inner diameter was used to pack the adsorbents in small quantities (MOFs, molecular sieve carbons etc).

The use of 1/8 inch stainless steel tubing for the transport of gases from cylinders to the reactor column facilitates the operation of system at very low flow rates. Type K thermocouple was installed inside the reactor column to observe operating temperatures and any variation of temperatures inside the column.

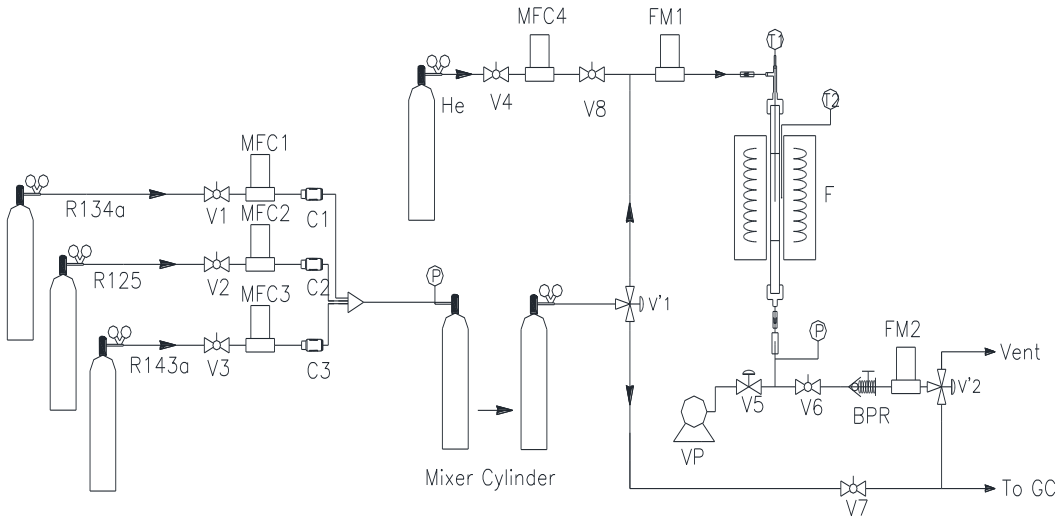

Figure 3-1 Schematic diagram of the adsorption reactor system, MFC – mass flow controller, FM – flow meter, P – pressure gauge, T – thermocouple, VP–vacuum pump, BPR – back pressure regulator, GC – gas chromatograph, V – ball valve, V' – three way valve

Prior to the breakthrough experiments, the adsorbents packed in the column was activated at relevant temperature under high vacuum for at least 8 h. During breakthrough experiments, the adsorbent column was maintained at a constant temperature by a circulator bath (Julabo F34).

The composition of the gas mixture after passing through the adsorbent column was monitored by an inline gas chromatograph (GC 2014, Shimadzu)

Chapter 4

Absolute Separation of R22, R32 and R125 Fluorocarbons in 4A Molecular Sieve Zeolite

Overview: This chapter reports the adsorption-based separation of blends of difluoromethane (R32), chlorodifluoromethane (R22) and pentafluoroethane (R125) into their pure components using 4A molecular sieve zeolite under ambient conditions. Pure gas equilibrium isotherm measurements indicate that the uptake capacity follows the order of R32 > R22 > R125 on 4A zeolite with negligible uptake capacity for R125. As evidenced by the gas breakthrough results, R32, R22 and R125 could be successfully separated into pure components using 4A zeolite. Steric effects were responsible for the separation of R32 and R22 from R125 while both steric and kinetics effects (due to the larger molecular size of R22 compared to R32) facilitated the successful separation of R22 from R32. The regular pore structure, excellent match of pore size of 4A zeolite with the molecular sizes of the fluorocarbon make the product gases very pure, to the extent of direct industrial applications.

4.1 Introduction

While numerous examples have been reported for the adsorption separation of CO_2/N_2, CO_2/CH_4, CO_2/CO, and etc, [21, 104, 105, 106] adsorption based separations of fluorocarbons are rarely reported in the literature.[24, 26, 107, 108] Myers et. al., reported the adsorption of HFC134 and HFC134a on X and Y zeolites,[107] while Akkimaradi et. al., studied the HFC-134a adsorption characteristics on activated charcoal.[108] Recently Motkuri et. al., reported R32, R22, R12, R13 and R14 adsorption on novel metal organic frameworks.[9] However, most of these reported literatures are based on thermodynamic equilibrium separation. For thermodynamic based separation, it can be due to enthalpy or entropic effects. In enthalpy separation, gas molecules that have stronger interaction with adsorbent can be retained preferentially over the other gases in the mixture.[14, 20, 109] But the applicability of this type of equilibrium separations for industrial

application is rather difficult because of the low product purity. Steric gas separation on the other hand is able to obtain very pure product. During steric gas separation, gas molecules with smaller molecular sizes than the pore aperture of adsorbent allow to enter into the pore of the adsorbent while larger ones are prevented from penetrating into the pore structure. Still applicability of this type of steric separations are very few, since availability of adsorbents with matching pore sizes for target molecular separations are limited. In this work, we report the adsorption separation of R32 (difluoromethane/HFC32), R22 (chlorodifluoromethane /HCFC22) and R125 (pentafluoroethane /HFC125) using type A zeolite molecular sieves.

4.2 Materials and Methods

Type 4A and 5A molecular sieve zeolites were purchased from Union K.K and Tosoh Japan in the form of spherical particles with diameter of 1.5 -2.5 mm and cylindrical extrudes with diameter of 1.5 mm, respectively. R32, R22 and R125 were purchased from Lie Ku Pte Ltd Singapore. For isotherm measurements, all gases were further dried over 3A molecular sieve zeolite. Characteristics of the selected fluorocarbon compounds are summarized in Table 4-1.[8, 10, 11, 110]

Table 4-1 Properties of R22, R32 and R125

Name	Molecular size/Å	Boiling point/˚C	Dipole moment(μ)/D	Polarizability(α)/ (cm^3/mol)
R22	4.2	−40.8	1.42	-
R32	3.9	−51.7	1.97	13.2
R125	4.4	−48.1	1.54	14.3

4.3 Results and Discussion

4A and 5A zeolite are in the sodium and calcium exchanged form of LTA zeolite with effective pore sizes of around 4 Å and 5 Å, respectively. Both N_2 adsorption isotherms (Figure 4-1) of 4A and 5A zeolite exhibit type I adsorption.[20] BET surface areas for 4A and 5A zeolite are 626 m^2/g and 484 m^2/g, respectively.

When compare the BET surface areas of 4A and 5A zeolites, 5A zeolite has lower surface area than 4A zeolite. However, both surface areas are within the range of 500-600 m^2/g which is typical of type A zeolites. Depending on the binder content used to form the spherical and cylindrical particles, such variation of surface area can be expected.

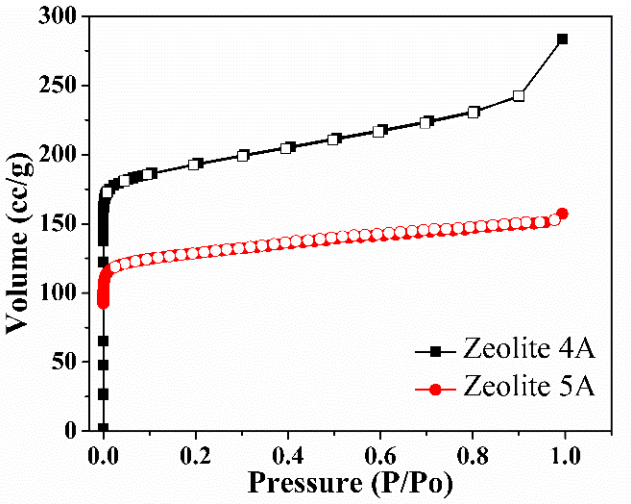

Figure 4-1 N_2 adsorption isotherms of 4A and 5A zeolite measured at 77 K.

4.3.1 Pure gas adsorption isotherms

Pure gas adsorption isotherms of R32, R22 and R125 on 4A and 5A zeolite are shown in Figure 4-2 and 4-3. Based on the adsorption isotherm results, R32 has higher adsorption amount on 4A zeolite than R22, while the adsorption of R125 is insignificant. Thus, it is possible to separate R22 and R32 from R125 in a mixture containing these three fluorocarbons. At 293 K and 1 bar, the adsorption amount of R32 on 4A zeolite is 3.5 mmol/g and it reduces to 1.6 mmol/g for R22. Under similar conditions, Motkuri et. al., reported higher adsorption amounts for R32 and R22 on MIL-101 metal organic framework (5 mmol/g and 6.5 mmol/g, respectively), due to much larger surface area of MIL-101 (5 times larger) as compared to 4A zeolite.[9] However, the measured gas adsorption amounts in our study should be in the lower bound as the 4A zeolite used in these measurements is pelletized which contains substantial amount of binders (about 20 wt%). The extra-framework cations in the 4A zeolite create polar surfaces, which should be beneficial for adsorption of polar fluorocarbon gas molecules such as R32 and R22.

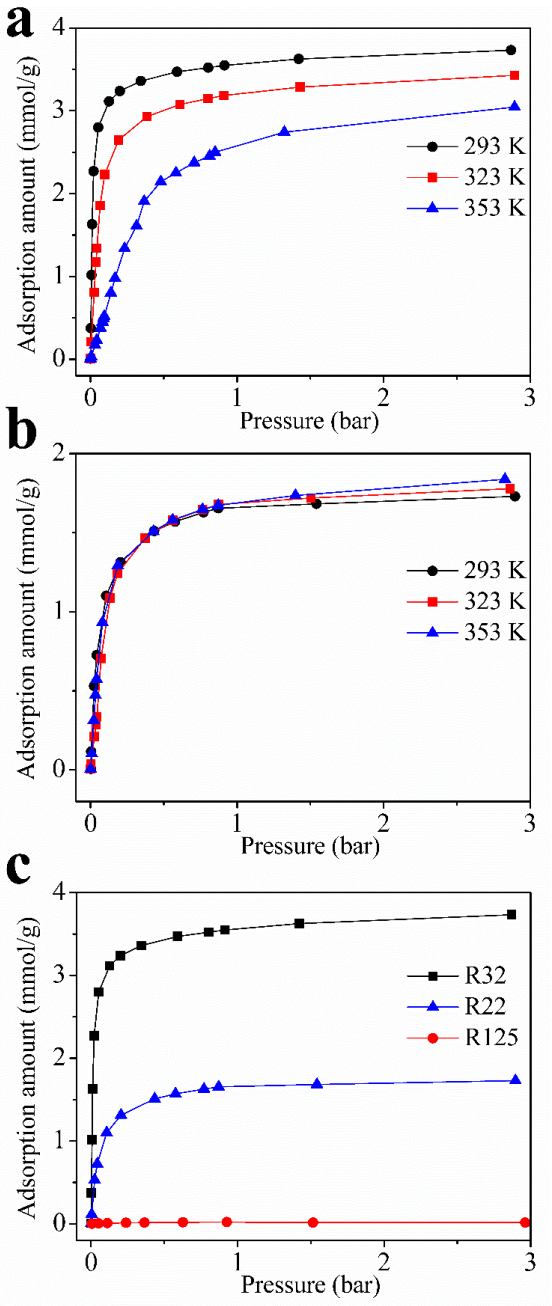

Figure 4-2 (a) R32 and (b) R22 adsorption in 4A zeolite at 293 K, 323 K and 353 K. (c) Isotherm comparison for R32, R22 and R125 at 293 K.

All three gases could be readily adsorbed onto 5A zeolite, indicating larger pore size of 5A zeolite compared to the gas molecules. Adsorption capacities of R32, R22 and R125 on 5A zeolite at 1 bar and 293 K reach 4.6, 2.8, and 2.7 mmol/g, respectively. These adsorption capacities are higher than those on 4A zeolite under similar conditions. 4A zeolite is the sodium exchanged form of the type A zeolite in which Na^+ cations are preferably located in two sites:

(1) near the 8- membered ring and (2) near the 6- membered ring windows. When Na^+ cations are exchanged with Ca^{2+} cations to form 5A zeolite, all Na^+ cations will be removed from the 8-membered ring window, while Ca^{2+} and remaining Na^+ cations will occupy the sites near the 6-membered ring window, which increases adsorption capacity of all tested gases in 5A over 4A zeolite, due to change of accessibility of active sites on the zeolite pore surface.

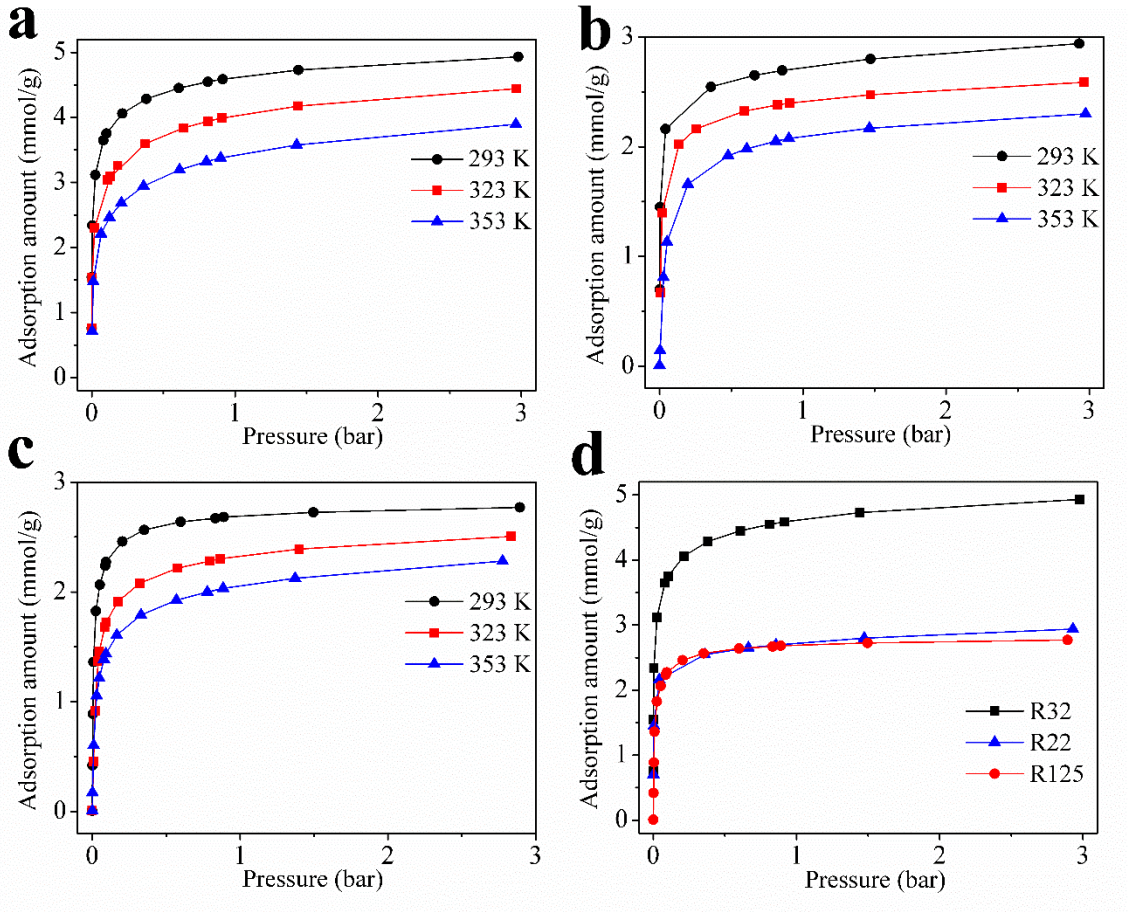

Figure 4-3 (a) R32, (b) R22, and (c) R125 adsorption in 5A zeolite measured at 293 K, 323 K and 353 K. (d) Isotherm comparison for R32, R22 and R125 at 293 K.

4.3.2 Diffusion of R32, R22 and R125 in zeolite 4A

IsorbHP high pressure gas adsorption analyzer uses the volumetric method to determine the gas uptake at different equilibrium pressures. During the analysis, the analysis cell is dosed with known amount of adsorbate and let the adsorbent to adsorb it. The instrument monitors the change of pressure inside the analysis cell and once the pressure variation within the cell reach

the equilibrium criteria, it calculates the gas uptake amount at that final pressure (equilibrium pressure) inside the cell. The general characteristic of the pressure variation inside the cell is, soon after dosing the cell with gas, the uptake rate is quite high due to the higher sorption of gas by the adsorbent. But uptake rate drops quickly and finally maintain very slow uptake rate until it reaches the equilibrium criteria. Significant diffusion limitations exist in microporous adsorbents such as 4A during gas adsorption due to the more comparative size of fluorocarbon molecules and pore size of 4A zeolite.

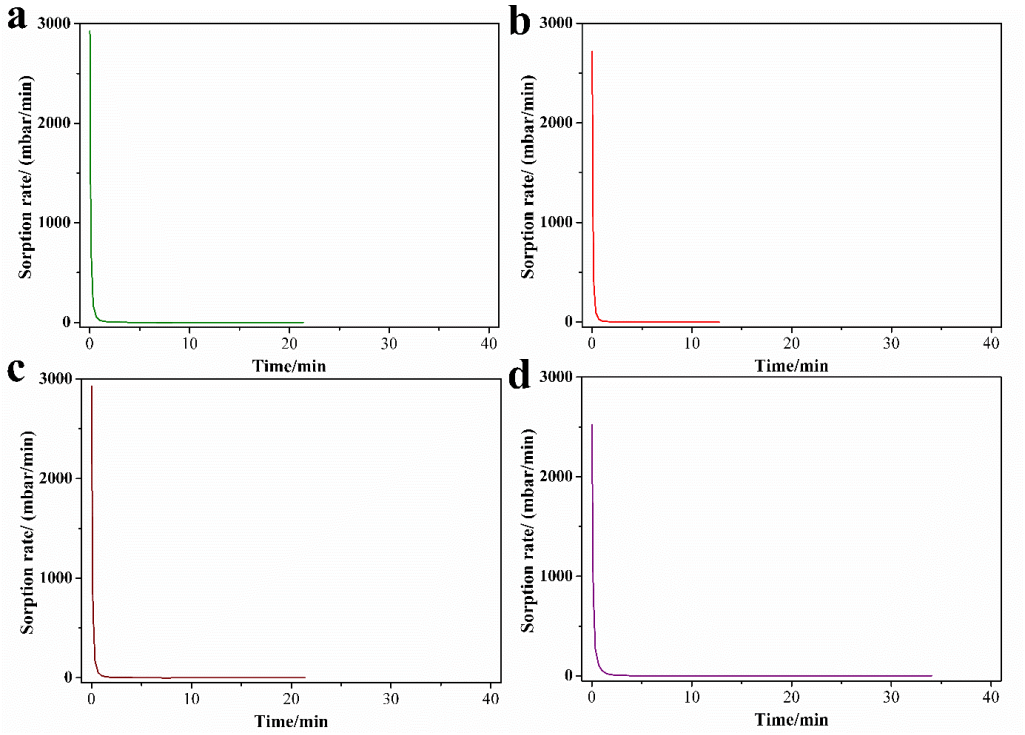

Figure 4-4 Variation of R32 sorption rate with time at equilibrium pressure of (a) 0.002 bar, (b)0.0067 bar, (c) 0.011 bar, and (d) 0.02 bar.

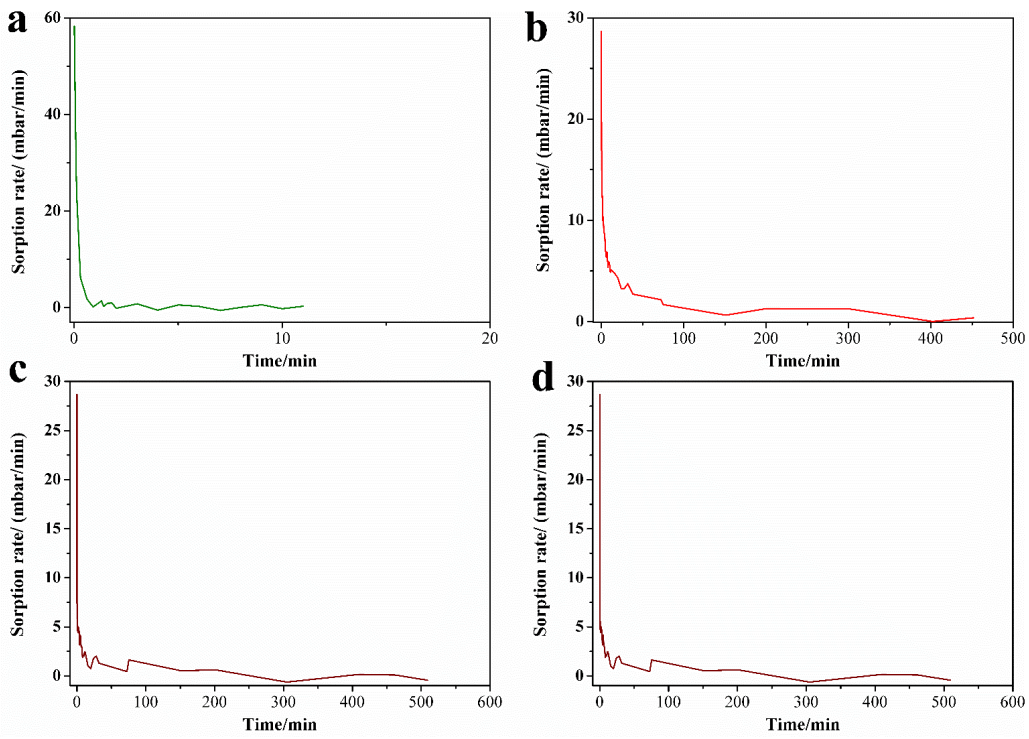

Figure 4-5 Variation of R22 sorption rate with time at equilibrium pressure of (a) 0.0015 bar, (b) 0.025 bar, (c) 0.042 bar, and (d) 0.1 bar.

By comparing the kinetics of adsorption, it is interesting to note that the sorption rate of R22 onto 4A zeolite is much slower compared to that of R32. Figure 4-4 and 4-5 show the uptake rates of R22 and R32 in 4A zeolite at low pressure region. For R32, almost 98% of adsorption at an equilibrium pressure takes place within 2-5 minutes while it takes 50-80 min for R22. These differences of uptake rates might create potential kinetic based separation for R22 and R32 using 4A zeolite.

Figure 4-6 shows the time taken by R22 and R32 to reach equilibrium adsorption up to 1 bar. It is very clear that R22 takes more time as much as 100 times of the R32 to reach 1.6 mmol/g at 1 bar.

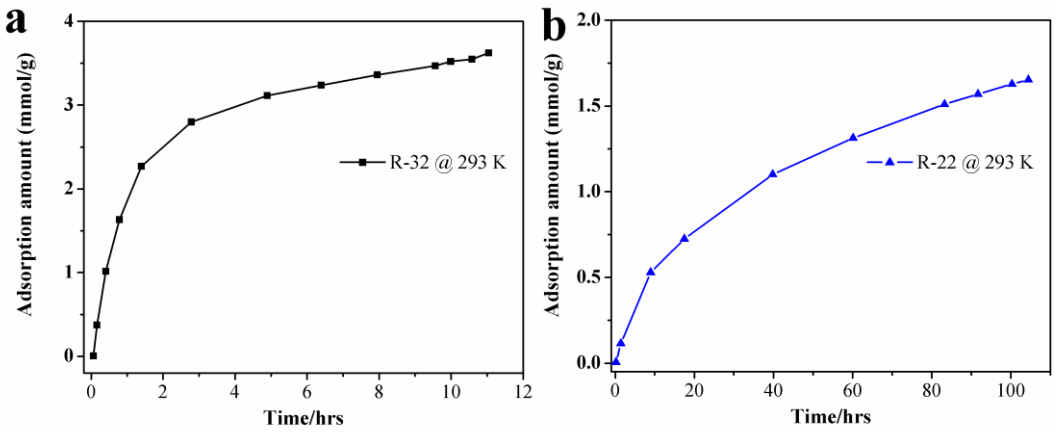

Figure 4-6 Time taken to reach equilibrium adsorption at 293 K and 1 bar (a) R- 32, (b) R22.

4.3.3 Dynamic column breakthrough experiments

4.3.3.1 Separate R32 from R125

The column breakthrough experiments to separate R32 from R125 were carried out using 32 g of 4A zeolite at atmospheric pressure and 298 K. Instead of mixing R32 and R125 for the preparation of desired mixture, R-410A blended from R32 and R125 (each component 50% by weight) was used. Figure 4-7a shows the breakthrough behavior of R32 and R125 over 4A zeolite. Sharp breakthrough front of R125 was observed immediately followed by R32 after 32 min, indicating the size selective adsorption of 4A zeolite. The R125 obtained after breakthrough showed no detectable R32 and the concentration of R32 in the adsorbed phase was always greater than 99.7%. Therefore, 4A molecular sieve zeolite can be readily used for the separation of R32 from R125 to meet the industrial standards.

4.3.3.2 Separate R32 from R22

The breakthrough results for the mixture of R32 and R22 (70% R22 and 30% R32) over 4A zeolite are displayed in Figure 4-7b, which shows the concentration ratio of the outlet to inlet gas against the contact time at atmospheric pressure and 298 K. R22 starts to breakthrough almost immediately after starting the experiment with very sharp breakthrough front, followed by breakthrough of R32 after 20 min. This observation indicates that R32 was adsorbed by the

4A zeolite while the adsorption of R22 is insignificant within the short amount of adsorption time. Although both R32 and R22 can be adsorbed on 4A zeolite based on the pure gas adsorption measurements, the much lower uptake rate of R22 leads to its immediate breakthrough. This fact can be further explained by comparing the time taken for each gas to reach the equilibrium adsorption at 1 bar. As shown in Figure 4-6, to reach 1.6 mmol/g at equilibrium pressure of 1 bar, R22 takes about 104 hrs while R32 takes only about 11 hrs to reach 3.5

mmol/g under same equilibrium pressure. Therefore, it is clear that the uptake of R22 by 4A zeolite is much slower compared to R32. To identify the adsorbed phase composition, desorption was carried out by placing the column in a heated furnace at 473 K. R32 in the adsorbed phase was around 74% while it was 30% in the feed mixture. With these results, it can be concluded that, R22 also adsorbed by 4A zeolite during breakthrough experiments but because of the much lower uptake rate compared to R32, immediate breakthrough of R22 has resulted.

4.3.3.3 Separate R22 from R125

By comparing the breakthrough profiles of R22 and R32 on 4A zeolite, it could be seen clearly that R22 was detected immediately after starting of the experiment, even though R22 could still be adsorbed on 4A zeolite. Thus, to achieve successful separation of R22 from R125, proper design of experimental conditions such as adsorbent amount, operating temperature and flow rate have to be considered. Increasing amount of adsorbent, operating temperature or decreasing feed flow rate can increase the residence time for adsorption. In our experiment, we used a combination of slower feed flow rate (10 cm^3/min) and higher operating temperature (323 K) while maintaining the adsorbent amount, which obviously delayed the breakthrough of R22 as shown in Figure 4-7c. Desorption by heating the column at 473 K with He purging released adsorbed R22 with a composition of more than 99.6%, while it was only 41.5% in the feed gas mixture.

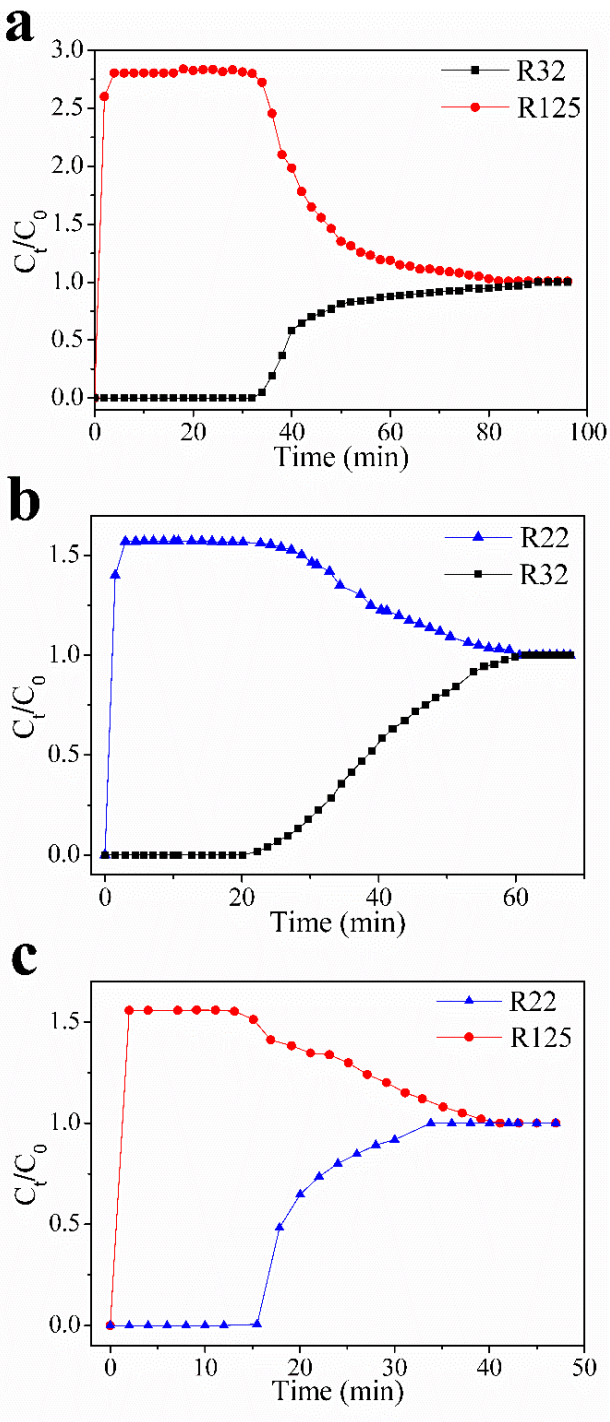

Figure 4-7 Dynamic gas breakthrough profiles of (a) R32/R125 (b) R22/R32 separation measured under atmospheric pressure and 298 K (c) R22/R125 measured under atmospheric pressure and 323 K.

4.3.3.4 Separation of mixture containing R32, R22 and R125

To demonstrate the applicability of our proposed method for the separation of R32, R22 and R125 mixtures in industrial scale, the adsorption reactor system was upgraded with larger

column in which 440 g of 4A zeolite can be packed. Mixture of R32, R22 and R125 with composition of 38.6%, 38.5% and 22.9% respectively were sent through the column with a flow rate of 300 cm^3/min at 298 K and atmospheric pressure. As shown in Figure 4-8a, R125 was breakthrough immediately with a very sharp front followed by R22 and R32 at 12 and 24 min respectively. By optimizing the operating conditions, especially the flow rate, our method should be applicable to make pure R22, R32 or R125 from their mixtures. As shown in Figure 4-8b, under similar conditions but simply by decreasing the mixture feed flow rate, the breakthrough time difference between each gas can be regulated.

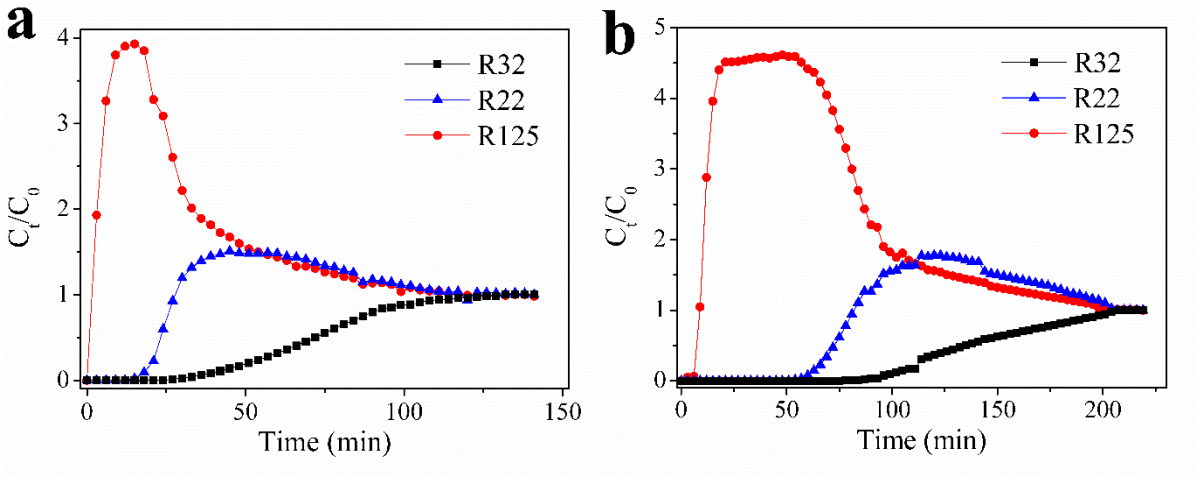

Figure 4-8 Dynamic breakthrough profiles for a gas mixture containing R32, R22 and R125 at a feed flow rate of (a) 300 cm^3/min (b) 180 cm^3/min

4.3.4 Heat of adsorption

It is interesting to notice that all isotherms measured on 4A and 5A zeolite are not fully reversible indicating the strong adsorbate-adsorbent interaction. Isosteric heat of adsorption was estimated by fitting the isotherms measured at 293 K, 323 K and 353 K to the Clausius-Clapeyron equation in the software (Figure 4-9). The heat of adsorption for R32 (46.4 kJ/mol) on 5A zeolite is lower than that for R22 (48.5 kJ/mol). The heat of adsorption of R32 for 4A (47.2 kJ/mol) was slightly higher than that for 5A. But, both of which are much higher than the reported values on MIL-101 metal organic frameworks indicating the much stronger attraction of these fluorocarbons on the polar zeolite surface.[9]

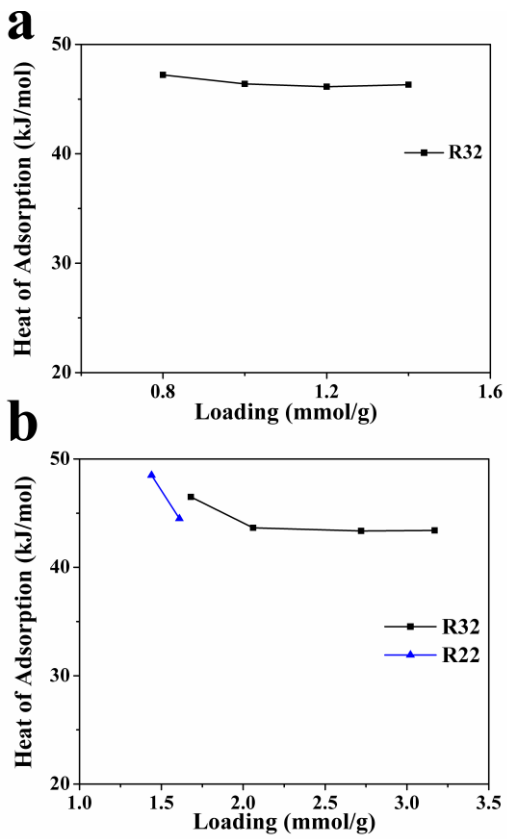

Figure 4-9 Isosteric heats of adsorption (a) R32 on 4A (b) R32 and R22 on 5A

4.4 Conclusions

In summary, we proposed a facile strategy to successfully separate R32, R22 and R125 from their mixtures using 4A zeolite under ambient conditions. The steric effect is responsible for the separation of R32 and R22 from R125, while lower uptake rate of R22 as compared to R32 facilitates the separation of R22 from R32. Our proposed method should attract immediate attention from industry as an alternative strategy to recycle fluorocarbon mixtures.

Chapter 5

Adsorption Separation of R134a, R125 and R143a Fluorocarbon Blends using Zeolite 13X and Surface Modified Zeolite 5A.

Overview: This chapter reports a facile method for the adsorption separation of fluorocarbon blends containing tetrafluoroethane (R134a), pentafluoroethane (R125) and trifluoroethane (R143a) refrigerants into their pure components using commercial zeolite 13X and pore size modified 5A zeolite under ambient condition. Based on the measured R134a, R125 and R143a pure gas equilibrium adsorption isotherms, the adsorption capacity varies in the order of R134a > R143a > R125 on zeolite 13X. The mixed gas breakthrough experiments reveal that zeolite 13X selectively adsorbs R134a over R125 and R143a. By running two adsorption cycles, it is possible to obtain R134a with ultrahigh purity. Furthermore, through chemical modification of tetraethyl orthosilicate (TEOS), the pore size of 5A zeolite could be successfully narrowed to the extent to just adsorb R125 while excluding R143a. The modified 5A zeolite was utilized to separate refrigerant mixtures containing R125 and R143a into their pure components.

5.1 Introduction

Because of the industrially important applications of fluorocarbons, they have been studied on several types of adsorbent systems.[23, 111, 112, 113, 114] However, separation of different fluorocarbon blends that contain R134a, R125 and R143a into their pure components has never been reported in the literature. In the previous chapter,[91] we have successfully demonstrated the separation of low GWP refrigerant R32 from a mixture of R32, R22 and R125 with purity greater than 99.5% using 4A molecular sieve zeolite. However, the separation of fluorocarbon mixtures that contain R134a, R125 and R143a into their pure components is much more challenging due to unavailability of commercial adsorbent with matching pore size for the size-selective separation.

Herein, we report a facile industrially applicable method to separate fluorocarbon mixtures containing R134a, R125 and R143a (molecular structures of these gases are shown in Figure 5-1) into their pure components using commercial zeolite 13X and surface modified 5A zeolite. The reason to choose zeolite 13X was based on the previously reported NMR and molecular simulation studies on the hydrofluorocarbon binding characteristics to NaX and NaY zeolite.[115, 116] The results suggested that R134a showed higher binding affinity to NaX zeolite than R125. Therefore, we expected 13X molecular sieve zeolite as a potential adsorbent candidate for the separation of R134a from R125 and R143a. Furthermore, based on our measured pure gas adsorption isotherms of R134a, R125 and R143a on 4A and 5A zeolite, it was found that none of these gases could be adsorbed by 4A zeolite while all of them were adsorbed by 5A zeolite. More importantly, it was noticed that the uptake rate of R143a by 5A zeolite is considerably slower than that of the other two gases, suggesting the larger molecular size of R143a. Therefore, we proposed to chemically modify the 5A zeolite to reduce its pore size,[117, 118, 119] so that the modified 5A zeolite could be used to separate R125 from R143a based on a size-selective separation.

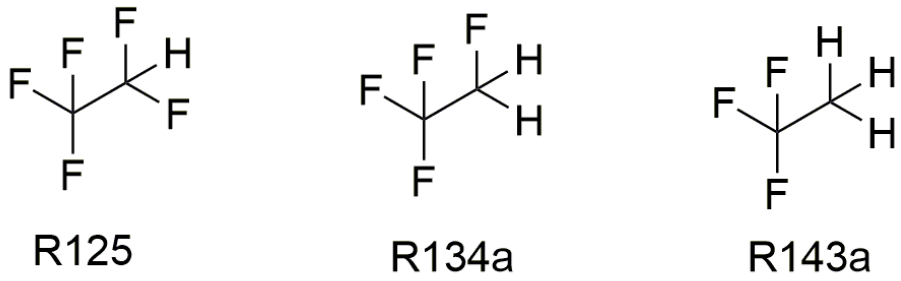

Figure 5-1 Molecular structures of R125, R134a and R143a

5.2 Experimental Section

5.2.1 Materials and methods

5A and 13X molecular sieve zeolites were purchased from Sigma-Aldrich in the form of powders and cylindrical extrudes, respectively. Tetraethyl orthosilicate (TEOS) and toluene

were also purchased from Sigma-Aldrich and toluene was further purified over 3A molecular sieve zeolite. R125, R134a and R143a were obtained from Lie Ku Pte Ltd Singapore. For isotherm measurements, all gases were further dried over 3A molecular sieve zeolite.

5.2.2 Pore size modification of 5A zeolite

TEOS was applied to modify 5A zeolite to reduce its pore size according to a reported procedure.[120] In a typical experiment, 5 g of activated 5A zeolite powder was dispersed in 40 ml of dry toluene, followed by drop wisely adding calculated amount of TEOS under stirring. Afterwards, the mixture was sealed and stirred at room temperature for 5 h. Finally, the product was harvested by centrifugation and subsequently calcined at 600 ˚C for 4 h to obtain pore size modified 5A zeolite.

5.2.3 Characterization of pore size modified 5A zeolite

X-ray diffraction (XRD) was carried out on a D2 phaser X-ray diffractometer (Bruker) equipped with LynxEye detector. Change of pore structure and surface area upon pore size modification was evaluated using N_2 adsorption isotherms measured at 77 K by Quantrachrom AS6 pore size and surface area analyzer. Prior to the analysis, about 100 mg of the sample was activated by heating them at 423 K under high vacuum for 12 h. For the surface area and micropore volume analysis, Brunauer−Emmett−Teller (BET) and t-plot method were used, respectively. Thermogravimetric analysis (TGA) was performed on bare and surface modified 5A zeolite on a Pyris diamond TGA at a heating rate of 10 K/min up to 973 K with flow of air.

5.3 Results and Discussion

5.3.1 Separation of R134a/R 125 and R134a/R143a using commercial zeolite 13X

5.3.1.1 Pure gas adsorption isotherms

Pure gas equilibrium adsorption isotherms were measured on zeolite 13X at 293 K, 313 K, and 333 K as shown in Figure 5-2. Table 5-1 lists the physical and textural properties of the used

zeolite 13X. All isotherms exhibit type I adsorption, which is the characteristic for microporous adsorbents.

Table 5-1 Characteristics of zeolite 13X

Zeolite 13X	
Size of the pellet	3 mm in diameter, 6 mm in length
Surface area[a]	588 m^2/g
Pore volume[b]	0.306 cc/g

[a]Calculated based on BET method
[b]Calculated based on BJH method

The adsorption capacity varies according to R134a > R143a > R125 over the tested pressure and temperature ranges. At 100 kPa and 293 K, the measured adsorption capacities of R134a, R143a and R125 reach 2.7, 2.4, and 2.3 mmol/g, respectively. Savitz et al reported an adsorption capacity of 5.5 mmol/g at 373 K and 60 kPa for R134a on NaX zeolite powder[112]. Our measured adsorption capacity of R134a on zeolite 13X is a little bit lower than the reported value. In our measurements, zeolite 13X was used in the form of pellets, which contains about 20-30 wt% of binders. Additionally, lower degassing temperature of 423 K to activate zeolite was used as compared to the reported study (623 – 673 K), which collectively results in a lower measured adsorption capacity in our experiments.

A dual-site Langmuir-Freundlich equation (Eq 1) was employed to describe the experimental adsorption isotherms over the tested pressure and temperature ranges as shown below:[121]

$$q = \frac{q_{sat,1} b_1 p^{1/n_1}}{1 + b_1 p^{1/n_1}} + \frac{q_{sat,2} b_2 p^{1/n_2}}{1 + b_2 p^{1/n_2}} \qquad \text{Eq 1}$$

where q (mmol/g) is the total adsorption quantity of a single gas and p (kPa) is the partial pressure, $q_{sat,1}$ and $q_{sat,2}$ are the saturated loading for site 1 and 2. b_1, b_2 and n_1, n_2 are Langmuir and Freundlich parameters for site 1 and 2, respectively. All our experimental isotherms can be

well described by the dual-site Langmuir-Freundlich model with a R^2 value greater than 0.99. The fitted isotherms and parameters are presented in Table 5-2.

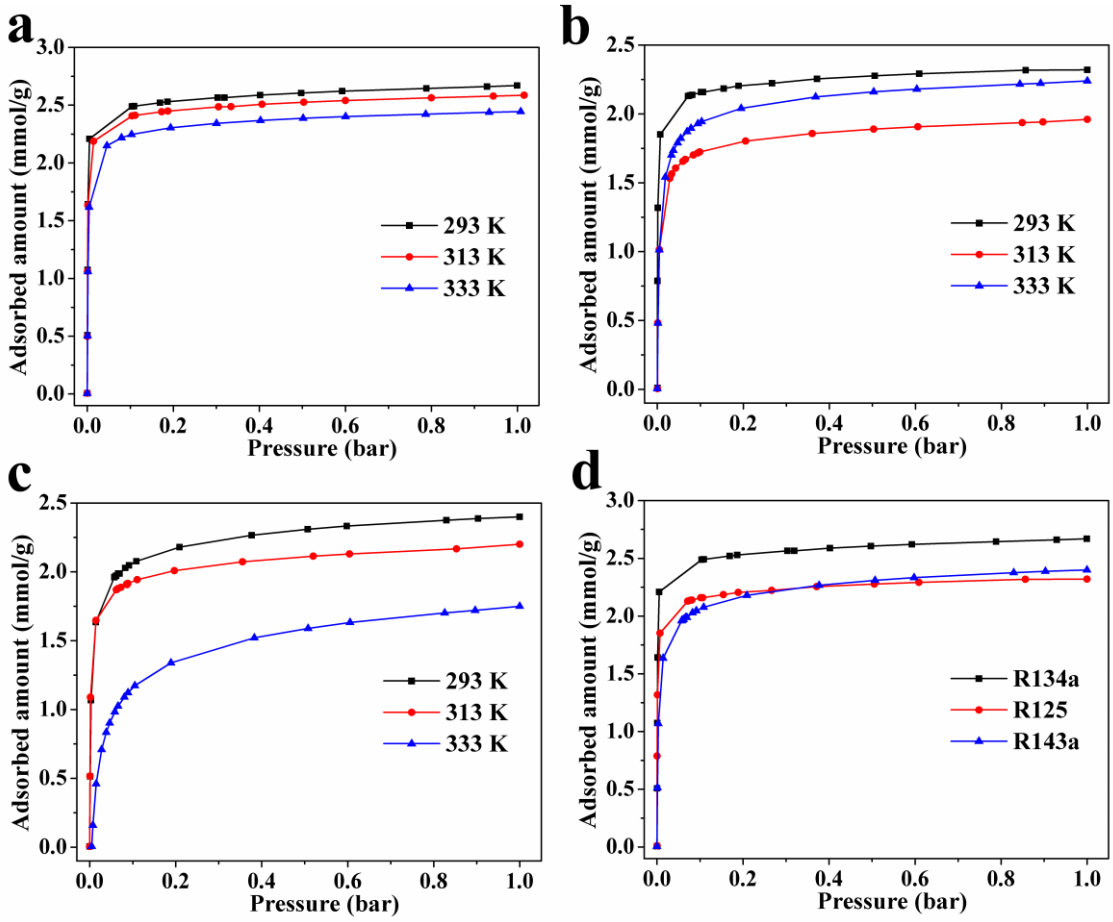

Figure 5-2 Adsorption isotherms on zeolite 13X for (a) R134a, (b) R125, and (c) R143a. (d) Isotherm comparison at 293 K.

Based on pure gas adsorption isotherms, adsorption selectivity for R134a over R125 and R143a was revealed using Ideal Adsorption Solution Theory (IAST)(Figure 5.3).[103] The adsorption selectivity, $S_{a,b}$, is defined by the following equation (Eq. 2) :

$$S_{a,b} = \frac{X_a/Y_a}{X_b/Y_b} \qquad \text{Eq 2}$$

where X_a, Y_a and X_b, Y_b are mole fraction of a and b in the adsorbed phase and bulk phase, respectively. We used the isorbHP software to calculate the isosteric heat of adsorption by fitting

the measured adsorption data (at 293 K, 313 K and 333 K) to the Clausius-Clapeyron equation (Eq. 3):

$$\Delta H°_{ad} = R \left[\frac{\partial \ln P}{\partial(\frac{1}{T})}\right]_{\theta} \qquad \text{Eq 3}$$

where ΔH°_{ad} is the heat of adsorption, R is the universal gas constant, θ is the fraction of the adsorbed sites at a pressure P and temperature T.

Table 5-2 Dual-site Langmuir-Freundlich parameters for the adsorption of R134a, R125 and R143a on zeolite 13X.

	R134a			**R125**			**R143a**		
	293 K	313 K	333 K	293 K	313 K	333 K	293 K	313 K	333 K
$\mathbf{q_{sat,1}}$	2.253	1.946	0.7732	1.62	0.8835	0.6818	1.292	0.8662	1.152
$\mathbf{q_{sat,2}}$	0.6182	0.7744	1.799	0.746	1.518	1.35	1.405	1.458	0.7403
$\mathbf{b_1}$	40.04	47.47	0.4126	118.3	0.2853	0.2629	0.3515	0.2947	0.05076
$\mathbf{b_2}$	0.2	0.4338	11.51	0.5659	2.984	6.167	5.938	22.4	0.3554
$\mathbf{n_1}$	0.733	0.7439	1.886	0.6584	1.693	1.416	2.051	1.635	0.9607
$\mathbf{n_2}$	2.051	2.002	0.8348	1.513	0.9769	0.8542	0.86	0.7801	0.4346
$\mathbf{R^2}$	0.999	0.9999	0.9999	0.9982	0.9999	0.9985	0.9932	0.9996	0.9984

The calculated isosteric heat of adsorption for R134a, R125 and R143a at a loading of 0.002 mmol/g is 42.7, 40.8, and 42.6 kJ/mol, respectively, indicating strong adsorption of R134a, R125 and R143a into the zeolite 13X framework.

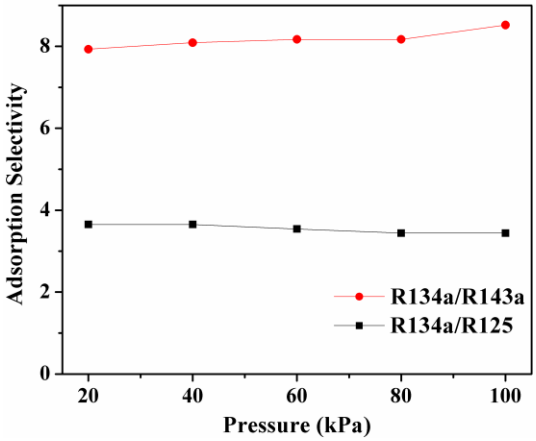

Figure 5-3 Adsorption selectivity for R134a/R125 (50 % each) and R134a/R143a (50% each) estimated using IAST at 293 K.

5.3.1.2 Dynamic column breakthrough experiments

To further confirm the selective adsorption of R134a over R125 and R143a, dynamic column breakthrough experiments were conducted. We used binary fluorocarbon mixtures containing R134a/R125 and R134a/R143a for the column breakthrough experiments. The gas mixture was fed into the adsorption column filled with zeolite 13X at a flow rate of 20 cm^3/min. Figure 5-4a and b display the gas breakthrough profiles.

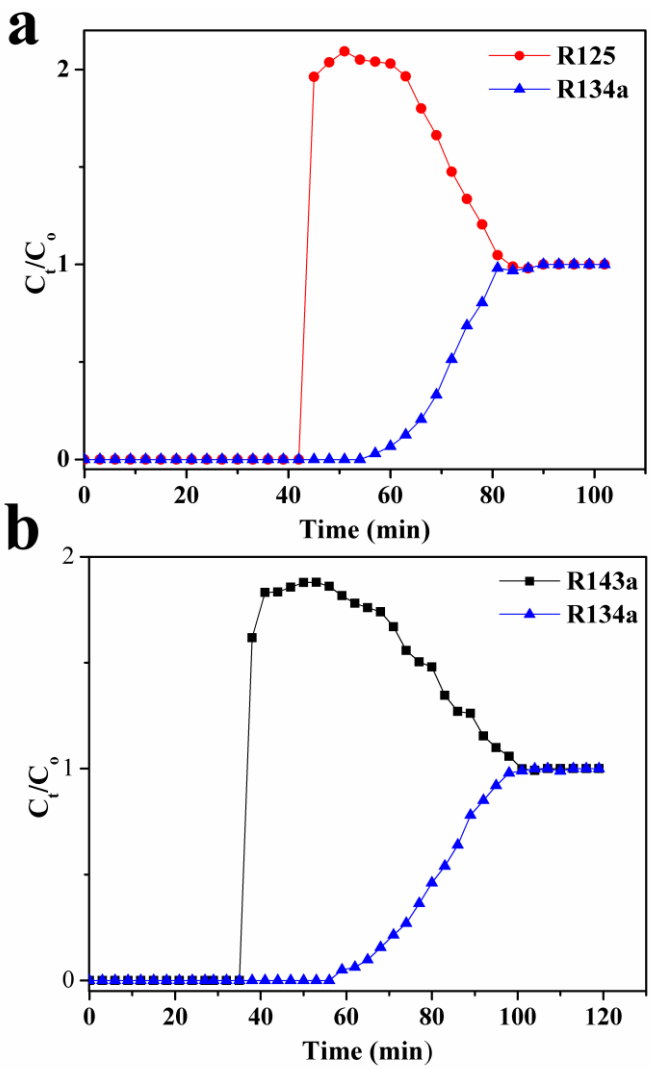

Figure 5-4 Binary gas mixture breakthrough curves for fluorocarbon mixtures containing (a) 50% R125 and 50% R134a, and (b) 50% R143a and 50% R134a.

For the mixture containing R134a and R125, breakthrough of R125 at 45 min was observed followed by R134a after 70 min, while for the R134a and R143a mixture, breakthrough of R143a at 38 min was noticed followed by R134a at 59 min. After gas breakthrough, the adsorbent bed was purged with He to remove the residual gases left in the void space in the column. Subsequently, the adsorbed gases were desorbed at 423 K and the composition was analyzed by gas chromatography. Based on that, we re-calculated the adsorption selectivity for the R134a/R125 and R134a/R143a binary mixtures, which gives a value of 4.96 and 7.88, respectively, close to the one calculated from IAST.

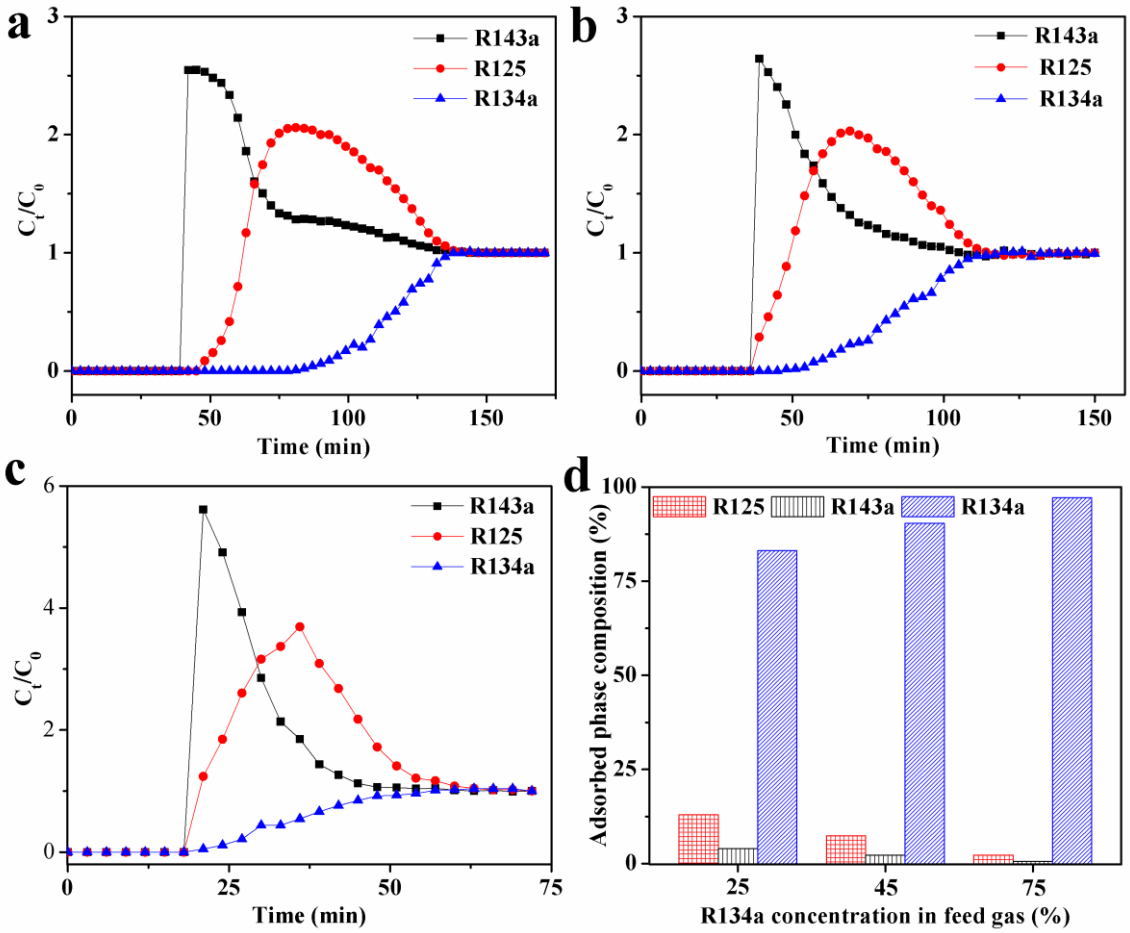

Figure 5-5 Dynamic gas breakthrough profiles of fluorocarbon blends containing (a) 25% R134a, 44% R143a, and 31% R125; (b) 45% R134a, 34% R143a, and 21% R125; (c) 75% R134a, 15% R143a, and 10% R125 measured under atmospheric pressure and 298 K, and (d)

Following, we conducted ternary fluorocarbon gas mixture breakthough experiments to evaluate the applicability of zeolite 13X to separate R134a from a mixture containing R125, R134a and R143a. The composition of R134a in the blend was varied to investigate the effect of concentration on the adsorbed phase of R134a to determine the number of adsorption cycles required to obtain pure R134a.The column temperature and adsorbent amount were maintained at 298 K and 14 g throughout the experiments and the gas mixture was fed into the column with a flow rate of 20 cm^3/min. As shown in Figure 5-5 at the beginning of the experiments, all three gases could be adsorbed on zeolite 13X. At 25% of R134a in the mixture, after around 40 min, breakthrough of R125 and R143a were observed followed by R134a after 80 min. If the concentration of R134a in the feed gas mixture was increased, similar breakthrough trend was

observed but with much quicker breakthrough of R134a. As summarized in Figure 5.5d, with increase in the concentration of R134a in the feed gas mixture, the composition of R134a in the adsorbed gas also increases. At 25% in the feed gas, the adsorbed phase concentration of R134a reaches as high as 83% while it increases to 90 and 97% when the composition of R134a in the feed gas increases to 45 and 75%, respectively. Based on these dynamic gas breakthrough results, it is clear to see that zeolite 13X is selective towards R134a instead of R125 and R143a. The better selectivity of R134a with zeolite 13X can be explained by its higher boiling point (boiling point of R134a is 246.9 K, while it is 225.8 K and 224.9 K for R143a and R125, respectively), which indicates stronger gas-gas interaction and thus it is more likely to have stronger host-gas interaction as well. To explain the preferential adsorption of R134a over the other two gases, different interactions of fluorocarbon molecules with zeolite 13X need to be carefully considered. zeolite 13X provides both acidic and basic adsorption sites for the adsorption of fluorocarbons. The highly electronegative -F groups in fluorocarbons are more attracted to the extraframework Na cations to form Na-F interactions while framework oxygen sites attract the hydrogen containing $-CF_2H$ and $-CFH_2$ groups to form hydrogen bonds. Both R134a and R125 molecules contain $-CF_3$ group at one side while at the other side of the molecules, they have $-CFH_2$ and $-CF_2H$ groups. A previous NMR and molecular simulation study indicates that, if the end group of a molecule contains higher numbers of hydrogen atoms, it should show stronger interaction with the faujasite type framework.[115] Furthermore, the presence of strongly electronegative F atoms on the same carbon tends also to increase the acidity of H atoms, which can facilitate the formation of hydrogen bonds with the oxygen sites in the zeolite.[113, 116] These findings explained our experimental results of selective adsorption of R134a over R125 on zeolite 13X. This hypothesis can be further used to explain the earlier breakthrough of R143a as well. As can be noticed from the ternary gas breakthrough results, R143a elutes from the column even before R125. Similar to R125 and R134a, R143a also has the $-CF_3$ group in its molecular structure, but the other end contains the less polar $-CH_3$ group. The interaction of this less polar $-CH_3$ group with the zeolite surface is much weaker compared

to the -CHF_2 and -CH_2F groups in R125 and R134a, which leads to earlier breakthough of R143a as compared to R125 and R134a.

5.3.2 Separation of R125/R143a using pore size modified 5A zeolite

To further separate the remaining R125 and R143a mixture into their pure components, we examined 5A zeolite as a potential adsorbent. Figure 5-6a displays the pure gas adsorption isotherms, from which the adsorption capacity of R125 on 5A zeolite is determined to be 2.12 mmol/g while it is only 1.55 mmol/g for R143a. Figure 5.6b compares the uptake rate of R125 and R143a on 5A zeolite at gas pressure of 300 kPa. R125 reached its equilibrium adsorption within 47 min while it took around 430 min for R143a, clearly indicating slower uptake rate of R143a.

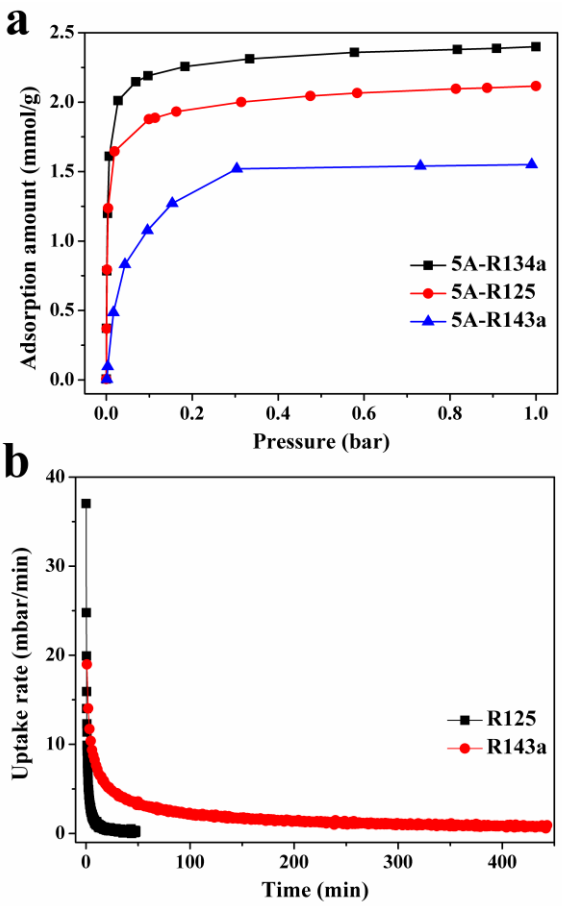

Figure 5-6 (a) Pure gas adsorption isotherms of R125, R143a and R134a on 5A zeolite at 293 K, and (b) uptake rate of R125 and R143a on 5A zeolite.

The kinetics of adsorption corresponding to the isotherms of R143a and R125 on 5A zeolite are shown in Figure 5-7 & 5-8, respectively. When comparing the time taken for the completion of these isotherms, it was around 12 hours for R125 (Figure 5-7) while R143a took around 5-6 days (Figure 5-8). The slower uptake rate indicates slower diffusion of R143a in 5A zeolite probably due to its larger molecular size as compared to R125. Since R125 has higher numbers of F atoms compared to R143a, it is questionable about the molecular sizes of these two gases. Unfortunately, we were unable to find reliable literatures on their molecular sizes. Though R125 has higher numbers of F atoms, the information regarding their spatial distribution and possible distortion of the molecular structure due to the polarization effects are still unknown. Therefore, with our experimental findings, we suggest that R143a is more difficult to enter the 5A zeolite pore structure as compared to R125. Thus, reducing the pore size of 5A zeolite should be expected to exclude the adsorption of R143a while at the same time still allow the adsorption of R125.

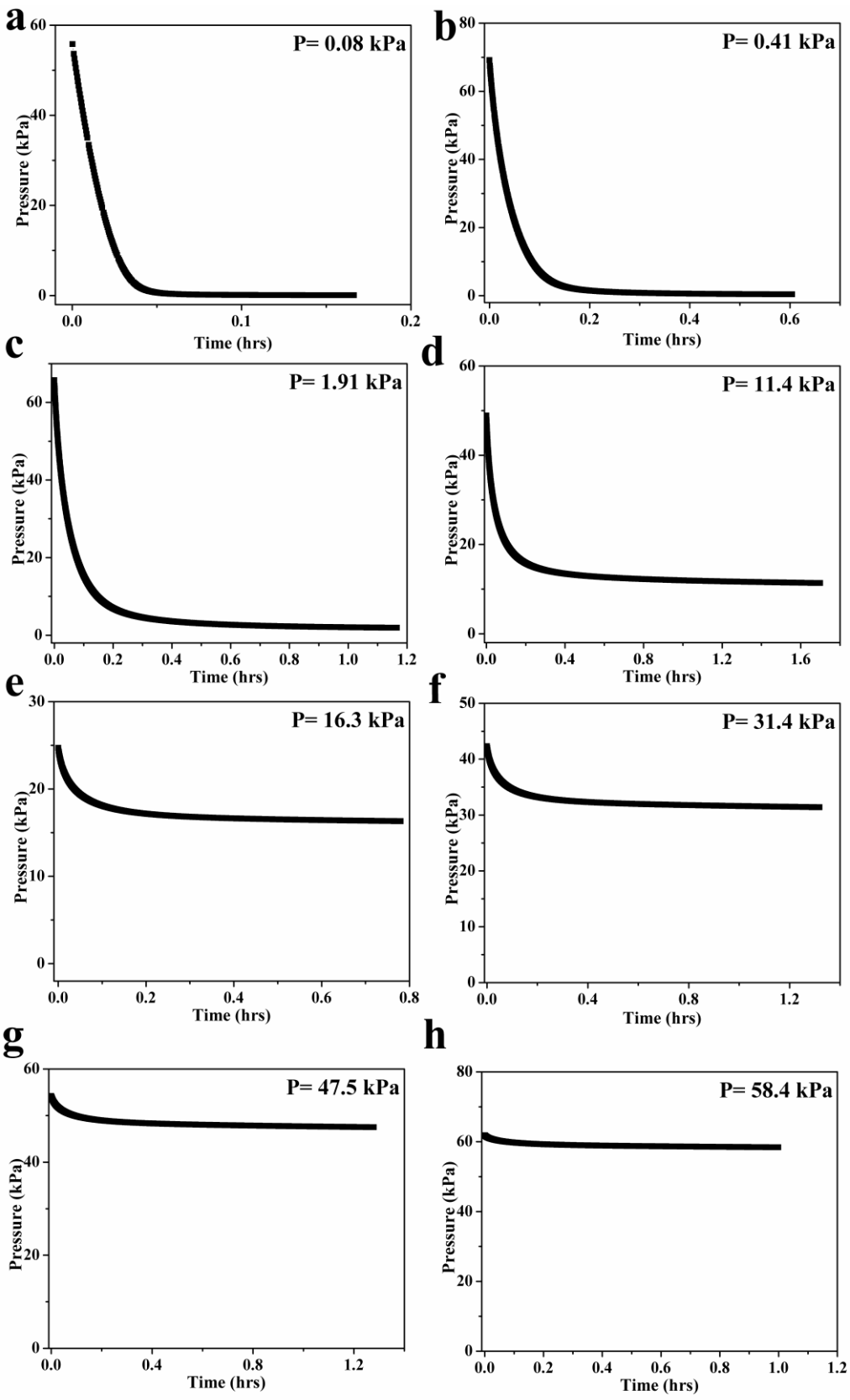

Figure 5-7 Kinetics of R125 adsorption on 5A zeolite: a-h corresponding to points 2,4,5,6,8,9-11 in the adsorption isotherm in Figure 5-6a.

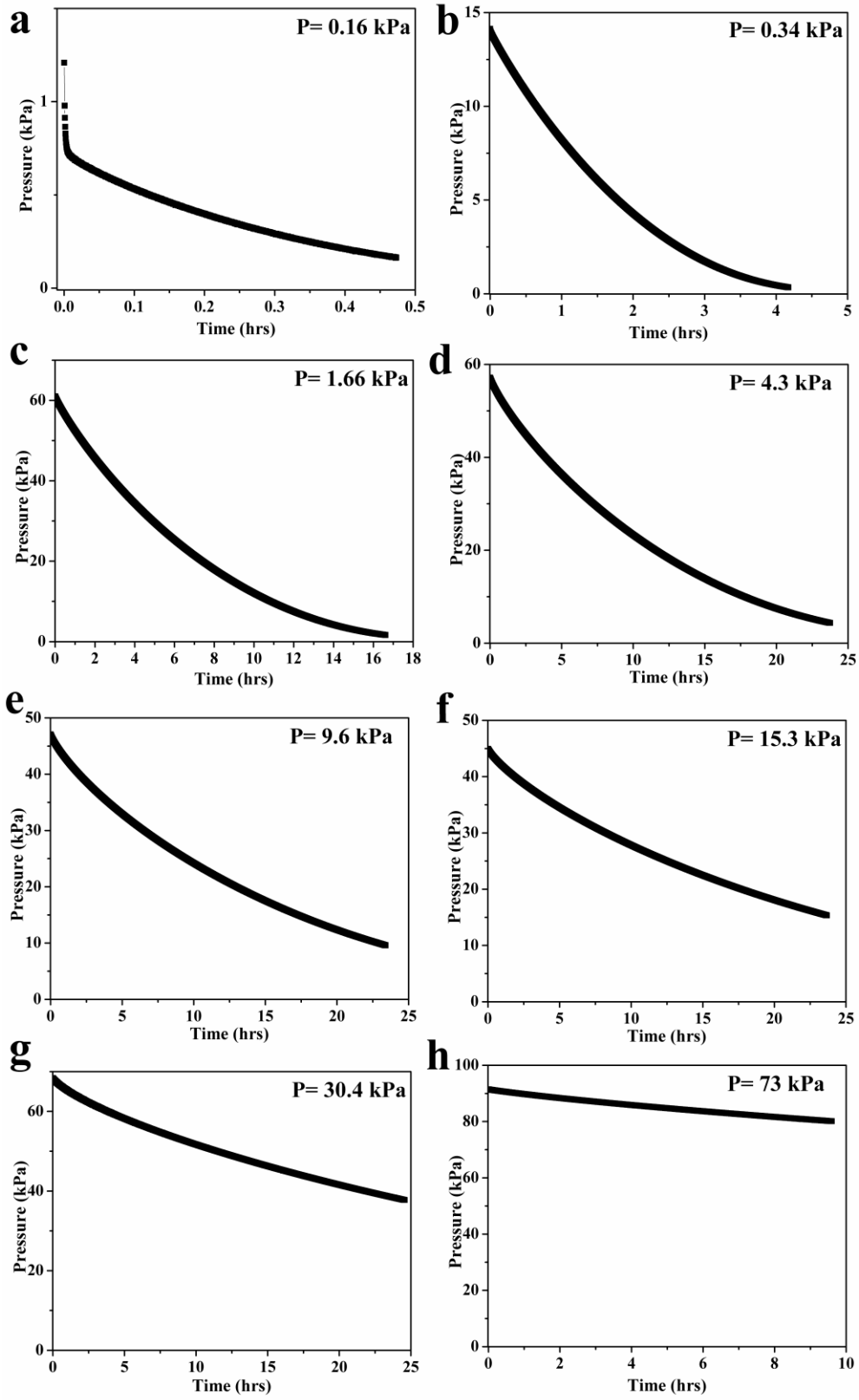

Figure 5-8 Kinetics of R143a adsorption on 5A zeolite: a-h corresponding to points 1-8 in the adsorption isotherm in Figure 5-6a.

Silylation through chemical vapor deposition (CVD) or chemical liquid deposition (CLD) are typical methods to modify the pore size of zeolites,[122, 123, 124, 125, 126] among which, CLD method has attracted much attention because of its easy applicability in the industrial scale.[127, 128] By selecting proper silylation agent (e.g., TEOS), the pore openings on the external surface of zeolite can be engineered without affecting the internal pore structure and internal surface properties. The degree of surface modification of 5A zeolite using TEOS chemical liquid deposition depends both on type of zeolite and the reaction medium. When carryout the silylation of high Al content zeolites, higher degree of surface deposition of silica can be expected due to the presence of high density of acid sites in the external surface. When using non-polar solvents like hexane and toluene as the reaction medium, the degree of water present in the solvent and the zeolite have high impact on the TEOS hydrolysis and condensation rate. Because the alkoxy group of the TEOS undergoes rapid hydrolysis and condensation in an aqueous environment. Also, TEOS which is incapable of entering to the internal pore structure of 5A zeolite is converted in to smaller $Si(OH)_4$ having kinetic diameter of about 0.5 nm. Consequently, deposition of silica in the inside pore channels may be resulted with higher degree of pore narrowing.

5.3.2.1 Characterization of pore size modified 5A zeolite

5A zeolite was treated with different amounts of TEOS, denoted as 5A-X% where X% represents the percentage ratio of the silicon content in added TEOS to 5A zeolite. Figure 5-9a shows the XRD patterns of the pristine and modified 5A zeolite after calcination. 5A zeolite modified with different amounts of TEOS show identical XRD patterns as the pristine 5A zeolite, indicating that the CLD method exerts little impact on the crystallinity of modified 5A zeolite.

The measured N_2 adsorption isotherms at 77 K are displayed in Figure 5-9b. Table 5-1 summarizes the BET surface area, micropore volume and external surface area of unmodified 5A, 5A-0.06%, 5A-0.12% and 5A-0.48% zeolite. Compared to unmodified 5A zeolite, BET surface area and micropore volume of 5A-0.06%, 5A-0.12% and 5A-0.48% were decreased by

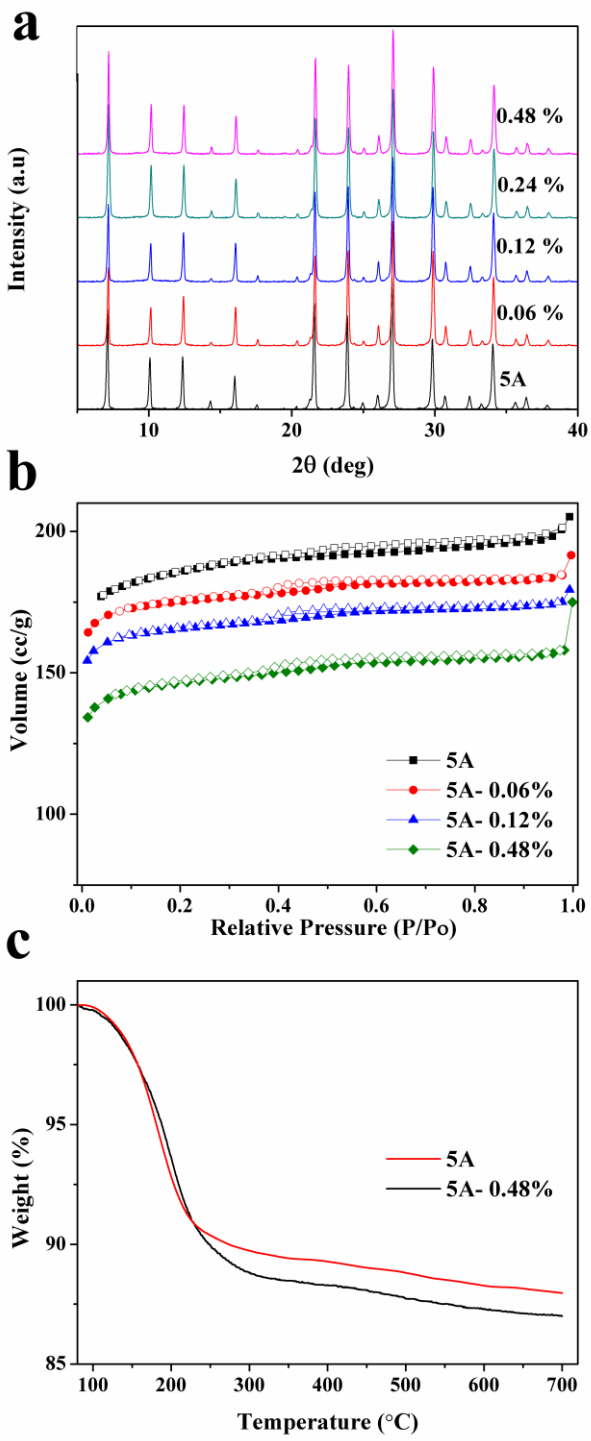

Figure 5-9 (a) XRD patterns of 5A and modified 5A zeolite. (b) N_2 adsorption isotherms measured at 77 K, and (c) TGA profiles for pristine and TEOS modified 5A zeolite.

6%, 3.6%, 11%, 7.1%, 22% and 21%, respectively. Based on these results, it can thus be concluded that the internal pore structures of modified 5A zeolite are not much affected. Most of the TEOS reaction should take place just on the external surface of 5A zeolite since the

molecular size of TEOS (8.9 Å) is much larger than the pore size of 5A zeolite.[129] Therefore, the pore narrowing is mainly occurring at the pore mouth regions on the external surface of the zeolite crystals. The TEOS modified 5A zeolite prior to calcination was further studied by TGA as shown in Figure 5-9c.

Slightly higher weight loss percentage in the temperature range from 473 to 973 K was observed in 5A-0.48% as compared to pristine 5A zeolite, which indicates successful grafting of TEOS onto the zeolite surface. Grafted organic ligands started to decompose at 473 K and further weight loss occurred with increase of temperature above 673 K due to the condensation of grafted TEOS and silanol groups.[130, 131]

5.3.2.2 Pure gas adsorption isotherms on modified 5A zeolite

Pure gas adsorption isotherms of R125 and R143a on modified 5A zeolite were measured at 293 K (Figure 5-10). As shown in Figure 10a and b, after pore size modification, the adsorption of R143a can be completely suppressed while at the same time the modified 5A zeolite still allows adsorption of R125. The adsorption capacities of R125 on 5A, 5A-0.06%, 5A-0.12%, 5A-0.24% zeolite measured at 100 kPa and 293 K reach 2.12, 1.72, 1.19, and 0.88 mmol/g, respectively. It is clear to observe that, with increase of TEOS modification concentration, the adsorption capacity of R125 decreases, which is mainly attributed to the greater degree of pore mouth narrowing and pore clogging. But the 5A-0.06% zeolite only exhibits 19% reduction of the R125 adsorption capacity, suggesting that the pore size modification by TEOS does not affect too much of the internal pore structure and internal surface property of 5A zeolite. All experimental isotherms can be well fitted by the dual-site Langmuir-Freundlich model as shown in Table 5-3.

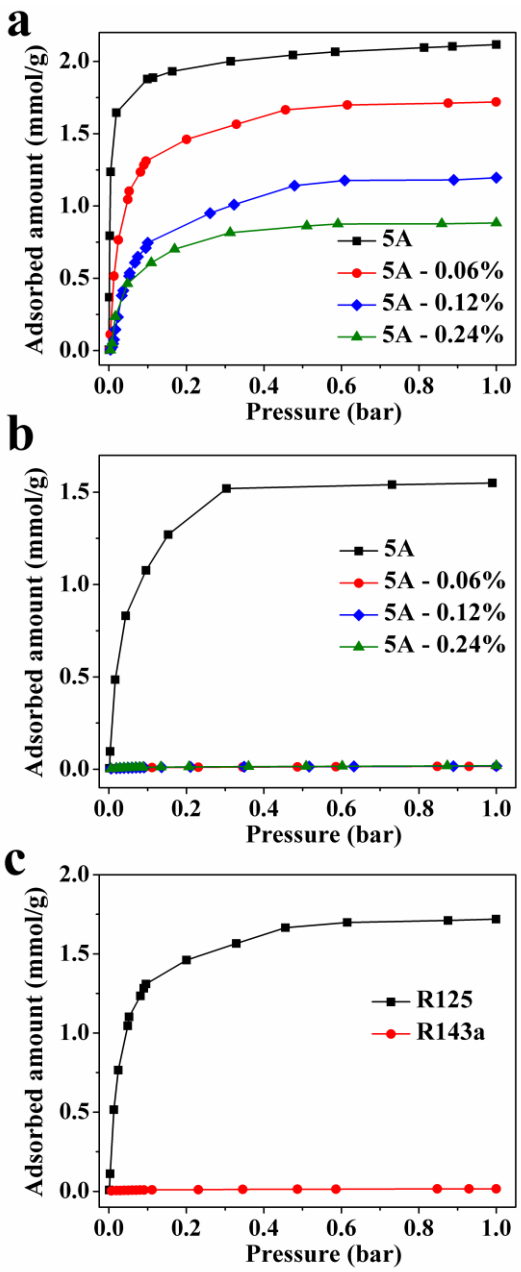

Figure 5-10 Pure gas adsorption isotherms for (a) R125 on 5A and modified 5A zeolite, (b) R143a on 5A and modified 5A zeolite, and (c) adsorption isotherm comparison for R125 and R143a on 5A-0.06% zeolite measured at 293 K.

Table 5-3 Dual-site Langmuir-Freundlich parameters for the adsorption of R125 on 5A and modified 5A zeolite as well as R143a and R134a on 5A zeolite.

	R125				R143a	R134a
	5A	**5A-0.06%**	**5A-0.12%**	**5A-0.48%**	**5A**	**5A**
$q_{sat,1}$	1.451	0.902	0.336	0.4573	0.5236	1.637
$q_{sat,2}$	0.8275	0.9217	0.9618	0.4354	1.077	0.9993
b_1	12.75	6.1	0.03754	0.00468	1.182	5.81
b_2	0.2773	0.05	0.05	0.2821	0.05	0.5723
n_1	0.661	1.03	0.3097	0.4938	0.537	0.8426
n_2	1.73	0.6711	0.8794	0.3519	0.7036	2.687
R^2	1	1	1	0.9999	0.9932	1

5.3.2.3 Dynamic column breakthrough experiments

Dynamic column breakthrough experiments were conducted using gas mixtures that consist of R125 and R143a on both unmodified 5A and 5A-0.06% zeolite. As shown in Figure 5-11a, even without pore size modification, immediate breakthrough of R143a was observed followed by R125 after 9 min. But it took around 70 min for R125 to reach the equilibrium, indicating shape-selective adsorption of R125 over R143a. The reason for the earlier breakthrough of R125 could be due to the slower diffusion of R125 gas molecules into the pore of 5A zeolite. The concentration of R125 and R143a was fixed at 57 and 43% in the feed gas mixture. Figure 5-11c compares the composition of the adsorbed gases. The concentration of R125 in the adsorbed phase increases to 74%. Breakthrough results for pore size modified 5A zeolite are displayed in Figure 5-11b. Immediate breakthrough for R125 and R143a was observed. Even though it still took around 70 min for R125 to reach the equilibrium, the concentration of R125 in the adsorbed phase could reach as high as 85% while it was only 19% in the feed gas mixture. Therefore, through pore size modification of 5A zeolite, we could get much purer R125 from the R125 and R143a mixture.

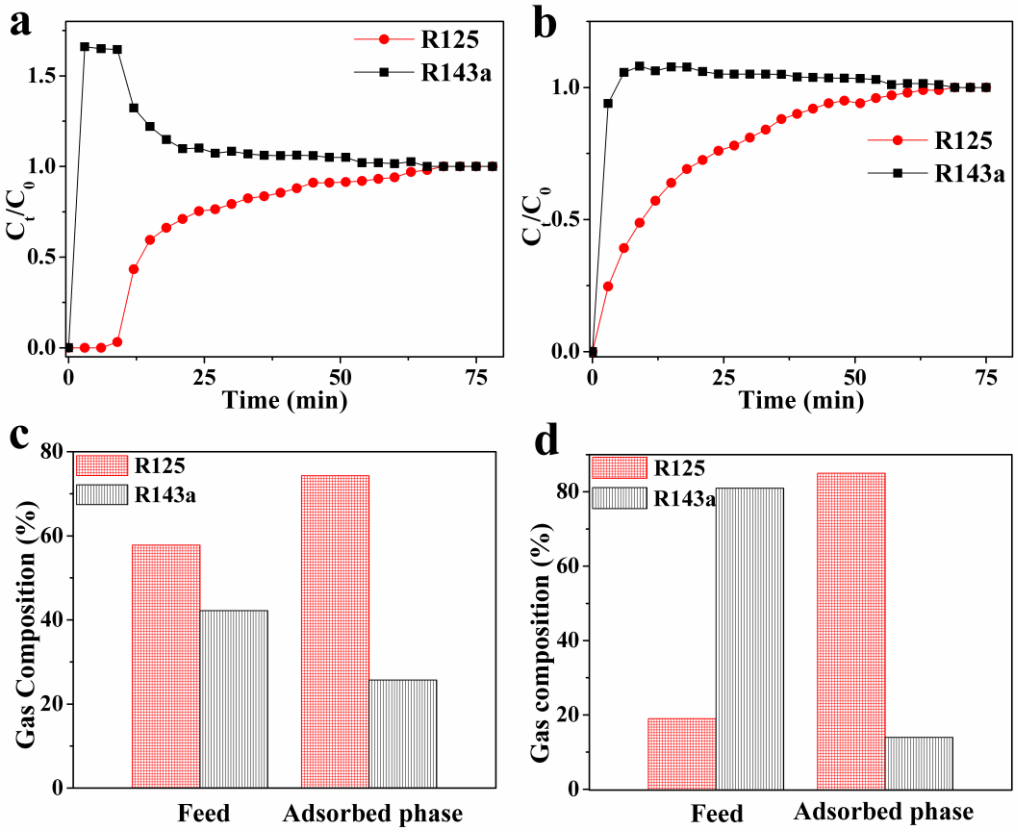

Figure 5-11 Dynamic gas breakthrough profiles for mixture of R125 and R143a on unmodified 5A zeolite (feed gas contains 57% R125 and 43% R143a) (a), and 5A-0.06% (feed gas contains 19% R125 and 81% R143a) (b) measured under atmospheric pressure and 298K.

5.3.3 Recycling stability and adsorbent regeneration

Stable adsorption capacity and recycling stability are very important considerations for industrial scale applications. 13X and surface modified 5A zeolite were subjected to 10 adsorption-desorption cycles of R134a and R125, respectively, to determine change of the adsorption capacity over the cyclic operation. Between each run, the regeneration was accomplished at 423 K for 2 h. Figure 5-12 shows the adsorption capacity of various adsorbents at 298 K and 100 kPa for 10 cycles. Over 10 adsorption-regeneration cycles, both 13X and surface modified 5A zeolite exhibit stable adsorption capacity. Figure 5.13 compares the XRD patterns of 13X and 5A-0.06% zeolite before and after 10 cycles of adsorption and regeneration operations. It is clear to see that both 13X and 5A-0.06% zeolite preserve their original

crystalline structure. To determine the degree of regeneration using Temperature Swing Adsorption (TSA), high temperature (423 K) pure gas adsorption isotherms for R134a on zeolite 13X and R125 on 5A-0.06% zeolite were measured. The measured isotherms at 423 K were compared with the ones measured at 293 K to determine the degree of regeneration at 423 K (Figure 5-14). The calculated regeneratibility of zeolite 13X for R134a is 71% while it is around 45% for 5A-0.06% for R125. Based on these results, it can be concluded that zeolite 13X has higher regenarability than modified 5A zeolite when using 423 K as the regeneration temperature. Since the pore size of 5A zeolite is much closer to the molecular size of R125, it is reasonable to observe moderate regeneration at 423 K. Therefore, by raising the regeneration temperature or using combined Vacuum-Pressure Swing Adsorption, the degree of regeneration of modified 5A should be increased.

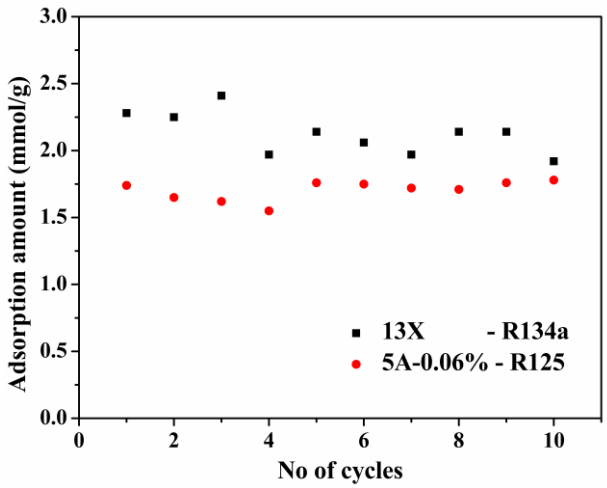

Figure 5-12 Cyclic adsorption capacity of R134a on zeolite 13X (■) and R125 on 5A-0.06% (•).

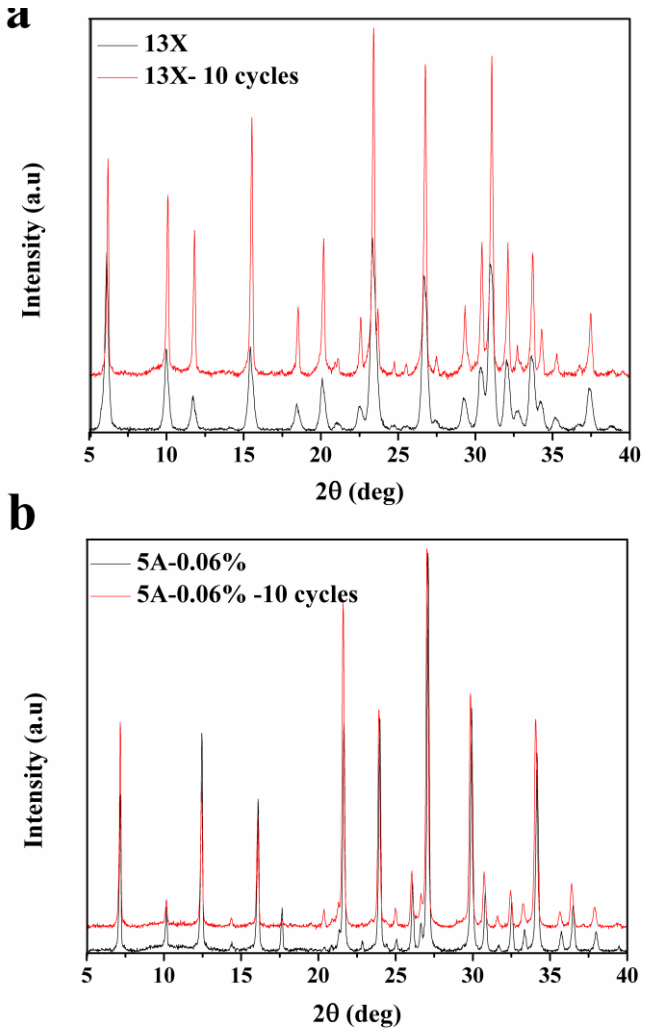

Figure 5-13 XRD patterns of zeolite 13X (a) and 5A-0.06% zeolite (b) before and after 10 cycles of adsorption and regeneration operations.

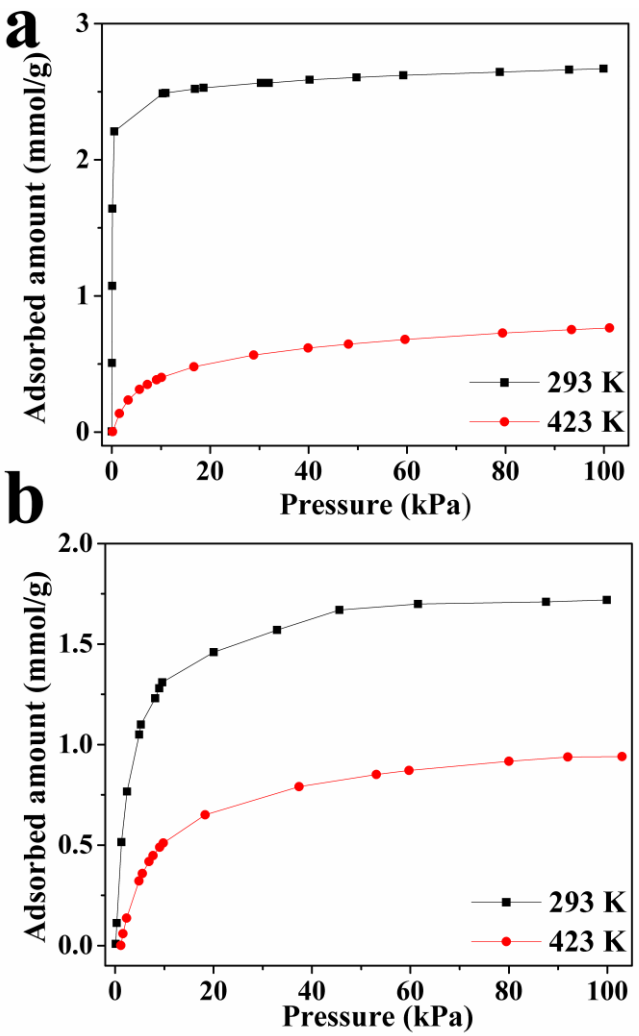

Figure 5-14 Adsorption isotherms at 293 K and 423 K for (a) R134a adsorption on zeolite 13X (b) R125 adsorption on 5A-0.06%

5.4 Conclusions

In conclusion, we have successfully demonstrated a facile strategy to separate mixtures of fluorocarbons containing R125, R134a and R143a to their pure components from their mixtures using zeolite 13X and surface modified 5A zeolite, under ambient conditions. Separation of R134a/R125 and R134a/R143a was achieved using zeolite 13X in which R134a adsorbs preferentially over R125 and R143a. Pore size modified 5A zeolite was used to separate the R125/R143a mixtures based on the molecular sieving property where the modified 5A only adsorbs R125 while completely suppressing the adsorption of R143a.

Chapter 6

HKUST-1 and UiO-66(Zr) Metal Organic Frameworks for the Adsorption Separation of Fluorocarbon blends via Temperature Swing Adsorption.

Overview: This chapter reports the performances of UiO-66(Zr) and HKUST-1 metal organic frameworks for the adsorption-based separation of R32, R22, R125 fluorocarbon blends in comparison with conventional zeolite 13X under ambient conditions. HKUST-1 and zeolite 13X behave as polar adsorbents due to the existence of coordinatively unsaturated Cu^{2+} sites (CUS) and extra framework Na^{+} ions in their structures respectively, whereas UiO-66(Zr) is behave as less polar adsorbent (not carrying any specific polar functional groups). The pore aperture sizes of these three adsorbents are large enough for adsorbates to diffuse, so that the mechanism of separation is expected to be thermodynamic. The performance of these adsorbents for the separation of blends of aforementioned fluorocarbons was compared with benchmark zeolite 13X based on their adsorption capacity, selectivity, working capacity and regenerability. Compared to zeolite 13X, exceptionally high gas adsorption capacities were observed in HKUST-1 and UiO-66(Zr) metal organic frameworks. The binary mixture gas breakthrough experiment results revealed the successful separation of R32/R125, R32/R22 into their individual fractions using HKUST-1 and UiO-66(Zr) among which, UiO-66(Zr) perform better than HKUST-1 in terms of selectivity. The calculated isosteric heats of adsorption values are consistent with high selectivity of R125 and R22 over R32 by HKUST-1 and UiO-66(Zr). Zeolite 13X exhibit reverse selectivity during R32/R125 separation and was unable to separate R32/R22 based on their thermodynamic properties. Compared to zeolite 13X, considerably higher adsorption capacities, higher selectivities, working capacities and lower temperatures for regeneration suggest the possibility of exploiting UiO-66(Zr) and HKUST-1 for the separation of R32/R125 and R32/R22 fluorocarbon blends.

6.1 Introduction

With the rising concerns over the ozone layer depletion and global warming, implementation of proper strategies to control the usage and emissions of greenhouse gases has become an urgent requirement. Though hydrochlorofluorocarbon (HCFC) and hydrofluorocarbon (HFC) derivatives are of great industrial importance because of their useful applications in refrigerants, solvents, fluoropolymers, and etc, they are potent greenhouse gases with very high global warming potential (GWP) and some even can cause ozone layer depletion. With the implementation of Montreal and Kyoto protocols, being the largest sector of fluorocarbon consumption, the refrigerant and air conditioning industry undergoes major transition from the use of ozone depleting CFCs and HCFCs to non-ozone depleting HFCs. For an example CFC-12(CCl_2F_2/R12) that has been used in domestic refrigerators and mobile air conditioning systems is now replaced with HFC-134a(CH_2FCF_3/R134a) because of its' ozone layer deletion potential. Also, R410A which is blended from HFC-32 (CH_2F_2/R32) and HFC-125(CHF_2CF_3/R125) is now widely being used in residential air conditioning and refrigeration systems as a replacement for ozone depleting HCFC-22(CHClF2/R22).

Due to the high growth rate of R410A in the air conditioning and refrigeration sector, it has predicted that, by 2030, the estimated consumption of R410A will constitute the highest proportion of HFC consumption leading to high demand for R32 and R125. Meanwhile, many air conditioning and refrigeration manufacturers are changing from R410A to R32, driven by several factors including low GWP (GWP of R32 and R410A are 675 and 2090 respectively), zero ozone layer depletion and superior energy efficiency, etc. However, most of the developed countries are planning for a stepwise phase out of most of the HFCs because of their very high global warming potential. The refrigerant industry foresees a high demand for HFCs and HCFCs especially in the service sector, since there is still requirement to operate and maintain the existing equipments which use the fluorocarbon refrigerants that are proposed to phase out in near future. Therefore, planning and design of fluorocarbon reclamation processes, especially to recover low GWP refrigerants and those are likely to phase out, is an urgent requirement.

Herein, we report the utilization of HKUST-1 and UiO-66(Zr) MOFs for the separation of R32/R22/R125 fluorocarbon mixtures, especially R32/R125 (R410A), into their individual fractions. Before selecting these materials, four types of MOFs (MIL-101, HKUST-1, ZIF-8 and UiO-66(Zr)) were screened based on their pure gas adsorption isotherms. Since the separation of these fluorocarbons using zeolites also rarely reported, we have included the performance of zeolite 13X for the comparison purpose. zeolite 13X has open three-dimensional pore system, which leads to lower mass transfer resistances and higher adsorption capacities compared to other zeolites. The single component adsorption isotherms of R32, R22 and R125 on these selected three adsorbents were measured at different temperatures. The working capacity and regeneration performances were evaluated using the measured high temperature adsorption isotherms. Furthermore, dynamic column breakthrough experiments were conducted to confirm their selectivity as suitable for practical applications.

6.2 Materials & Methods

All the starting materials including solvents were purchased from Sigma Aldrich and were used without further purification. zeolite 13X was also purchased from Sigma Aldrich in a form of cylindrical extrudes.

Synthesis of Materials

HKUST-1 [132], UiO-66(Zr) [133], MIL-101[40], ZIF-8[64] was synthesized according to procedures reported in the literature.

Synthesis of HKUST-1. Briefly, 0.9 g $Cu(NO_3)_2.5H_2O$ and 0.4 g PVP were dissolved in 50 mL of methanol under stirring. Then, 0.43 g of H_3BTC was dissolved in 50 ml methanol and was added into the above solution drop by drop to form a blue colloidal suspension. The colloidal solution was aged at room temperature without any interruption for 24 h. The resulting blue precipitate was centrifuged and washed several times with methanol and finally dried in an oven at 60 ºC. Prior to the gas adsorption measurements, HKUT-1 was activated by heating at 170 ºC for 24 hours under dynamic vacuum.

Synthesis of UiO-66(Zr). 125 mg $ZrCl_4$, 5 ml DMF, and 1 ml concentrated HCl were sonicated for 20 minutes until fully dissolved. Then 123 mg H_2BDC in 10 ml DMF were added to the above mixture and was sonicated an additional 20 minutes before being heated at 80 °C overnight. The resulting solid was then filtered and washed first with DMF (2x30 mL) and then with EtOH (2x 30 mL). Prior to the gas adsorption measurements, UiO-66(Zr) was activated by heating at 150 ºC for 12 hours under dynamic vacuum.

6.3 Results & discussion

6.3.1 Characterization of Materials

The obtained XRD patterns were used to verify the crystalline structure of synthesized MOFs (Figure 6-1). The calculated BET surface area and micropore volume using measured N_2 adsorption isotherms (Figure 6-2) are given in table 6-1 and are comparable with the reported values. The characteristic IR spectra of HKUST-1 and UiO-66(Zr) were obtained from the FTIR experiments and are shown in figure 6-3. The FESEM images of these MOFs are shown in Figure 6-4.

Material selection

Initially performances of four types of MOFs were screened based on their R22 and R125 pure gas adsorption isotherms: microporous HKUST-1[56, 57, 134, 135] which contain abundant coordinatively unsaturated metal sites (CUS) for the gas adsorption,[55] UiO-66(Zr) with exceptionally high thermal stability[62, 136, 137], MIL-101(Cr) with hierarchical pore structure and giant cell volume (~702,000 $Å^3$)[87] and ZIF-8 with small aperture size which is suitable for shape-selective gas separation . Figure 6-5 compares the measured R22 and R125 pure gas adsorption isotherms on these MOFs and zeolite 13X measured at 293 K. At 1 bar, for both R22 and R125, the adsorption capacities vary according to MIL-101 > HKUST-1 > UiO-66(Zr) > ZIF-8 > zeolite 13X. Importantly, it should be noted that both R22 and R125 adsorption capacity of MIL-101 and HKUST-1 are more than two times higher than zeolite 13X. Interestingly, both HKUST-1 and zeolite 13X adsorption isotherms indicate steep slope at low pressure region

(<0.2 bar) indicating strong binding affinity of R22 and R125 to these materials, mainly because of the existence of open Cu^{2+} sites and extra framework Na^{+} ions respectively.

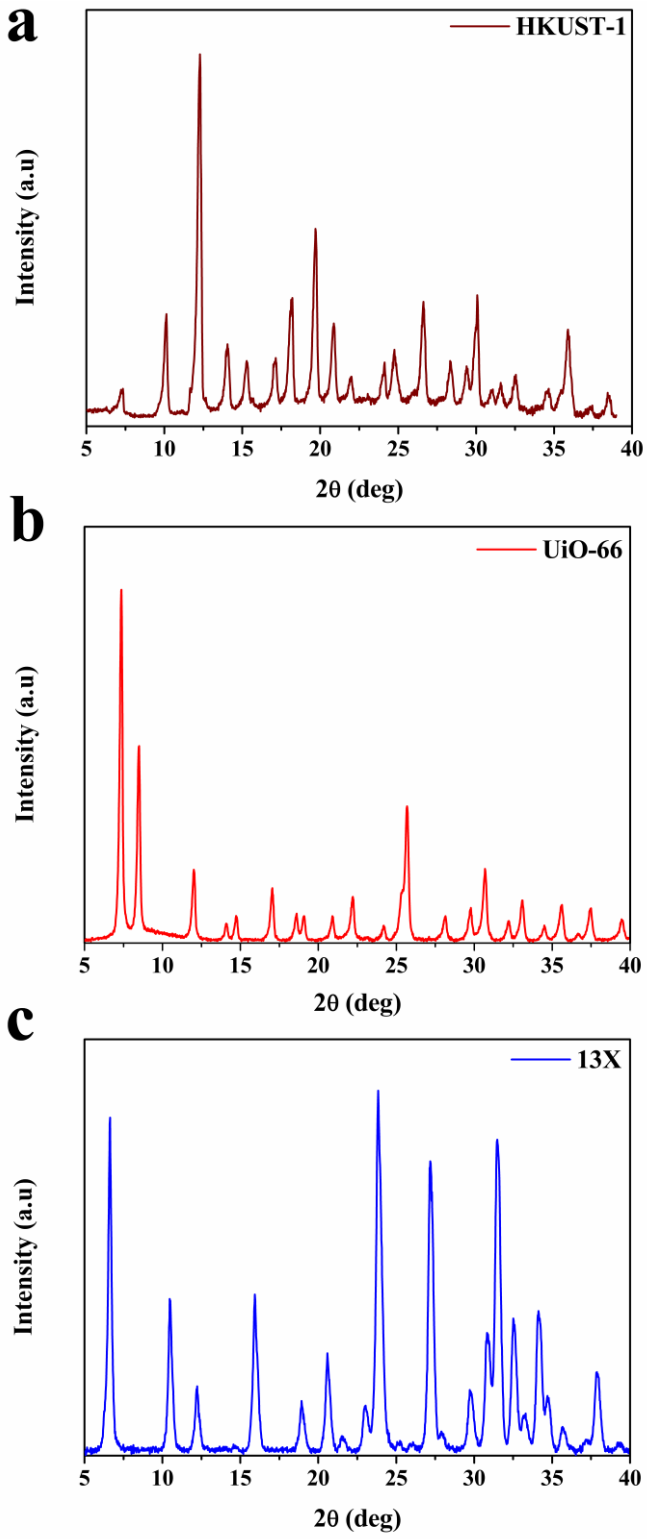

Figure 6-1 XRD patterns of (a) HKUST-1 (b) UiO-66(Zr) (c) Zeolite 13X

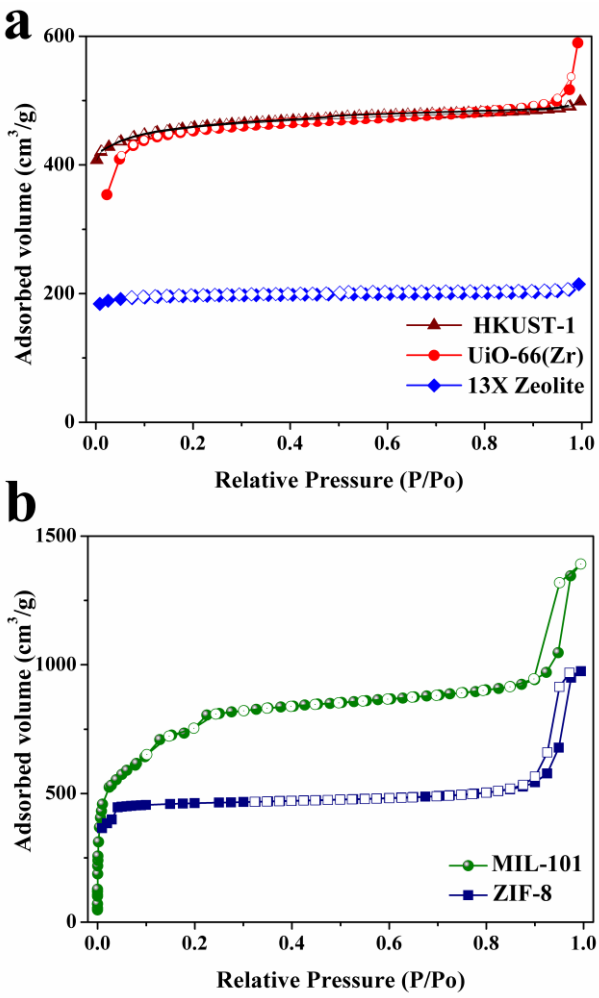

Figure 6-2 N_2 adsorption isotherms measured at 77 K.

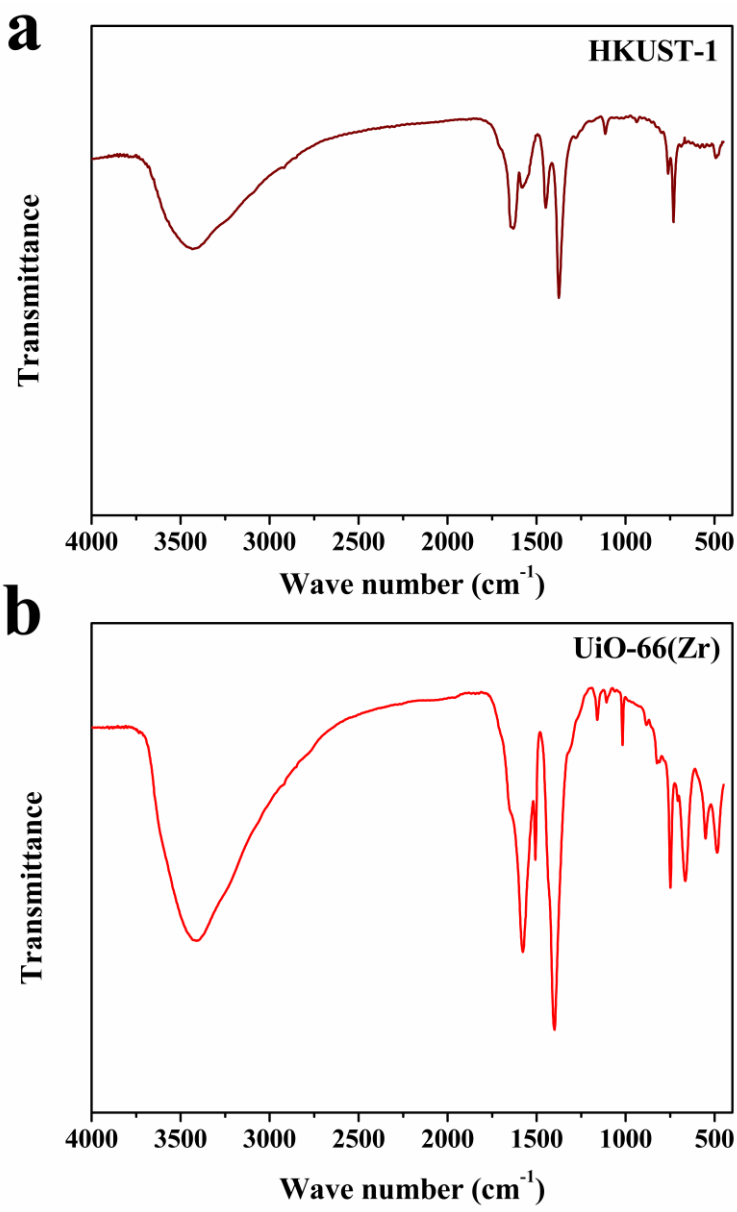

Figure 6-3 FTIR spectra of (a) HKUST-1 (b) UiO-66(Zr)

Such steep adsorption at low pressure region was not observed in UiO-66(Zr) due to the lack of strong adsorption sites in its framework(Figure 6-5). Also, both R22 and R125 adsorption isotherms on ZIF-8 did not indicate considerable difference in their adsorption capacities as suitable for shape-selective separation. Considering their higher adsorption capacities, different surface polarities and the availability of synthesis routes for bulk production, HKUST-1, UiO-66(Zr) metal organic frameworks were selected for the detail investigation of their potentials for the separation of R32, R22 and R125 fluorocarbon mixtures. Since these selected MOFs have larger pore aperture size compared to the molecular sizes of our fluorocarbons (R32-3.9 Å, R22-

4.2 Å, R125-4.9 Å), the mechanism of their separation is mainly expected to be arising from thermodynamic selectivity rather than from steric or kinetic selectivity. The selectivity of zeolite 13X is also expected to be thermodynamic, because the pore aperture of 13X is

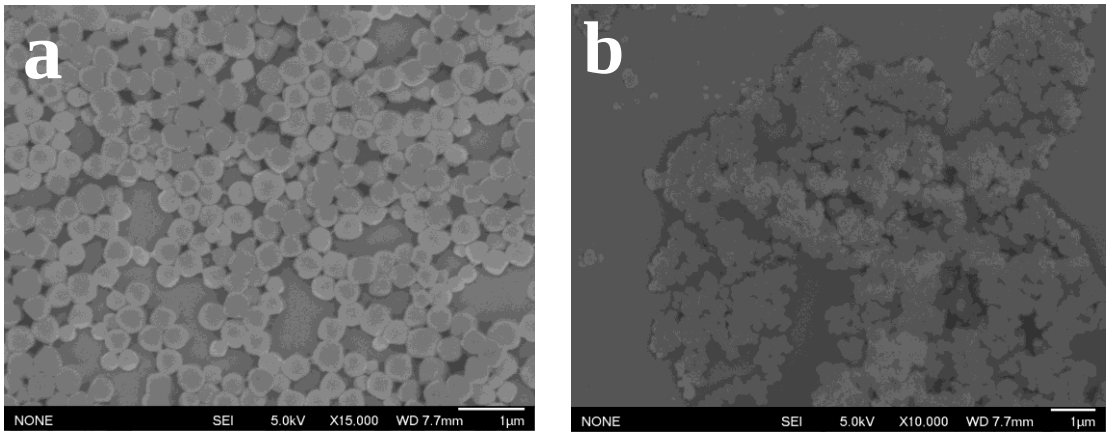

Figure 6-4 FESEM images of (a) HKUST-1 and (b) UiO-66(Zr)

also much larger than the molecular sizes of the R32, R22 and R125. For thermodynamic equilibrium separations, the pore aperture of the adsorbent should be large enough to allow all adsorbates to diffuse, and then the separation performances depend on the affinity of various adsorbates and the adsorbent surface.[138]

Description of the MOF and Zeolite structures

Basic chemical and physical properties of HKUST-1, UiO-66(Zr) and zeolite 13X are summarized in table 6-1. Briefly, HKUST-1[139] has three-dimensional pore structure with three types of cages generated by the connection of dimeric clusters of copper coordinated with four carboxylate groups of trimesic acid. The smallest cages, commonly known as side pockets with 6 Å internal diameters and 4.6 Å pore aperture are located at eight corners of a cube to form two types of big cages. These big cages having 12 and 10 Å internal diameter are connected through 6.5 Å pore aperture. In the as synthesized material, the axial ligand of the copper dimer is coordinated to water molecule that can be removed by heating.

UiO-66(Zr), a Zirconium carboxylate MOF, is one of the most studied MOF because of its excellent chemical, thermal and mechanical stability since it was first reported by Lillerud et al.[140] It consists of a cubic framework of cationic $Zr_6O_4(OH)_4$ nodes (formed *in situ* via hydrolysis of $ZrCl_4$) connected to 12 benzene-1,4-dicarboxylate (BDC) linkers to form the 3D arrangement of micropores with each centric octahedral cage surrounded by eight corner tetrahedral cages (free diameters of ca. 11 and 8 Å for the two types of cages, respectively) and connected through narrow windows (ca. 6 Å). This high degree of network connection is believed to be the main reason for its high stabilities.[133]

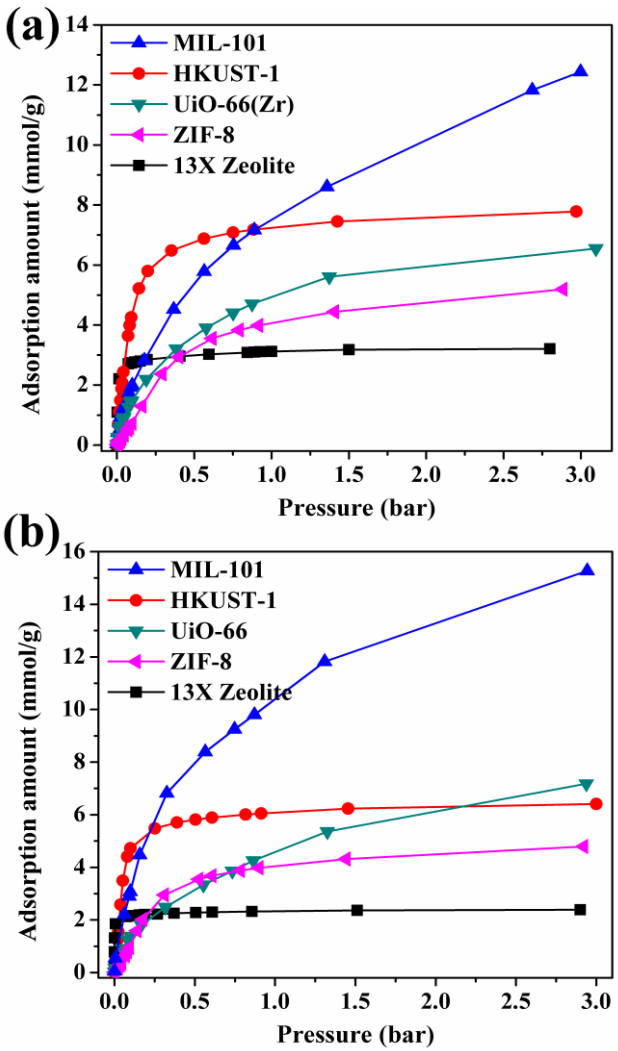

Figure 6-5 (a) R22 ad (b) R125 adsorption isotherms of selected MOFs and zeolite 13X at 293 K.

The crystallographic unit cell of zeolite 13X consists of an array of eight cages containing a total of 192 AlO_2 and SiO_2 tetrahedral units. The framework can be considered as a tetrahedral lattice of sodalite units connected through six-membered oxygen bridges. The resulting channel structure is very open with each cage connected to four other cages through twelve-membered oxygen rings of free diameter ~ 7.4 Å.[138]

Table 6-1 Chemical and Physical properties of selected adsorbents.

Property	HKUST-1	UiO-66(Zr)	13X
Chemical formula	$Cu_3(C_9H_3O_6)_2$	$Zr_6O_4(OH)_4(C_8H_4O_4)_6.nH_2O$	$[Na^+_{54}(H_2O)_{240}][Al_{58}Si_{134}O_{384}]$
Topology	-	-	FAU
CUS	Cu^{2+}	-	-
Counter ions	-	-	Na^+
Type of porosity	cages	cages	cages
Pore diameter/aperture (Å)	12/6.5 10/6.5 6/4.6	11/6 8/6	11/7.4
Surface area (m^2/g) [a]	1385	1383	588
Micro Pore volume (cm^3/g) [b]	0.67	0.66	0.30
Bulk Density (g/cm^3)	0.36[141]	0.17[141]	0.65[142]

[a] BET method, [b] t-plot method

6.3.2 Comparison of Adsorption isotherm data

Adsorption of R32, R22 and R125 on HKUST-1 measured at 293 K, 313 K and 333 K are shown in figure 6.6. The measured adsorption capacities of R32, R22 and R125 at 1 bar and 293 K were 11.3, 7.3, 6.1 mmol/g respectively. The observed R22 and R125 steep increase of adsorption at low pressure region and saturation capacity at around 1 bar reveal their strong affinity to the pore surface of HKUST-1. At low pressures (< 0.01 bar), the adsorption capacities of R22 and R125 are 4-5 times higher than R32. Generally, the gases with high polarity shows stronger interaction with the adsorbent surface than the less polar molecules.[143] This fundamental physical concept can be used to explain the steep adsorption of R22 and R125

compared to R32 by HKUST-1 at low pressure region. R22 and R125 have higher molar mass, boiling point, polarizability[11] and highly acidic H in its' structure compared to R32, resulting in stronger interaction with the unsaturated Cu^{2+} sites and the O sites in HKUST-1. But, the R32 adsorption continues at high pressures through the pore filling mechanism. Therefore, higher adsorption of R32 over R22 and R125 is resulted.

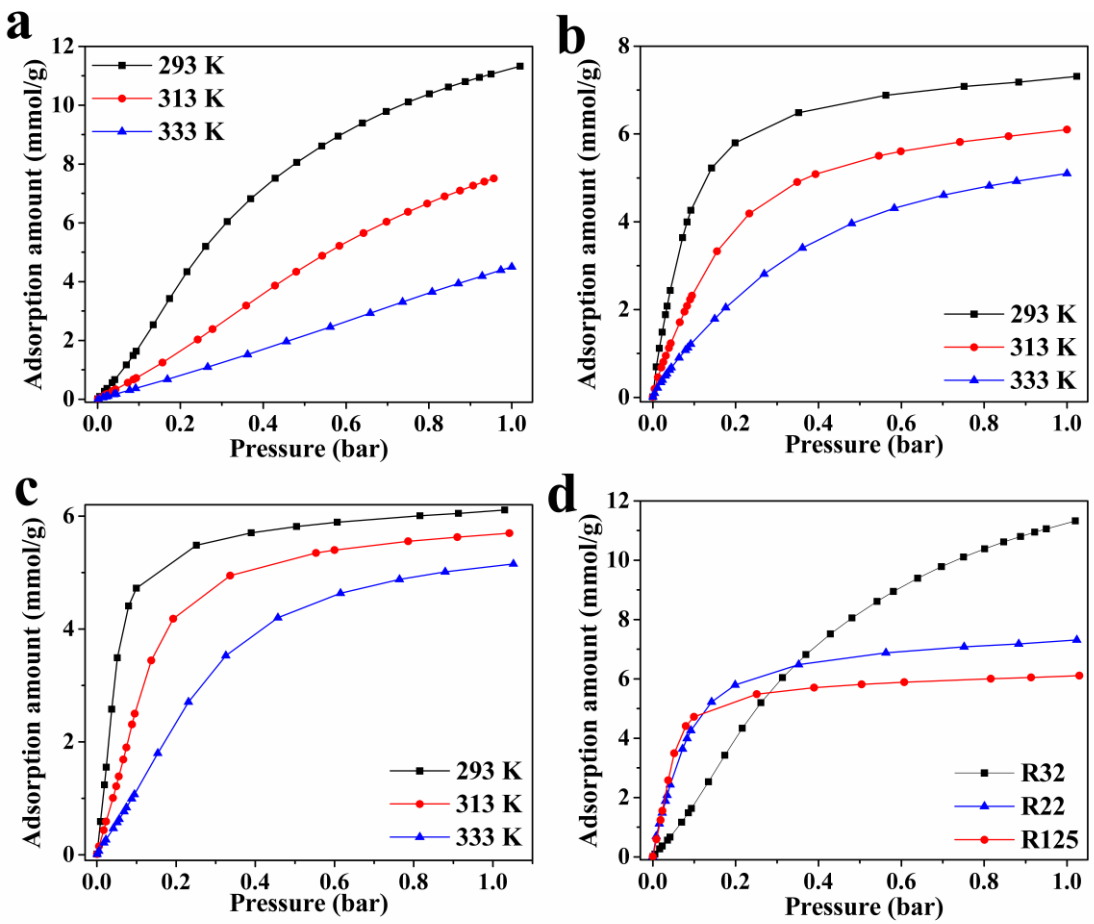

Figure 6-6 Pure gas adsorption isotherms for (a) R32 (b) R22 (c) R125 for HKUST-1 at 293, 313, 333 K and (d) isotherm comparison at 293 K.

As expected, the adsorption amounts of each gas decreased with the increase of temperature due to the higher thermal energy of gas molecules at high temperatures. When the temperature increased to 333 K, the steepness of the R22 and R125 isotherms at low pressure region was less pronounced compared to the isotherms measured at 293 K. For R32, the adsorption isotherm at 333 K become almost linear. This is due to the overcoming of the heat of adsorption

at the exposed open Cu^{2+} sites by thermal energy of gas molecules, resulting in an apparently homogeneous pore surface at high temperatures.[144] Importantly, at 333 K and 0.5 bar, the adsorption capacity of R32 (2.11 mmol/g) became considerably less than the that of R125(4.34 mmol/g) and R22(4.04 mmol/g) suggesting improved R125 and R22 selectivity at slightly higher temperatures.

Due to the inherent heterogeneity of the pore surface and the higher affinity of gases towards the exposed Cu^{2+} sites compared to the other adsorption sites in HKUST-1, dual-site Langmuir-Freundlich equation was used to model the experimental single-component isotherms (Eq 1).

$$q = \frac{q_{sat,1} b_1 p^{n_1}}{1+b_1 p^{n_1}} + \frac{q_{sat,2} b_2 p^{n_2}}{1+b_2 p^{n_2}} \qquad \text{Eq 1}$$

where q (mmol/g) is the total adsorption quantity of a single gas and p (bar) is the partial pressure, $q_{sat,1}$ and $q_{sat,2}$ are the saturated loading for site 1 and 2. b_1, b_2 and n_1, n_2 are Langmuir and Freundlich parameters for site 1 and 2, respectively. All our experimental isotherms can be well described by the dual-site Langmuir-Freundlich model with a R^2 value greater than 0.99. The fitted parameters are presented in Table 6-2.

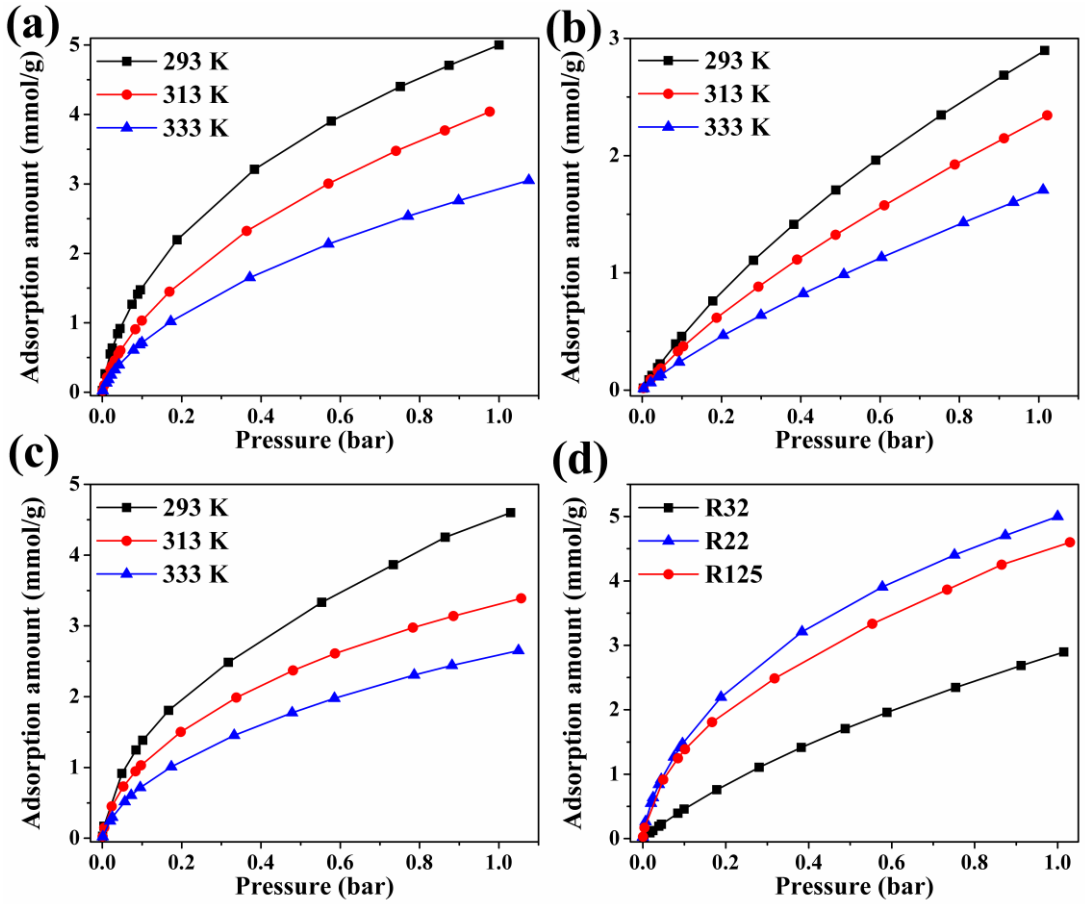

Figure 6-7 Adsorption isotherms on UiO-66(Zr) for (a) R22 (b) R32 (c) R125 measured at 293 K, 313 K, 333 K and (d) isotherm comparison at 293 K.

Figure 6-7 illustrates R32, R22 and R125 pure gas adsorption isotherms on UiO-66(Zr). At 1 bar and 313 K the adsorption capacities of R22 and R125 are 4.0, 3.4 mmol/g respectively, while it was only 2.3 mmol/g for R32. Compared to their pure gas adsorption isotherms on HKUST-1, especially in the case of R22 and R125, no steep adsorption at low pressure region was observed indicating moderate binding affinity of these gases in UiO-66(Zr) framework being the absence of strong adsorption sites. However, the considerable differences in their adsorption capacities suggests the potential of UiO-66(Zr) for the separation of R32/R125 and R32/R22 fluorocarbon blends. Higher polarizability and availability of highly acidic H to form stronger C-H···π, C-H···O interactions with phenyl groups in UiO-66(Zr) may have contributed to the higher adsorption capacity of R22 and R125 in UiO-66(Zr). To our knowledge, adsorption of R22, R32 and R125 in HKUST-1 and UiO-66(Zr) are not reported in the literature.

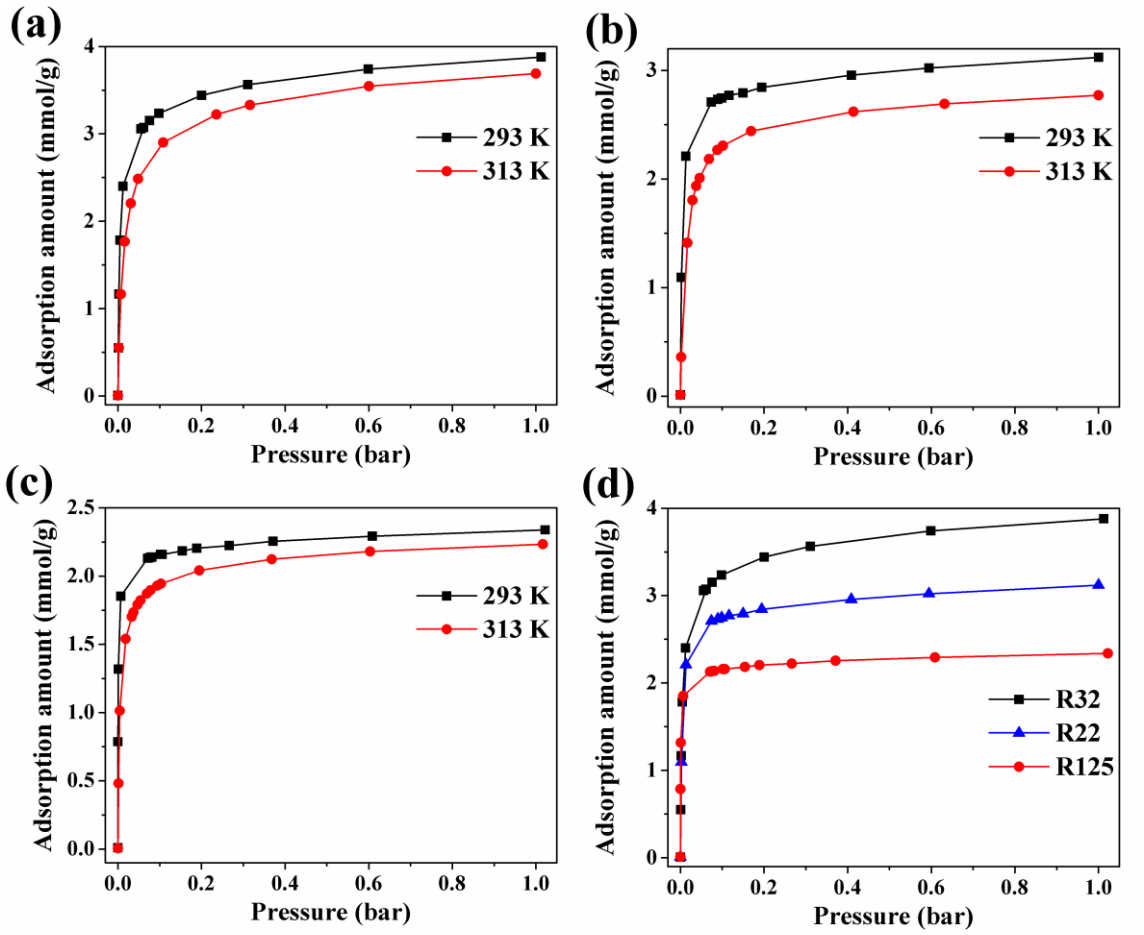

Figure 6-8 Pure gas adsorption isotherms for (a) R32 (b) R22 (c) R125 on 13X at 293, 313, 333 K

According to the measured pure gas adsorption isotherms on zeolite 13X (figure 6-8), the adsorption capacities of R32, R22 and R125 were observed to be 3.88, 3.12 and 2.34 mmol/g at 1 bar and 293 K. Strong adsorption affinities of all these three gases to the zeolite 13X was clearly understood by the steep type 1 isotherm and such steepness in the isotherms was not observed in the HKUST-1 and UiO-66(Zr). All these experimental isotherms also successfully fitted with dual-site Langmuir-Freundlich equation with the R^2 value greater than 0.99 and the obtained parameters are listed in Table 6-2, 6-3 & 6-4.

Table 6-2 Dual-site Langmuir-Freundlich parameters for the adsorption of R32, R22 and R125 on HKUST-1.

HKUST-1	R32			R22			R125		
	293 K	313 K	333 K	293 K	313 K	333 K	293 K	313 K	333 K
$q_{sat,1}$	1.667	9.711	5.989	2.277	1.885	4.982	5.783	3.967	3.52
$q_{sat,2}$	14.78	1.305		5.686	5.299	1.007	0.4143	2.17	2.47
b_1	113.5	2.065	2.447	447	72.42	4.821	215.1	7.52	3.341
b_2	1.867	5.928		7.16	3.943	20.53	3.951	893.4	37.93
n_1	3.125	1.852	1.938	2.341	2.253	1.529	1.684	1.01	0.9862
n_2	1.17	0.9883		0.8296	0.8588	1.007	3.612	3.073	2.57
R^2	1	1		1	1	1	0.9993	1	1

Table 6-3 Dual-site Langmuir-Freundlich parameters for the adsorption of R32, R22 and R125 on UiO-66(Zr) at 293 K.

UiO-66(Zr)	R22	R125	R32
$q_{sat,1}$	5.663	5.33	4.234
$q_{sat,2}$	1.939	1.817	3.873
b_1	2.162	1.872	1.117
b_2	1.374	1.431	0.1947
n_1	0.776	1.362	1.024
n_2	2.081	0.368	0.5473
R^2	0.9999	1	1

Table 6-4 Dual-site Langmuir-Freundlich parameters for the adsorption of R32, R22 and R125 on 13X.

13X	R32		R22		R125	
	293 K	313 K	293 K	313 K	293 K	313 K
$q_{sat,1}$	2.594	1.036	0.7634	0.3002	2.122	0.8743
$q_{sat,2}$	1.785	3.098	2.765	2.59	0.2924	1.516
b_1	827.7	1.729	0.9012	2.294	800	4.599
b_2	2.518	52.82	356.2	80.32	2.642	335.9
n_1	1.167	0.9112	0.9725	1.677	0.9194	0.6015
n_2	0.6089	0.9883	1.046	1.018	1.072	1.024
R^2	0.9999	1	0.9999	0.9997	0.9933	1

6.3.3 Dynamic column breakthrough experiment results

Both binary and ternary gas breakthrough experiments were carried out on HKUST-1, UiO-66(Zr) and zeolite 13X for the separation of R22, R32 and R125 fluorocarbon mixtures. Figure 6-9 shows the breakthrough results for the separation of R32/R22/R125 in HKUST-1.

Table 6-5 Operating conditions of dynamic column breakthrough experiments.

`		HKUST-1	UiO-66(Zr)	13X
Sample amount/g		4	2	12
Temperature (K)		298	298	298
Pressure (bar)		1	1	1
Feed gas composition (vol %)	R32/R125	36/64	36/64	36/64
	R32/R22	65/35	55/46	50/50
	R32/R22/R125	29/29/42	26/46/28	31/43/26
Feed flow rate (cm^3/min)	R32/R125	5	5	10
	R32/R22	12	8	12
	R32/R22/R125	8	8	16

All the operating conditions including sample amount, operating temperature and pressure, feed flow rate and feed gas compositions are given in table 6-5. The characteristic breakthrough profile of thermodynamic separation is observed from the R32 and R125 breakthrough experiments (Figure 6-9a), which is the sharp breakthrough font with marked roll-up.[143]

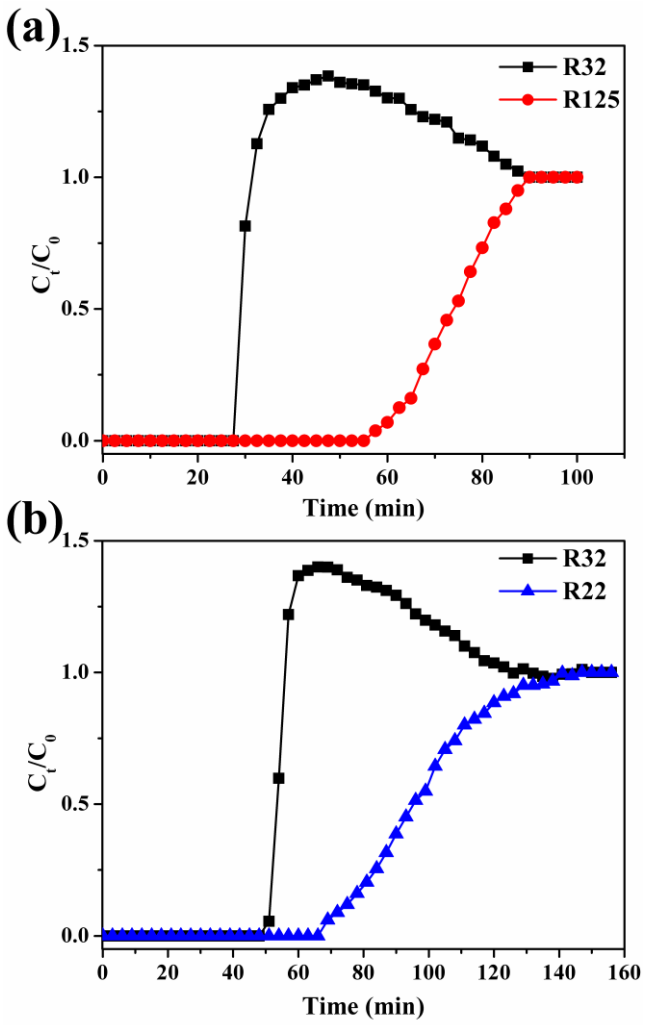

Figure 6-9 Breakthrough curves on HKUST-1 for (a) R32/R125 (b) R32/R22 and (c) R32/R22/R125 at 1 bar and 298 K

This roll-up means that the concentration of weakly adsorbed component, which elute from the column first, is higher than its initial feed concentration.

The interpretation of selective adsorption of R125 over R32 in HKUST-1 is challenging due to the existence of different types of cages and heterogeneity of its pore surface. As mentioned earlier higher polarizability of R125 is a decisive factor because it can strongly interact with the

open metal sites in HKUST-1. But the cage sizes also may have played an important role since the molecular size of R125 match perfectly well to the side pockets which are defined as strong adsorption sites in many publications because of the strong overlap of electric fields.

At first R32 is adsorbed to a higher concentration level which exceeds the final equilibrium value. It then desorbs to the equilibrium level as R125 penetrates.[138] The weakly adsorbed R32 elute from the column first and breakthrough gas flow contain only R32 until the elute of R125 is occurred at 57 min indicating the potential of HKUST-1 for the separation of R410A into individual fractions. Adsorbed phase R125 composition exceeded 93 % while it was only 64% in the feed gas mixture. Further, according to the pure gas adsorption isotherms of HKUST-1, at 1 bar, the reduction of R32 adsorption capacity with the increase of temperature from 293 K to 333 K was 60 % compared to that of 14% for R125, suggesting the possibility of increasing the adsorbed R125 purity by maintaining the column temperature at slightly higher value than the ambient temperature.

Similarly, the thermodynamic selectivity of R22 over R32 is observed during the column breakthrough experiments for the separation of R22/R32. Mixture of R22 and R32 was fed into the column with the flow rate of 12 cm^3/min at 298 K and 1 bar. Sharp breakthrough front with marked roll-up was observed for R32 at 51 min followed by R22 at 69 min. The adsorbed phase R22 composition exceeded 95 % while it was only about 35% in the feed mixture.

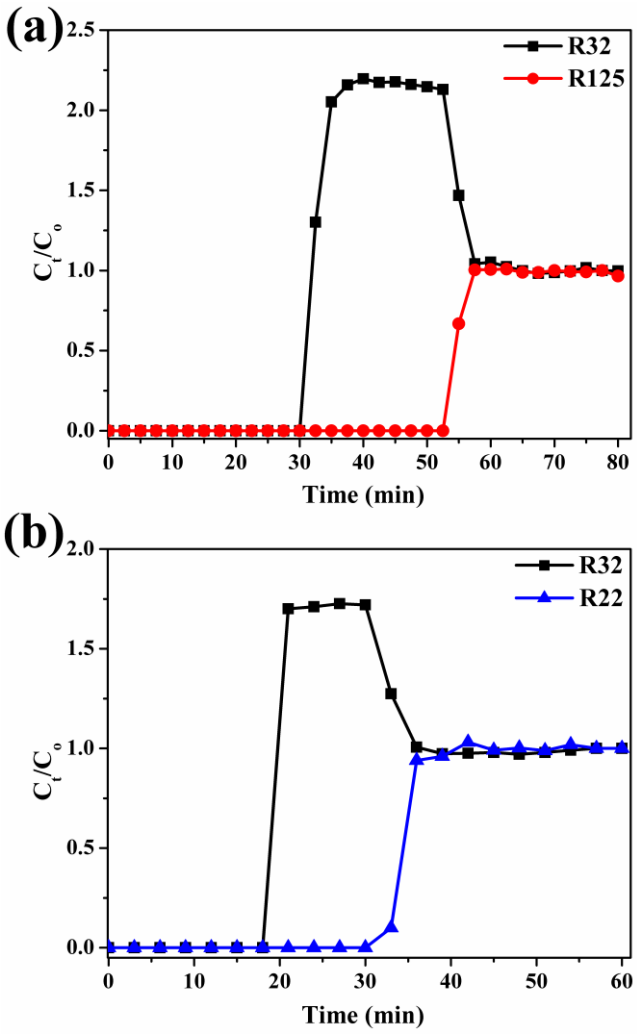

Figure 6-10 Breakthrough curves on UiO-66(Zr) for (a) R32/R125 (b) R32/R22 and (c) R32/R22/R125 at 1 bar and 298 K

Similar to HKUST-1, selective adsorption of R125 over R32 was observed in the column breakthrough experiment results (Figure 6-10a) of UiO-66(Zr), indicating successful separation of R410A into individual fractions. R32 breakthrough from the column first followed by R125 after 22 min. Importantly, adsorbed phase R125 composition exceeded 98% while it was only 64% in the feed gas mixture suggesting that UiO-66(Zr) perform better compared to HKUST-1 for the separation of R410A. When compare the R32/R125 separation breakthrough results of HKUST-1 and UiO-66(Zr), R125 takes longer time to reach the plateau of the breakthrough curve of HKUST-1 suggesting that R125 have diffusional limitations to reach the core of the adsorbent particles. But in the case of UiO-66(Zr), R125 elute from the column with sharp front

indicating fast adsorption kinetics and a more complete utilization of the adsorbent bed as suitable for large scale R410A separation applications. Further, R22/R32 experimental breakthrough results of UiO-66(Zr) (Figure 6-10b) reveal the selective adsorption of R22 over R32. The adsorbed phase R22 composition also exceeds 98% when it is around 46% in the feed mixture. Therefore UiO-66(Zr) is indeed suitable for separation of R32/R22 mixtures as well.

During our previous attempts to use Mg-MOF-74 for R32/R125 separation, it exhibited different adsorption behavior, which is the considerably high R32 adsorption capacity compared to R125(Figure 6-11). At 1 bar, the adsorption capacity of R32 in polar Mg-MOF-74 and HKUST-1 are considerably higher than R125, but in the case of non-polar UiO-66(Zr), the R32 adsorption capacity is considerably lower than R125 and it exhibited highest selectivity for R125. A recent report provides the details of R22 and R32 adsorption characteristics in MIL-101.[40] Even at1 bar, lower adsorption capacity of R32 over R22 (measured adsorption capacities are 5, 8.5 mmol/g respectively) by MIL-101 is reported. Unlike Mg-MOF-74 and HKUST-1, but similar to UiO-66(Zr), MIL-101 does not contain strong gas adsorption sites, resulting much poorer adsorption of less polar R32. Based on these findings, it can be concluded that surface polarity/type of available adsorption sites in the adsorbent play a major role during thermodynamic separation of R32/R125, R32/R22 fluorocarbon mixtures. Though our results are not sufficient to distinguish in between, it should be noted that, along with surface polarity, pore structure of the adsorbents also can influence the selectivity.[145]

The breakthrough experiment results for separation of binary R32/R125, R32/R22 and ternary R32/R22/R125 using zeolite 13X are shown in figure 6-12. Figure 6-12a shows the R32 and R125 results. Interestingly, compared to the HKUST-1 and UiO-66(Zr), zeolite 13X exhibited reverse selectivity, which is the preferential adsorption of R32 over R125. Although it is difficult to fully explain this separation behavior of 13X based only on adsorption isotherms and breakthrough results, plausible explanation can be hypothesized considering various sorbate-sorbent interactions and the size entropy/molecular packing effects.[146] During the process of fluorocarbon adsorption to zeolite 13X, a variety of interactions appear to be important:

$F/Cl_{sorbate}$…. $O_{framework}$ van der Waals interactions, $F/Cl_{sorbate}$…. Na^{+} electrostatic interactions and $H_{sorbate}$….$O_{framework}$ hydrogen bonding (H bonding).[82, 147, 148] When observe the single component adsorption isotherms on 13X, steep adsorptions at low pressure

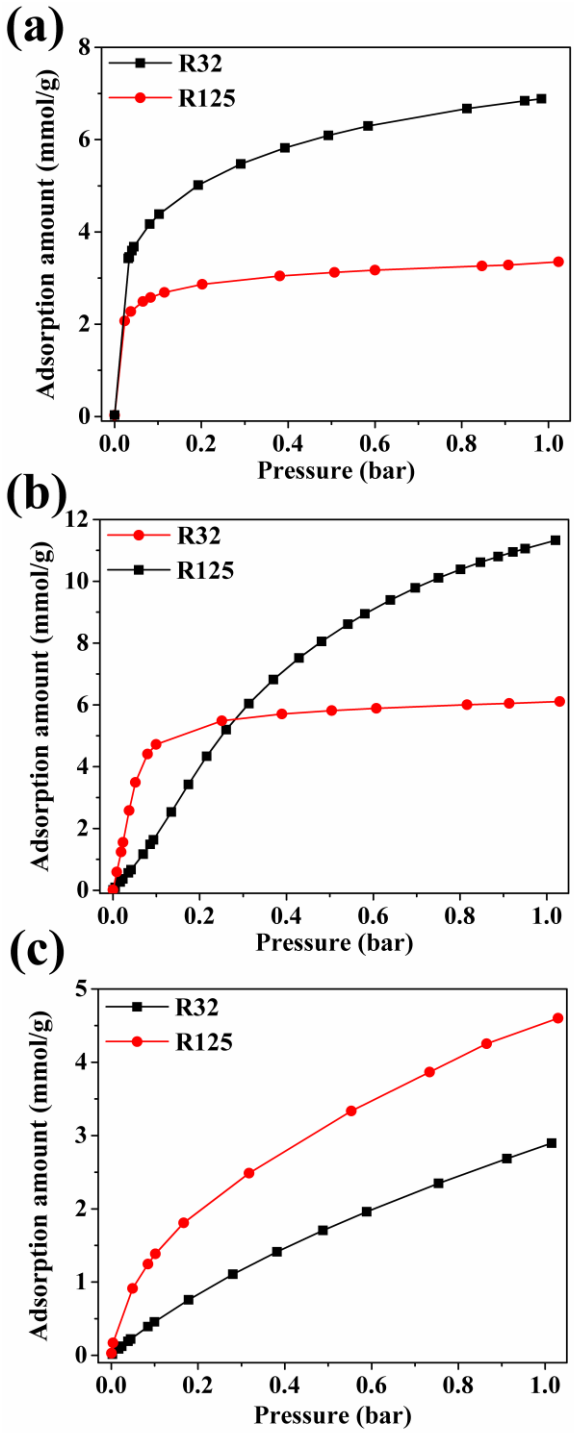

Figure 6-11 R32 and R125 adsorption isotherms at 293 K on (a) Mg-MOF-74 (b) HKUST-1 and (c) UiO-66(Zr).

region were noticeable for all the three gases indicating their strong adsorption affinity to zeolite 13X framework, which can be mainly due to the strong $F/Cl_{sorbate}\ldots.Na^{+}$ electrostatic interactions and $H_{sorbate}\ldots.O_{framework}$ hydrogen bonding.

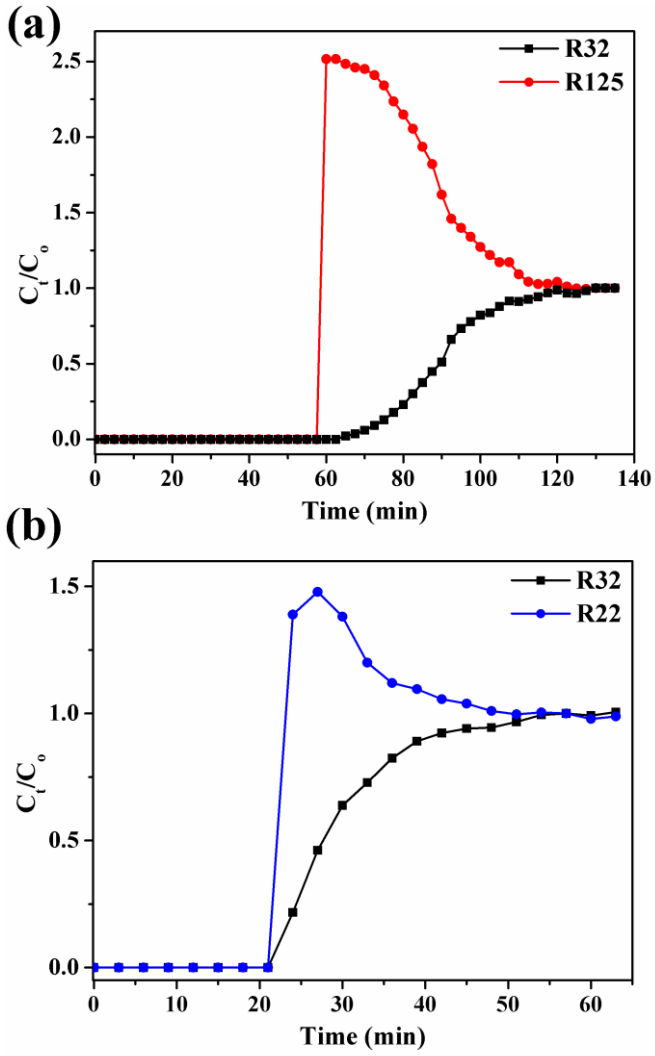

Figure 6-12 Breakthrough curves on 13X for (a) R32/R125 (b) R32/R22 and (c) R32/R22/R125 at 1 bar and 293 K

Because of this strong electric field of zeolite 13X and the existence of highly electronegative F atoms in both R32 and R125, it seems that 13X is unable to do selective separation based on the thermodynamic properties of gas mixture. Further, compared to open Cu sites in HKUST-1, extra framework Na ions in the 13X can be considered as more accessible or exposed to the fluorocarbon molecules and they have the flexibility even to pulled away from their equilibrium position to optimize the interaction with adsorbates. Equally high accessibility and binding of

both R32 and R125 may have suppressed the selective adsorption of more polar molecules from the mixture. Besides, due to the entropic and molecular packing effects[149] (which are related to the shape and volume of the adsorbates and their ability to fit into available adsorbent cavities or channels), smaller size R32 finds it easier to fill in the 'gaps' within the supercages in zeolite 13X resulting higher adsorption capacity.[146, 150] The measured pure gas adsorption isotherms on zeolite 13X also indicate higher adsorption capacity of R32 compared to R22 and R125 (Similar to this, in our previous publication, we have reported higher adsorption capacity of R32 over R125 in LTA-5A zeolite[91]). Therefore, as a combined effect, selective adsorption of R32 over R125 can be expected. However, judging from the breakthrough results, zeolite 13X have only moderate selectivity for R32/R125 separation (Adsorbed phase composition of R32 was about 78%).

During the R32/R22 breakthrough experiments (figure 6.12b), both R32 and R22 elute from the column together suggesting that they both have similar affinity to zeolite 13X irrespective of their difference in polarizabilities(polarizabilities of R32 and R22 are 3, 6.5 Å respectively[40]).

Further we have tested ZSM-5, 5A zeolites and MCM-41 for the separation of R410A and found that they have very poor thermodynamic selectivity. During our breakthrough experiments using commercial Na-Mordenite it was revealed that similar to 13X it selectively adsorbs R32 from a mixture of R32 and R125(Figure 6-13). But unlike in the zeolite 13X, the mechanism of this separation can be considered as combined effect of steric and thermodynamic selectivity because of its narrow tortuous pore structure. However, considering its low adsorption capacity (at 313 K and 1 bar adsorption capacities of R32, R125 and R22 are 2.5, 0.8, 1.6 mmol/g respectively, Figure 6-14) and degree of selectivity (about 92% of R32 in the adsorbed phase), the suitability of Na-Mordenite for the industrial scale applications is questionable.

By considering these pure gas adsorption isotherms and breakthrough results of MOF and Zeolite, it can be concluded that MOFs are much more suitable for the separation of R32/R22/R125 fluorocarbon blends in terms of both adsorption capacity and selectivity.

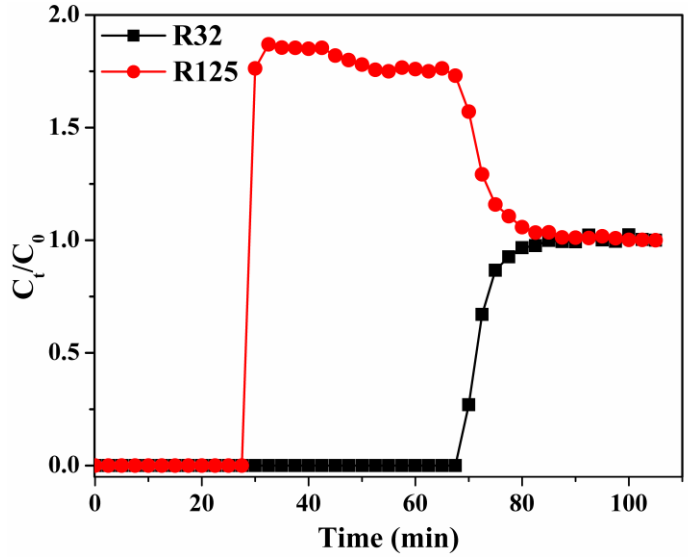

Figure 6-13 Breakthrough profile of R32/R125 (36/64 mole fraction) on Mordenite-Na at 1bar and 298 K.

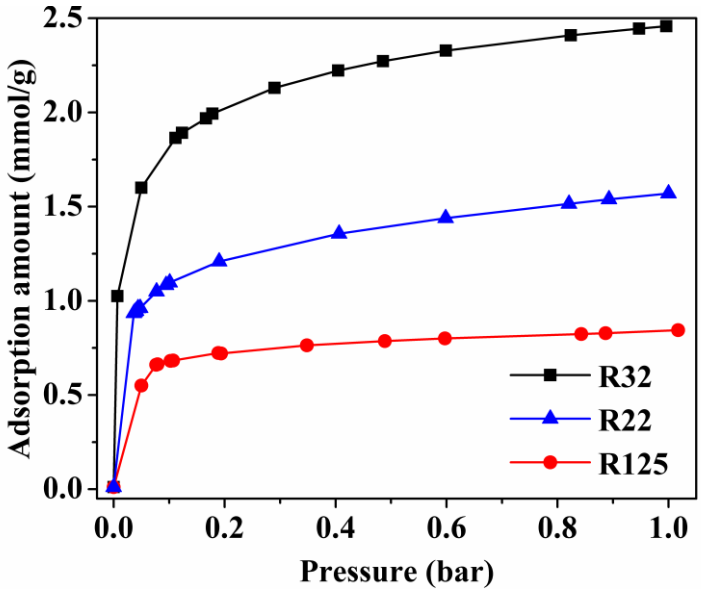

Figure 6-14 R32, R22 and R125 adsorption isotherms at 313 K.

6.3.4 Heat of Adsorption

We used the isorbHP software to calculate the isosteric heat of adsorption by fitting the measured adsorption data (at 293 K, 313 K and 333 K) to the Clausius-Clapeyron equation (Eq 2): where ΔH°_{ad} is the heat of adsorption, R is the universal gas constant, θ is the fraction of the adsorbed sites at a pressure p and temperature T.

$$\Delta H°_{ad} = R \left[\frac{\partial \ln P}{\partial(\frac{1}{T})}\right]_{\theta} \quad \text{Eq 2}$$

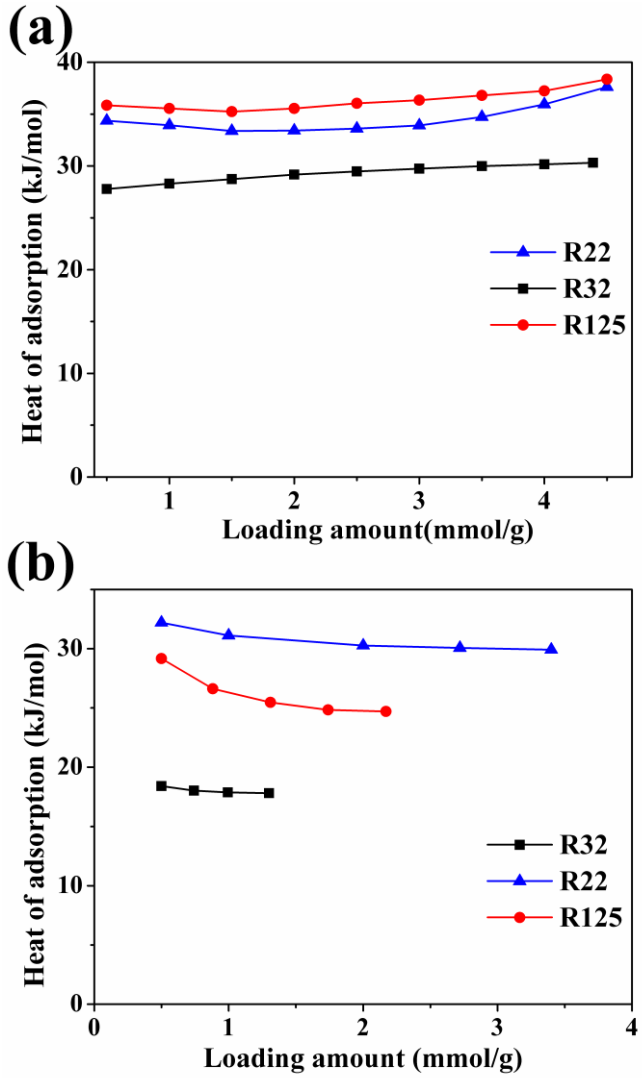

Figure 6-15 Isosteric heat of adsorption in (a) HKUST-1 and (b) UiO-66(Zr)

The values of heat of adsorption for R32, R22, R125 on HKUST-1 lie in the range of 27-30, 34-37 and 35-38 kJmol^{-1} respectively. As can be seen from figure 6-15a, there is no significant variation of heat of adsorption values with the change of loading. The lower heat of adsorption of R32 compared to R22 and R125 further confirm the selective adsorption of R125 and R22 by HKUST-1. Considerably lower heat of adsorption for R32 (18.4 kJ/mol at loading of ~ 0.4 mmol/g) on UiO-66(Zr) was observed compared to R22 (31.8 kJ/mol) and R125 (28.6 kJ/mol). Similarly, literature reports lower heats of adsorption of 32(~25 kJ/mol) compared to that of

R22 (~34.6 kJ/mol) on MIL-101.[40] Due to the coincided nature of adsorption isotherms of R32, R22, and R125 at low loading conditions, the heats of adsorption on zeolite 13X were calculated at the loading of 1.5 mmol/g. The calculated isosteric heats of adsorptions for R32, R22 and R125 on zeolite 13X were 31.5. 50.6, 51.5 kJ/mol respectively. Compared to the values of MOFs considerably high adsorption heats were observed for all three gases suggesting their stronger adsorption to the zeolite 13X framework. Interestingly, despite the larger adsorption capacity of R32 compared to R22 and R125 on zeolite 13X, lower adsorption heat was noticed for R32. Lower heats of adsorption during the adsorption of CF_4(R14) and C_2F_6(R116) on zeolite 13X is reported[82] mainly due to the unavailability of acidic H in their molecular structure compared to the CH_2F_2 (R32), $CHClF_2$ (R22) and C_2HF_5(R125). But similar heats of adsorption during the adsorption of CHF_3(R23) on zeolite 13X is reported.[151]

6.3.5 Working Capacity and Regeneration

Working capacity is far more important decisive metric than the absolute fluorocarbon uptake to evaluate the adsorbent performance in actual gas separation applications. The working capacity in a Temperature Swing Adsorption (TSA) process is directly related to the temperature dependence of the pure gas adsorption isotherms. An estimation of working capacity can be made based on their difference in adsorption capacities at the adsorption and desorption temperatures ($WC = q_{ad}-q_{des}$).[152, 153] For this purpose, pure gas adsorption isotherms at high temperatures (at 373 K and 393 K for R32, R125 on HKUST-1 and UiO-66(Zr); at 393 K and 413 K for R32, R125 on zeolite 13X) were measured. The adsorption amounts were obtained from pure gas adsorption isotherms at relevant loading conditions (for all the gases q_{ads} at P_{ads} = 0.5 bar, T_{ads} = 293 K: q_{des} at P_{des} = 1bar, T_{des}=393 K). Figure 6-16 & 6-17 shows the working capacity of HKUST-1and UiO-66(Zr) for R22 and R125 under the above-mentioned conditions. The calculated working capacities of HKUST-1 and UiO-66(Zr) are for R22 are 3.9 and 2.15 mmol/g respectively. For R125 those are 3.5, 2.05 mmol/g respectively. But it should be noted that this calculation slightly overestimates the working capacity of HKUST-1, since the gas desorbed at T_{des} is not 100% R125. However, it can be reasonably use as an easily calculated

metric for comparing different materials. However, compared to HKUST-1 and UiO-66(Zr), the working capacities are much lower in zeolite 13X as shown in figure 6-18.

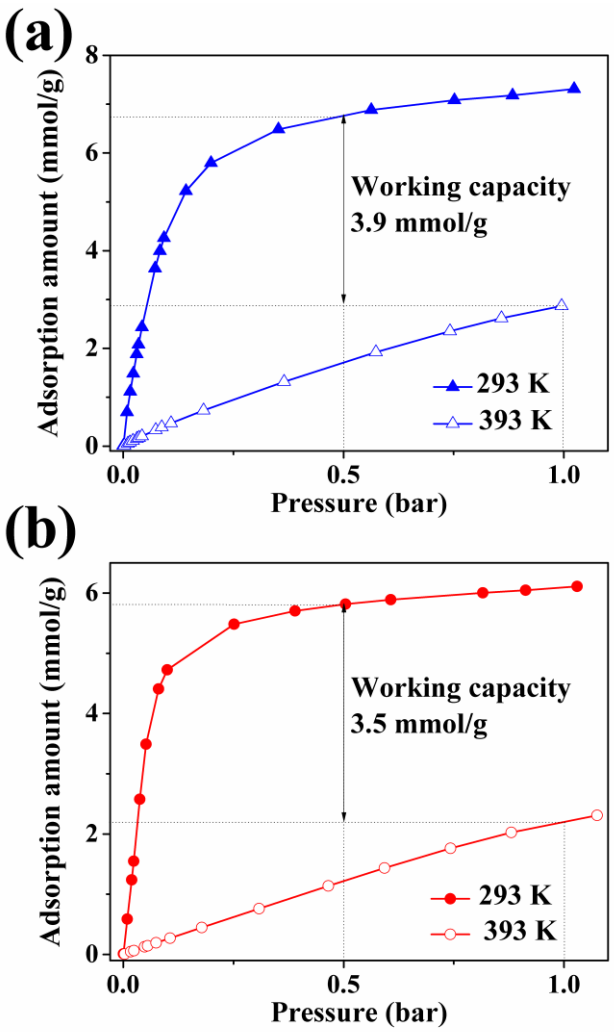

Figure 6-16 Working capacity of R22 and R125 on (a) HKUST-1.

The degree of regenerability of HKUST-1, UiO-66(Zr) and zeolite 13X under moderately high temperatures was evaluated using the measured high temperature pure gas adsorption isotherms.The regenerability (R) of the adsorbents were defined as below (Eq3):

$$R\ (\%) = (\Delta N_1/N_1^{ads})\ x100 \qquad \text{Eq 3}$$

Where ΔN_1 is the desorbed amount of gas by raising the temperature from 293 K to the 393 K and N_1^{ads} is the adsorption amount under adsorption conditions. The regenerability was lowest for zeolite 13X (23.4 % for R32 and 30.2 % for R125) when compared to the UiO-66(Zr) (66.7

% for R32 and 73.3 % for R125) and HKUST-1 (91.6 % for R32 and 62.2 % for R125). It was noted that by raising the temperature even up to 413 K, the regenarability of zeolite 13X was only 26% and 35% for R32 and

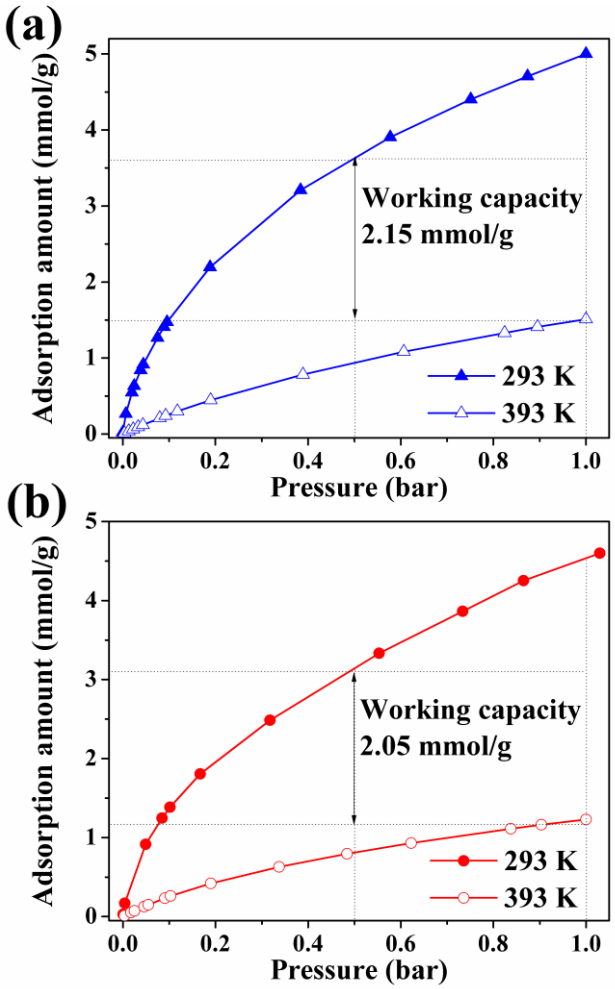

Figure 6-17 Estimated working capacity of (a) R22 and (b) R125 on UiO-66(Zr).

R125 respectively. Therefore, it seems that, zeolite 13X have difficulties in using even for R32/R125 separation applications. Both HKUST-1 and UiO-66(Zr) indicated higher regenerability at moderately high temperatures suggesting their suitability for economical, industrial scale fluorocarbon separation applications via Temperature Swing Adsorption.

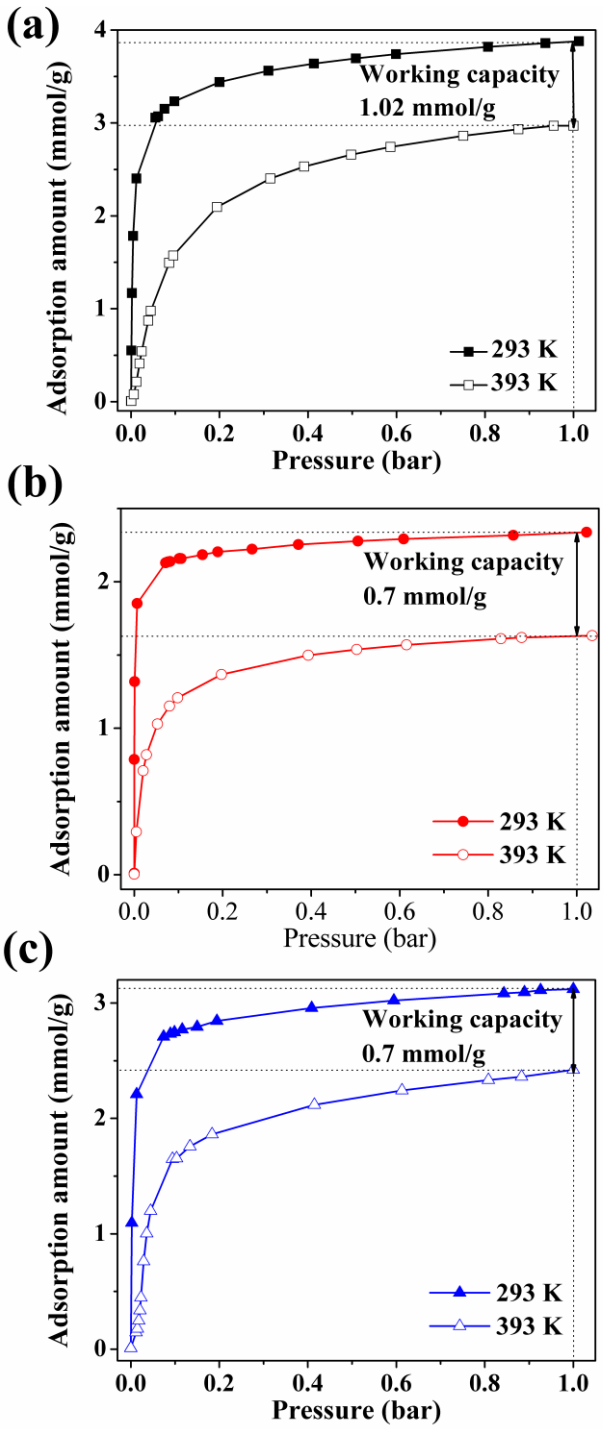

Figure 6-18 Estimated working capacity of (a) R32, (b) R125, and (c) R22 on zeolite 13X at 1 bar.

Because of the excellent selectivity of UiO-66(Zr), its' cycling stability was further assessed by repeatedly adsorbing and desorbing R22 and R125. Over 15 adsorption-regeneration cycles, UiO-66(Zr) exhibits stable adsorption capacity as shown in Figure 6-19. Figure 6-20 compares

the XRD patterns of UiO-66(Zr) before and after 15 cycles of adsorption and regeneration operations. It is clear to see that UiO-66(Zr) well preserves its original crystalline structure.

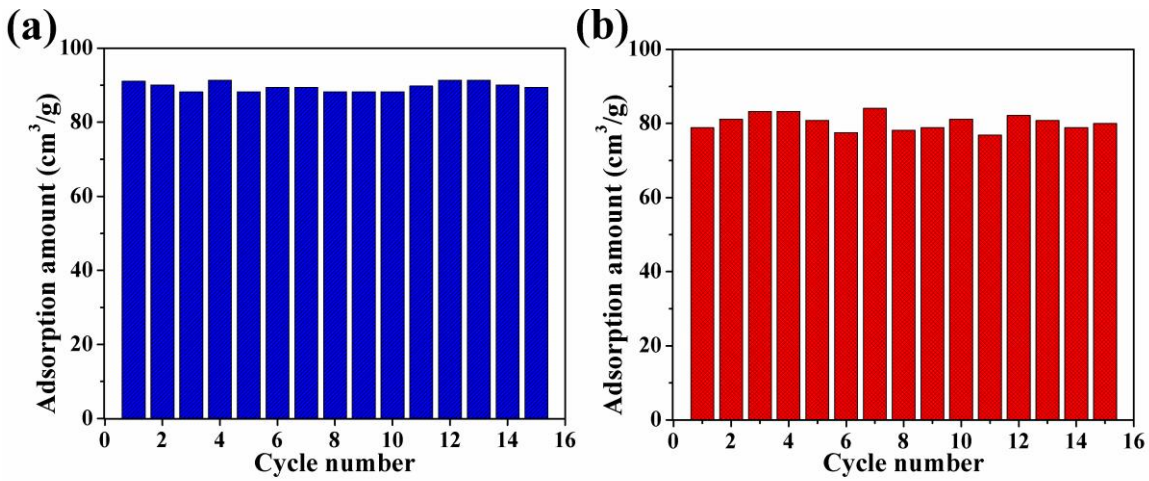

Figure 6-19 Cyclic R22 (a) and R125 (b) adsorption in UiO-66(Zr).

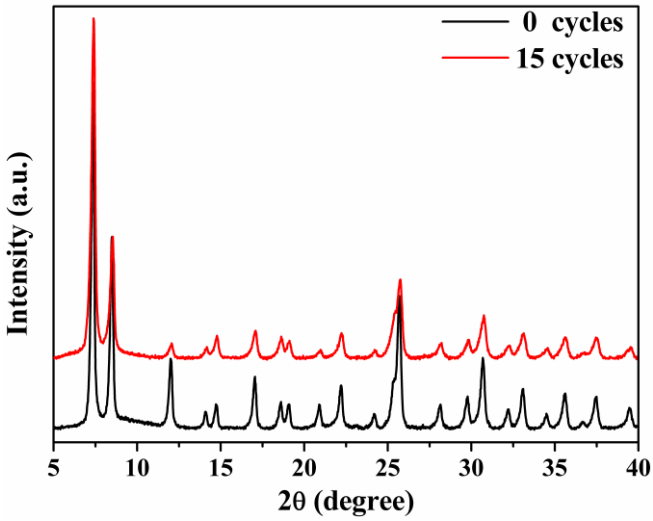

Figure 6-20 XRD patterns of UiO-66(Zr) before and after 15 adsorption-regeneration cycles.

6.4 Conclusions

In conclusion, the exceptionally high adsorption capacity, selectivity, high working capacity, regenerability under moderately high temperatures of HKUST-1 and UiO-66(Zr) suggest the possibility of utilizing these adsorbents for the separation of R22/R32/R125 fluorocarbon mixtures. Taking UiO-66(Zr) as an example, MOFs without strong adsorption sites might be more suitable for the R32/R125 and R22/R32 separation. The tested zeolite 13X not only exhibit

poor adsorption capacity and selectivity but also difficulties in regeneration under moderately high temperatures. These findings clearly promote the potential of MOFs for the sustainable separation of fluorocarbon mixtures.

Chapter 7

General conclusions and recommendations for future research directions

In this dissertation, materials selections, working principles and up-to-date development of facile methods for the industrial scale separation of various fluorocarbon blends have been discussed in detail.

The significant contributions of this research project towards the development of effective fluorocarbon separation can be summarized as follows:

1. We demonstrated absolute separation of fluorocarbon blends containing R32, R22 and R125 over 4A molecular sieve zeolite. More importantly, we can separate near azeotropic R410A (blend of R32 and R125) fluorocarbon blend to obtain R32 which has high economic value. The purity of the separated R32 exceeded the industry purification standards for their reuse. Further, due to its' low GWP compared to many other common fluorocarbon refrigerants, air conditioning and refrigeration industry is moving towards the use of R32 in their new equipment. Therefore, recycling of used R32, positively contribute to the environment sustainability. Our proposed method can be immediately commercialized since the 4A molecular sieve zeolite is readily available in commercial scale.

2. We demonstrated two stage separation of ternary R125/R134a/R143a fluorocarbon blend over zeolite 13X and surface modified zeolite 5A. R134a could be separated from R125 and R143a over zeolite 13X through the equilibrium separation while R125 and R143a could be separated over surface modified 5A zeolite through steric effects. It should be noted that both zeolite 13X and zeolite 5A also readily available in commercial scale. The method we used for the surface modification of zeolite 5A to enhance the adsorption selectivity is very simple but highly effective and can be easily adopted for industrial scale surface modification of zeolite 5A.

3. The successful utilization of HKUST-1 and UiO-66(Zr) metal organic frameworks for the separation of different fluorocarbon blends was introduced. The adsorption capacity, thermodynamic equilibrium selectivity, working capacity and the regeneration of these MOFs were outstanding when compared to molecular sieve zeolite. Currently HKUST-1 is commercially available for purchase and the scale up synthesis of UiO-66(Zr) is also reported. Importantly these MOFs can be easily regenerated under milder temperatures compared to conventional zeolite, which is very important for the design of energy efficient fluorocarbon separation processes.

General design aspects of adsorbents for the separation of fluorocarbons

Design of adsorbents for steric separation

Like any other steric separation of gas mixtures, steric separation of fluorocarbons relies on the pore aperture size of adsorbent. For ideal separation, the pore aperture size should lie between the kinetic diameters of the fluorocarbon molecules in the mixture. Based on our experimental findings, the kinetic diameters of R32, R22, R125, R134a and R143a are lower than 5Å. So primarily, adsorbents with pore aperture size smaller than 5Å can be considered for their separation. Through our study, we realized by pore size modifications of zeolites via grafting various surface groups, the steric selectivity can be improved. It can be either entire pore structure modification or modification of pore mouth regions in external surface. Besides zeolite 5A, other microporous zeolites such as ZSM-5, mordenite-Na, chabazite may also possible to use separation of these fluorocarbon after pore size modification. Utilization of ultra microporous metal organic frameworks for the real time steric separation of these fluorocarbons seems a challenging task. Unlike zeolites, ultramicroporous MOFs possess very low surface area and pore volume resulting much lower adsorption capacity. However, either by grafting bulkier functional groups to the ligands or to the metal center, pore size of the MOFs can be tuned to facilitate successful steric separation of these fluorocarbons.

Design of adsorbents for thermodynamic equilibrium separation

Unlike in steric separation, selectivity during thermodynamic separation is mainly controlled by the chemical properties of the adsorbent pore surface and the molecular properties such as dipole

moments, quadrupole moments and polarizability. Generally, gas molecules with permeant dipole moment are more attracted by the adsorbents with charged pore surface(e.g low silica zeolites). On the other hand, adsorbents without charged pore surface selectively adsorb molecules with higher polarizability. For example, in our case, R32 have higher dipole moment than R125 but R125 have higher polarizability than R32. When the molecule form both electrostatic interaction and van der waals interactions with a charged pore surface, electrostatic interactions becomes dominant than van-der-Waalls interactions, hence in our case the selectivity of R32 increase than R125. But in non-polar adsorbents, selectivity of R125 increases due to its high polarizability. So, it is beneficial to use highly polar adsorbents or entirely non-polar adsorbents to get the optimum selectivity.

Recommendations for future research directions

Besides the utilization of HKUST-1 and UiO-66(Zr) for the separation of binary R32/R22 and R32/R125 fluorocarbon blends, their applicability for the separation of binary R32/R134a, R22/R134a and ternary R32/R125/R134a fluorocarbon blends were also investigated with the aid of dynamic column breakthrough experiments.

Figure 7-1 compares the breakthrough curves of binary R32/R134a, R125/R134a and ternary R32/R125/R134a in UiO-66(Zr). Based on the binary breakthrough data, it is found that UiO-66(Zr) is highly suitable for separating R32/R134a with high separation efficiency, which exhibits large breakthrough time gap (Figure 7-1a) as well as high adsorbed species purity (R134a; ~99%). Additionally, UiO-66(Zr) is also capable to separate R125/R134a blends (Figure 7-1b). Therefore, it becomes possible to use UiO-66(Zr) to separate ternary R32/R125/R134a mixture.

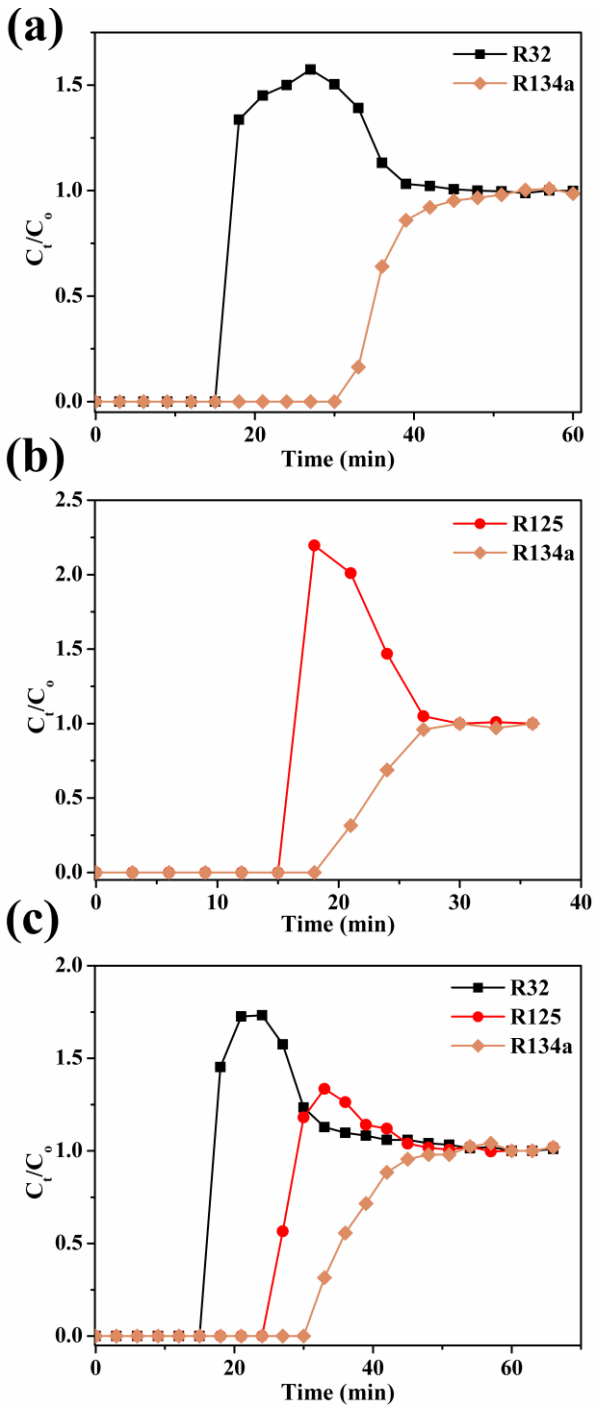

Figure 7-1 Breakthrough profiles on UiO-66(Zr) for (a) R32/R134a, (b) R125/R134a and (c) R32/R125/R134a at 1 bar and 298 K.

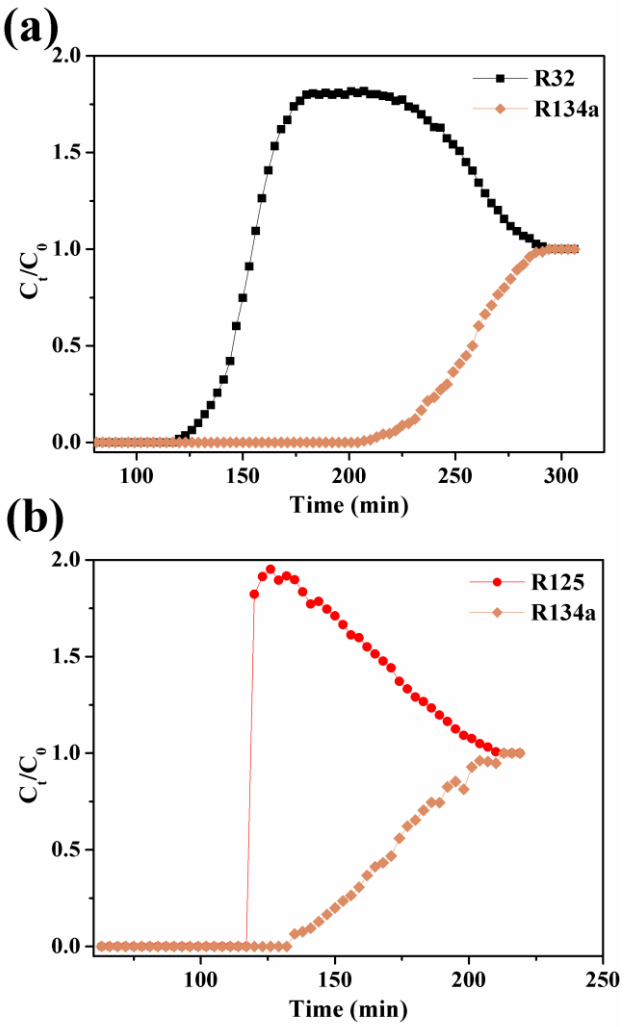

Figure 7-2 Binary R32/R134a (a) and R125/R134a (b) separation in HKUST-1 at 1 bar and 298 K.

The ternary gas breakthrough curve as shown in Figure 6c exhibits different breakthrough time in the order of R134a > R125 > R32, suggesting that the adsorption strength into UiO-66(Zr) decreases in the order R134a > R125 > R32. The better selectivity of R134a on UiO-66(Zr) can be attributed to the higher boiling point of R134a (boiling point of R134a is 246.9 K, while it is 221.3 K and 224.9 K for R32 and R125, respectively), which indicates stronger gas–gas interaction and thus it is more likely to have stronger host-gas interaction as well.[90] Besides, R134a also has higher dipole moment than R32 and R125 (dipole moments are 2.06, 1.97, 1.54 Debye for R134a, R125 and R32, respectively), which can also favorably contribute to the selective adsorption of R134a over R32 and R125. Similarly, HKUST-1 also exhibited excellent

R32/R134a separation performances as shown in figure 7.2. Therefore, UiO-66(Zr) and HKUST-1 metal organic frameworks have potential for the separation of ternary R32/R125/R134a fluorocarbon blends as well.

Fluorocarbon adsorption mechanisms in zeolites and metal organic frameworks

During our study, we noticed different thermodynamic selectivity trend in zeolites and metal organic frameworks. For example, during R32/R125 separation, zeolite 13X exhibited higher selectivity for R32 whereas both HKUST-1 and UiO-66(Zr) showed higher selectivity towards R125. Also, zeolite 13X have highest R32 adsorption capacity than R22 and R125 while UiO-66(Zr) indicate lower R32 adsorption capacity than R22 and R125. This different adsorption behavior can be tentatively rationalized using their different physical and chemical properties, though a thorough study is required to fully understand the mechanisms of fluorocarbon adsorption in porous materials with different surface properties.

List of Publications

Wanigarathna, D. J. A.; Gao, J.; Takanami, T.; Zhang, Q.; Liu, B. Adsorption Separation of R-22, R-32 and R-125 Fluorocarbons using 4A Molecular Sieve Zeolite. ChemistrySelect 2016, 1, 3718-3722.

Wanigarathna, D. K. J. A.; Gao, J.; Liu, B. Adsorption Separation of R134a, R125, and R143aFluorocarbon Mixtures Using 13X and Surface Modified5A Zeolites. AIChE J. 2017. DOI 10.1002/aic.15955

Wanigarathna, D. K. J. A.; Gao, J. ; Liu, B. Fluorocarbon Separation in a Thermally Robust Zirconium Carboxylate Metal Organic Framework. Submitted.

Wanigarathna, D. K. J. A.; Gao, J.; Liu, B. Adsorption and Adsorption-based Separation of Fluorocompounds in Metal Organic Frameworks: A Review. In preperation

References

1. Xiang B, *et al.* Global emissions of refrigerants HCFC-22 and HFC-134a: unforeseen seasonal contributions. *Proc. Natl. Acad. Sci.* **111**, 17379-17384 (2014).
2. Zhao Y, *et al.* Mesoscopic constructs of ordered and oriented metal-organic frameworks on plasmonic silver nanocrystals. *J. Am. Chem. Soc.* **137**, 2199-2202 (2015).
3. World bank data. HFC gasemissions .URL: https://data.worldbank.org/indicator/EN.ATM.HFCG.KT.CE
4. Phan NTS, Nguyen TT, Nguyen KD, Vo AXT. An open metal site metal–organic framework Cu(BDC) as a promising heterogeneous catalyst for the modified Friedländer reaction. *Appl. Catal. A: Gen.* **464-465**, 128-135 (2013).
5. Zacher D, Baunemann A, Hermes S and Fischer RA. Deposition of microcrystalline $[Cu_3(btc)_2]$ and $[Zn_2(bdc)_2(dabco)]$ at alumina and silica surfaces modified with patterned self assembled organic monolayers: evidence of surface selective and oriented growth. *J. Mater. Chem.* **17**, 2785 (2007).
6. Sircar S. Basic Research Needs for Design of Adsorptive Gas Separation Processes. *Ind. Eng. Chem. Res.* **45**, 5435-5448 (2006).
7. Ahmed MJ, Theydan SK. Modeling of propane separation from light hydrocarbons by adsorption on 4A molecular sieve zeolite. *J. Nat. Gas Sci. Eng.* **18**, 1-6 (2014).
8. Meyer CW, Morrison G. Dipole Moment of Seven Refrigerants. *J. Chem. Eng. Data* **34**, 3860-3866 (1991).
9. Motkuri RK, *et al.* Fluorocarbon adsorption in hierarchical porous frameworks. *Nat. Commun.* **5**, 4368 (2014).
10. Meyer CW, Morrison G. Dlpole Moments of Seven Partlally Halogenated Ethane Refrigerants. *J. Phys. Chem. C* **95**, 3860-3866 (1991).
11. Morrison G. Alternative refrigerant properties measurement and correlation program at NIST (national institute of standards and technology). *Pure&Appl Chem.* **63**, 1465-1472. (1991).

12. Aguado S, Bergeret G, Daniel C, Farrusseng D. Absolute molecular sieve separation of ethylene/ethane mixtures with silver zeolite A. *J. Am. Chem. Soc.* **134**, 14635-14637 (2012).

13. Chudasama CD, Sebastian J, and Jasra RV. Pore-Size Engineering of Zeolite A for the Size-Shape Selective Molecular Separation. *Ind. Eng. Chem. Res*. 1780-1786 (2005).

14. Ruthven DM. *Principles of adsorption and adsorption processes / Douglas M. Ruthven*. New York : Wiley, c1984. (1984).

15. Yang RT. *Adsorbents - fundamentals and applications*. A John Wiley & Sons, Inc., (2003).

16. Webster CD, Cottone A. and Drago RS. Multiple Equilibrium Analysis Description of Adsorption on Na-Mordenite and H-Mordenite. *J. Am. Chem. Soc.* **121**, 12127-12139 (1999).

17. Villarreal A, *et al.* Adsorption and separation of CO 2 from N 2 -rich gas on zeolites: Na-X faujasite vs Na-mordenite. *J. CO_2 Util.* **19**, 266-275 (2017).

18. Moura PAS, Bezerra DP, Vilarrasa-Garcia E, Bastos-Neto M, Azevedo DCS. Adsorption equilibria of CO_2 and CH_4 in cation-exchanged zeolites 13X. *Adsorption* **22**, 71-80 (2015).

19. Bezerra DP, *et al.* CO_2 adsorption in amine-grafted zeolite 13X. *Appl. Surf. Sci.* **314**, 314-321 (2014).

20. Yang RT. *Adsorbents [electronic resource] : Fundamentals and Applications*. Hoboken : John Wiley & Sons, Inc., 2003. (2003).

21. Sircar S, Golden TC, Rao MB. Activated Carbon for Gas Separation and Storage *Carbon* **31**, 1-12 (1996).

22. Shiflett MB, Corbin DR, Elliott BA, Yokozeki A. Sorption of trifluoromethane in zeolites and ionic liquid. *J. Chem. Thermodyn. Thermochem.* **64**, 40-49 (2013).

23. Askalany AA, Saha BB, Ahmed MS, Ismail IM. Adsorption cooling system employing granular activated carbon–R134a pair for renewable energy applications. *Int. J. Refrig.* **36**, 1037-1044 (2013).

24. Askalany AA, *et al.* Adsorption Isotherms and Heat of Adsorption of Difluoromethane on Activated Carbons. *J. Chem. Eng. Data* **58**, 2828-2834 (2013).

25. Loh WS, Ismail AB, Xi B, Ng KC, Chun WG. Adsorption Isotherms and Isosteric Enthalpy of Adsorption for Assorted Refrigerants on Activated Carbons. *J. Chem. Eng. Data* **57**, 2766-2773 (2012).

26. Peng Y, Zhang F, Zheng X, Wang H, Xu C, Xiao Q, Zhong Y, Zhu W. Comparison Study on the Adsorption of CFC-115 and HFC-125 on Activated Carbon and Silicalite-1. *Ind. Eng. Chem. Res.* **49**, 10009–10015 (2010).

27. Berlier K, Ferey M, Bougard J. Adsorption of Dichlorodifluoromethane, Chlorodifluoromethane, and Chloropentafluoroethane on Activated Carbon. *J. Chem. Eng. Data* **40**, 1137-1139 (1995).

28. Akkimaradi BS, Prasad M, Dutta P and Srinivasan K. Adsorption of 1,1,1,2-Tetrafluoroethane on Activated Charcoal. *J. Chem. Eng. Data* **46**, 417-422 (2001).

29. Frere M, Berlier K, Bougard J and Roger Jadot. Adsorption of Dichlorodifluoromethane, Chlorodifluoromethane, Chloropentafluoroethane, 1,l-Difluoroethane, and 1,1,1,2-Tetrafluoroethane on Silica Gel. *J. Chem. Eng. Data* **39**, 697-699 (1994).

30. Impens NREN, van der Voort P, Vansant EF. Silylation of micro-, meso- and non-porous oxides: a review. *Microporous Mesoporous Mater.* **28**, 217–232 (1999).

31. Ates A, Hardacre C. The effect of various treatment conditions on natural zeolites: ion exchange, acidic, thermal and steam treatments. *J. Colloid Interface Sci.* **372**, 130-140 (2012).

32. Sadowska K, *et al.* Desilication of highly siliceous zeolite ZSM-5 with NaOH and NaOH/tetrabutylamine hydroxide. *Microporous Mesoporous Mater.* **168**, 195-205 (2013).

33. Xiao L, Mao J, Zhou J, Guo X, Zhang S. Enhanced performance of HY zeolites by acid wash for glycerol etherification with isobutene. *Appl. Catal. A: General* **393**, 88-95 (2011).

34. Cheng C-H, Bae T-H, McCool BA, Chance RR, Nair S and Jones CW. Functionalization of the Internal Surface of Pure-Silica MFI Zeolite with Aliphatic Alcohols. *J. Phys. Chem. C* **112**, 3543-3551 (2008).

35. Li JR, Sculley J, Zhou HC. Metal-organic frameworks for separations. *Chem. Soc. Rev.* **112**, 869-932 (2012).

36. Li L, *et al.* High gas storage capacities and stepwise adsorption in a UiO type metal-organic framework incorporating Lewis basic bipyridyl sites. *Chem. Commun.* **50**, 2304-2307 (2014).

37. Fracaroli AM, *et al.* Metal-organic frameworks with precisely designed interior for carbon dioxide capture in the presence of water. *J. Am. Chem. Soc.* **136**, 8863-8866 (2014).

38. Zhao M, *et al.* Ultrathin 2D Metal-Organic Framework Nanosheets. *Adv. Mater.* **27**, 7372-7378 (2015).

39. Xydias P, Spanopoulos I, Klontzas E, Froudakis GE, Trikalitis PN. Drastic enhancement of the CO_2 adsorption properties in sulfone-functionalized Zr- and Hf-UiO-67 MOFs with hierarchical mesopores. *Inorg. Chem.* **53**, 679-681 (2014).

40. Motkuri RK, *et al.* Fluorocarbon adsorption in hierarchical porous frameworks. *Nat. Commun.* **5**, (2014).

41. Jiang J, Furukawa H, Zhang YB, Yaghi OM. High Methane Storage Working Capacity in Metal-Organic Frameworks with Acrylate Links. *J. Am. Chem. Soc.* **138**, 10244-10251 (2016).

42. Rodenas T, *et al.* Metal-organic framework nanosheets in polymer composite materials for gas separation. *Nat. Mater.* **14**, 48-55 (2015).

43. Manna K, Ji P, Greene FX, Lin W. Metal-Organic Framework Nodes Support Single-Site Magnesium-Alkyl Catalysts for Hydroboration and Hydroamination Reactions. *J. Am. Chem. Soc.* **138**, 7488-7491 (2016).

44. Gonzalez MI, Bloch ED, Mason JA, Teat SJ, Long JR. Single-crystal-to-single-crystal metalation of a metal-organic framework: a route toward structurally well-defined catalysts. *Inorg. Chem.* **54**, 2995-3005 (2015).

45. Carson F, *et al.* Ruthenium complexation in an aluminium metal-organic framework and its application in alcohol oxidation catalysis. *Chemistry* **18**, 15337-15344 (2012).

46. Li ZQ, Wang A, Guo CY, Tai YF, Qiu LG. One-pot synthesis of metal-organic framework@SiO2 core-shell nanoparticles with enhanced visible-light photoactivity. *Dalton Trans.* **42**, 13948-13954 (2013).

47. Wang Y, Lü Y, Zhan W, Xie Z, Kuang Q, Zheng L. Synthesis of porous Cu2O/CuO cages using Cu-based metal–organic frameworks as templates and their gas-sensing properties. *J. Mater. Chem. A* **3**, 12796-12803 (2015).

48. Furukawa H, Cordova KE, O'Keeffe M, Yaghi OM. The Chemistry and Applications of Metal-Organic Frameworks. *Science* **341**, 1230444-1230444 (2013).

49. Furukawa H, *et al.* Ultrahigh Porosity in Metal-Organic Frameworks. *Science* **329**, 424-428 (2010).

50. Farha OK, *et al.* Metal-organic framework materials with ultrahigh surface areas: is the sky the limit? *J. Am. Chem. Soc.* **134**, 15016-15021 (2012).

51. Banerjee R, Furukawa H, Britt D, Knobler C, O'Keeffe M and Yaghi OM. Control of Pore Size and Functionality in Isoreticular Zeolitic Imidazolate Frameworks and their Carbon Dioxide Selective Capture Properties. *J. Am. Chem. Soc.* **131**, 3875–3877 (2009).

52. Eddaoudi M, Kim J, 1 Nathaniel R, David V, Wachter J, O'Keeffe M, Yaghi OM. Systematic Design of Pore Size and Functionality in Isoreticular MOFs and Their Application in Methane Storage. *Sci. Technol. Adv. Mater.* **295**, (2002).

53. Chen CX, *et al.* A Robust Metal-Organic Framework Combining Open Metal Sites and Polar Groups for Methane Purification and CO_2 /Fluorocarbon Capture. *Chemistry* **23**, 4060-4064 (2017).

54. Howarth AJ, *et al.* Chemical, thermal and mechanical stabilities of metal–organic frameworks. *Nat. Rev. Mater.* **1**, 15018 (2016).

55. Yang Y, Shukla P, Wang S, Rudolph V, Chen X-M, Zhu Z. Significant improvement of surface area and CO2 adsorption of Cu–BTC via solvent exchange activation. *RSC Adv.* **3**, 17065 (2013).

56. Gerardo Majano JPr-R. Room Temperature Synthesis and Size Control of HKUST-1. *Helv. Chem. Acta* **95**, (2012).

57. Majano G, Pérez-Ramírez J. Scalable Room-Temperature Conversion of Copper(II) Hydroxide into HKUST-1 (Cu3(btc)2). *Adv. Mater.* **25**, 1052-1057 (2013).

58. Bai Z-Q, *et al.* Introduction of amino groups into acid-resistant MOFs for enhanced U(vi) sorption. *J. Mater. Chem. A* **3**, 525-534 (2015).

59. Fei H, Sampson MD, Lee Y, Kubiak CP, Cohen SM. Photocatalytic CO2 Reduction to Formate Using a Mn(I) Molecular Catalyst in a Robust Metal-Organic Framework. *Inorg. Chem.* **54**, 6821-6828 (2015).

60. Bromberg L, Diao Y, Wu H, Speakman SA, Hatton TA. Chromium(III) Terephthalate Metal Organic Framework (MIL-101): HF-Free Synthesis, Structure, Polyoxometalate Composites, and Catalytic Properties. *Chem. Mater.* **24**, 1664-1675 (2012).

61. DeCoste JB, Peterson GW, Jasuja H, Glover TG, Huang Y-g, Walton KS. Stability and degradation mechanisms of metal–organic frameworks containing the $Zr_6O_4(OH)_4$ secondary building unit. *J. Mat. Chem. A* **1**, 5642 (2013).

62. Zhao Y, Zhang Q, Li Y, Zhang R, Lu G. Large-Scale Synthesis of Monodisperse UiO-66 Crystals with Tunable Sizes and Missing Linker Defects via Acid/Base Co-Modulation. *ACS Appl. Mater. Interfaces* **9**, 15079-15085 (2017).

63. Farha OK, *et al.* De novo synthesis of a metal-organic framework material featuring ultrahigh surface area and gas storage capacities. *Nat. Chem.* **2**, 944-948 (2010).

64. Schejn A, Balan L, Falk V, Aranda L, Medjahdi G, Schneider R. Controlling ZIF-8 nano- and microcrystal formation and reactivity through zinc salt variations. *CrystEngComm* **16**, 4493 (2014).

65. Schejn A, *et al.* Cu2+-doped zeolitic imidazolate frameworks (ZIF-8): efficient and stable catalysts for cycloadditions and condensation reactions. *Catal. Sci. Technol.* **5**, 1829-1839 (2015).

66. Hu X, *et al.* Facile synthesis of the Basolite F300-like nanoscale Fe-BTC framework and its lithium storage properties. *RSC Adv.* **6**, 114483-114490 (2016).

67. Zhuang J-L, Ceglarek D, Pethuraj S, Terfort A. Rapid Room-Temperature Synthesis of Metal-Organic Framework HKUST-1 Crystals in Bulk and as Oriented and Patterned Thin Films. *Adv. Funct. Mater.* **21**, 1442-1447 (2011).

68. U. Mueller HP, M. Hesse and H. Wessel. <WO2005049892A1.pdf> (2005).

69. Stock N, Biswas S. Synthesis of metal-organic frameworks (MOFs): routes to various MOF topologies, morphologies, and composites. *Chem. Soc. Rev.* **112**, 933-969 (2012).

70. Czaja AU, Trukhan N, Muller U. Industrial applications of metal-organic frameworks. *Chem. Soc. Rev.* **38**, 1284-1293 (2009).

71. Liu J, Thallapally PK, McGrail BP, Brown DR, Liu J. Progress in adsorption-based CO2 capture by metal-organic frameworks. *Chem. Soc. Rev.* **41**, 2308-2322 (2012).

72. Jenks JJ, Motkuri RK, TeGrotenhuis W, Paul BK, McGrail BP. Simulation and Experimental Study of Metal Organic Frameworks Used in Adsorption Cooling. *Heat Transfer Eng.* **38**, 1305-1315 (2016).

73. Chang MB, Chang JS. Abatement of PFCs from Semiconductor Manufacturing Processes by Nonthermal Plasma Technologies: A Critical Review. *Ind. Eng. Chem. Res.* **45**, 4101-4109 (2006).

74. Walter Worth TAT, P.E., Richard F. Cambio, P.E. *Analysis of Data for Perfluorocompound (PFC) Emission Control Systems.*

75. Kim M-B, Lee S-J, Lee CY, Bae Y-S. High SF_6 selectivities and capacities in isostructural metal-organic frameworks with proper pore sizes and highly dense unsaturated metal sites. *Microporous Mesoporous Mater*. **190**, 356-361 (2014).

76. Kim M-B, *et al.* High SF_6/N_2 selectivity in a hydrothermally stable zirconium-based metal–organic framework. *Chem. Eng. J.* **276**, 315-321 (2015).

77. Senkovska I, Barea E, Navarro JAR and Kaskel S. Adsorptive capturing and storing greenhouse gases such as sulfur hexafluoride and carbon tetrafluoride using metal–organic frameworks. *Microporous Mesoporous Mater*. **156**, 115-120 (2012).

78. Chowdhury P, Bikkina C, Meister D, Dreisbach F, Gumma S. Comparison of adsorption isotherms on Cu-BTC metal organic frameworks synthesized from different routes. *Microporous Mesoporous Mater*. **117**, 406-413 (2009).

79. Kim P-J, *et al.* Separation of SF_6 from SF_6/N_2 mixture using metal–organic framework MIL-100(Fe) granule. *Chem. Eng. J.* **262**, 683-690 (2015).

80. Chowdhury P, Bikkina C and Gumma S. Gas Adsorption Properties of the Chromium-Based Metal Organic Framework MIL-101. *J. Phys. Chem. C* **113**, 6616–6621 (2009).

81. Chen T-H, Popov I, Kaveevivitchai W, Chuang Y-C, Chen Y-S, Jacobson AJ and Miljanic OS. MesoporousFluorinated Metal–Organic Frameworks with Exceptional Adsorption of Fluorocarbonsand CFCs. *Angew. Chem. Int. Ed.* **54**, 13902 - 13906 (2015).

82. Ahn N-G, Min B-H. and Suh S-S. Adsorption Isotherms of Tetrafluoromethane and Hexafluoroethane on Various Adsorbents. *J. Chem. Eng. Data* **51**, 451-456 (206).

83. Cho W-S, Lee K-H, Chang H-J, Huh W, Kwon H-H. Evaluation of pressure-temperature swing adsorption for sulfur hexafluoride (SF_6) recovery from SF_6 and N_2 gas mixture. *Korean J. Chem. Eng.* **28**, 2196-2201 (2011).

84. Alkhabbaz MA, Bollini P, Foo GS, Sievers C, Jones CW. Important roles of enthalpic and entropic contributions to CO_2 capture from simulated flue gas and ambient air using mesoporous silica grafted amines. *J. Am. Chem. Soc.***136**, 13170-13173 (2014).

85. Li H, O'Keeffe M, Yaghi OM. Design and synthesis of an exceptionally stable and highly porous metal organic framework *Nature* **402**, (1991).

86. Lin R-B, Li T-Y, Zhou H-L, He C-T, Zhang J-P, Chen X-M. Tuning fluorocarbon adsorption in new isoreticular porous coordination frameworks for heat transformation applications. *Chem. Sci.* **6**, 2516-2521 (2015).

87. Ferey G, *et al.* A chromium terephthalate-based solid with unusually large pore volumes and surface area. *Science* **309**, 2040-2042 (2005).

88. Zheng J, *et al.* Pore-Engineered Metal-Organic Frameworks with Excellent Adsorption of Water and Fluorocarbon Refrigerant for Cooling Applications. *J. Am. Chem. Soc.* (2017).

89. Annapureddy HVR, *et al.* Computational studies of adsorption in metal organic frameworks and interaction of nanoparticles in condensed phases. *Mol. Simul.* **40**, 571-584 (2014).

90. Wanigarathna DKJA, Liu B, Gao J. Adsorption separation of R134a, R125, and R143a fluorocarbon mixtures using 13X and surface modified 5A zeolites. *AIChE J.*, (2017).

91. Wanigarathna DJA, Gao J, Takanami T, Zhang Q, Liu B. Adsorption Separation of R-22, R-32 and R-125 Fluorocarbons using 4A Molecular Sieve Zeolite. *ChemistrySelect* **1**, 3718-3722 (2016).

92. Bloch ED, Queen WL, Krishna R, Zadrozny JM, Brown CM, Long JR. Hydrocarbon separations in a metal-organic framework with open iron(II) coordination sites. *Science* **335**, 1606-1610 (2012).

93. Dybtsev DN, Yoon SH, Kim D. and Kimoon Kim. Microporous Manganese Formate: A Simple Metal-Organic Porous Material with High Framework Stability and Highly Selective Gas Sorption Properties. *J. Am. Chem. Soc.* **126**, (2004).

94. Uemura K, Maeda A, Maji TK, Kanoo P, Kita H. Syntheses, Crystal Structures and Adsorption Properties of Ultramicroporous Coordination Polymers Constructed from Hexafluorosilicate Ions and Pyrazine. *Eur. J. Inorg. Chem.* **2009**, 2329-2337 (2009).

95. Nugent P, *et al.* Porous materials with optimal adsorption thermodynamics and kinetics for CO2 separation. *Nature* **495**, 80-84 (2013).

96. Groen JC, Peffer LAA, Pérez-Ramírez J. Pore size determination in modified micro- and mesoporous materials. Pitfalls and limitations in gas adsorption data analysis. *Microporous Mesoporous Mater*. **60**, 1-17 (2003).

97. Scarlett B. *Powder Surface Area and Porosity*. Chapman and Hall Ltd (1984).

98. Konstantakou M, Steriotis A, Kainourgiakis M, Papadopoulos GK. Determination of pore size distribution in microporous carbons based on CO2 and H2 sorption data. *Stud. Surf. Sci. Catal.* **160**, 543-550 (2007).

99. Silvestre-Albero J, Silvestre-Albero A, Rodríguez-Reinoso F, Thommes M. Physical characterization of activated carbons with narrow microporosity by nitrogen (77.4K), carbon dioxide (273K) and argon (87.3K) adsorption in combination with immersion calorimetry. *Carbon* **50**, 3128-3133 (2012).

100. Bae T-H, *et al.* Evaluation of cation-exchanged zeolite adsorbents for post-combustion carbon dioxide capture. *Energy Environ. Sci.* **6**, 128 (2013).

101. Hofman PS, Rufford TE, Chan KI, May EF. A dynamic column breakthrough apparatus for adsorption capacity measurements with quantitative uncertainties. *Adsorption* **18**, 251-263 (2012).

102. Bae T-H, Liu J, Thompson JA, Koros WJ, Jones CW, Nair S. Solvothermal deposition and characterization of magnesium hydroxide nanostructures on zeolite crystals. *Microporous Mesoporous Mater*. **139**, 120-129 (2011).

103. Myers AL, Prausnitz JM. Thermodynamics of Mixed-Gas Adsorption. *A1ChE J.* **11**.

104. Rufford TE, Watson GCY, Saleman TL, Hofman PS, Jensen NK, May EF. Adsorption Equilibria and Kinetics of Methane + Nitrogen Mixtures on the Activated Carbon Norit RB3. *Ind. Eng. Chem. Res.* **52**, 14270-14281 (2013).

105. Jensen NK, Rufford TE, Watson G, Zhang DK, Chan KI, May EF. Screening Zeolites for Gas Separation Applications Involving Methane, Nitrogen, and Carbon Dioxide. *J. Chem. Eng. Data* **57**, 106-113 (2012).

106. Huang Q, Eić M. Commercial adsorbents as benchmark materials for separation of carbon dioxide and nitrogen by vacuum swing adsorption process. *Sep. Purif. Technol.* **103**, 203-215 (2013).

107. Savitz S, *et al.* Adsorption of Hydrofluorocarbons HFC-134 and HFC-134A on X and Y Zeolites: Effect of Ion-Exchange on Selectivity and Heat of Adsorption. *J. Phys. Chem. B* **103**, 8283-8289 (1999).

108. Basavaraj S. Akkimaradi MP, † Pradip Dutta, and Kandadai Srinivasan. Adsorption of 1,1,1,2-Tetrafluoroethane on Activated Charcoal. *J. Chem. Eng. Data* **46**, 417-422 (2001).

109. Peralta D, *et al.* Comparison of the Behavior of Metal–Organic Frameworks and Zeolites for Hydrocarbon Separations. *J. Am. Chem. Soc.* **134**, 8115-8126 (2012).

110. Russell AJ, Spackman MA. Anab initiostudy of vibrational corrections to the electrical properties of the fluoromethanes: CH_3F, CH_2F_2, CHF_3 and CF_4. *Molecular Physics* **98**, 633-642 (2000).

111. Banker ND, Prasad M, Dutta P, Srinivasan K. Activated carbon+HFC 134a based two stage thermal compression adsorption refrigeration using low grade thermal energy sources. *Appl. Therm. Eng.* **29**, 2257-2264 (2009).

112. Savitz S, Huber R, Tieri SM, Gorte RJ, Myers AL and Corbin DR. Adsorption of Hydrofluorocarbons HFC-134 and HFC-134A on X and Y Zeolites: Effect of Ion-Exchange on Selectivity and Heat of Adsorption. *J. Phys. Chem. B* **103**, 8283-8289 (1999).

113. Crawford MK, Dobbs KD, Smalley JR, Corbin DR, Maliszewskyj N, Cavanagh RR, Rush JJ and Grey CP. A Raman Spectroscopy Study of the Separation of Hydrofluorocarbons Using Zeolites. *J. Phys. Chem. B* **103**, 431-434 (1999).

114. Lin SH, Lin RC. Adsorption of 1,1,1,2-tetrafluoroethane by Various Adsorbents. *J. Environ. Eng.* **125**, 1048-1053 (1999).

115. Kwang HL, Fabien J, Scott MA and Clare PG. Double Resonance NMR and Molecular Simulations of Hydrofluorocarbon Binding on Faujasite Zeolites NaX and NaY: the

Importance of Hydrogen Bonding in Controlling Adsorption Geometries. *J. Phys. Chem. B* **105**, 9918-9929 (2001).

116. Crawford MK, Corbin DR, Smalley RJ. A Raman Study of Fluorinated Ethanes Adsorbed on Zeolite NaX. In: *Amazing Light: A Volume Dedicated To Charles Hard Townes On His 80th Birthday* (ed^(eds Chiao RY). Springer New York (1996).

117. Ohayon D, Ciaravino D, Hazel H, Cochennec A. Methods for pore size engineering in ZSM-5 zeolite. *Appl. Catal. A: General* **217**, 241-251 (2001).

118. Yue Y-H, Tang Y, Gao Z. Zeolite pore size engineering by chemical liquid deposition. *Stud. Surf. Sci. Catal.*, **105**, (1997).

119. Yue Y-H, Liu Y, and Gao Z. Chemical Liquid Deposition Zeolites with Controlled Pore-Opening Size and Shape-Selective Separation of Isomers. *Ind. Eng. Chem. Res.* **35**, 430-433 (1996).

120. Chudasama CD, Sebastian J, and Jasra RV. Pore-Size Engineering of Zeolite A for the Size/Shape Selective Molecular Separation. *Ind. Eng. Chem. Res.* **44**, 1780-1786 (2005).

121. Mason JA, *et al.* Methane storage in flexible metal–organic frameworks with intrinsic thermal management. *Nature* **527**, 357-361 (2015).

122. Miki Niwa KY, and Yuichi Murakami. Separation of Oxygen and Nitrogen Due to the Controlled Pore-Opening Size of Chemical Vapor Deposited Zeolite A. *Ind. Eng. Chem. Res.* **30**, (1991).

123. Fengxi Chen a, Shoucang Shen b, Xiao-Jun Xu c, Rong Xu a, Fethi Kooli. Modification of micropore-containing SBA-3 by TEOS liquid phase deposition. *Microporous Mesoporous Mater.* **75**, 85-91 (2005).

124. Mitsuyoshi D, Kuroiwa K, Kataoka Y, Nakagawa T, Kosaka M, Nakamura K, Suganuma S, Araki Y, Katada N. Shape selectivity in toluene disproportionation into para-xylene generated by chemical vapor deposition of tetramethoxysilane on MFI zeolite catalyst. *Microporous Mesoporous Mater.* **242**, 118e126 (2017).

125. Weber RW, Moller KP, O'Connor CT. The chemical vapour and liquid deposition of tetraethoxysilane on ZSM-5, mordenite and beta. *Microporous Mesoporous Mater.* **35–36**, 533–543 (2000).

126. Begum HA, Katada N, Niwa M. Chemical vapour deposition of silica on silicalite crystals and shape-selective adsorption of paraffins. *Microporous Mesoporous Mater.* **46**, 13-21 (2001).

127. Zhu Z, Xie Z, Chen Q, Kong D, Li W, Yang W. Chemical liquid deposition with polysiloxane of ZSM-5 and its effect on acidity and catalytic properties. *Microporous Mesoporous Mater.* **101**, 169–175 (2007).

128. Zhao Y-W, Shen B-X, Sun H. Chemical Liquid Deposition Modified ZSM-5 Zeolite for Adsorption Removal of Dimethyl Disulfide. *Ind. Eng. Chem. Res.* **55**, 6475-6480 (2016).

129. Cabral BJC, Guedes RC, Pai-Panandiker RS, Nieto de Castro CA. Hydrogen bonding and the dipole moment of hydrofluorocarbons by density functional theory. *Phys. Chem. Chem. Phys.* **3**, 4200-4207 (2001).

130. Van Der Vis MGM, Cordfunke EHP, Konings RJM. The thermodynamic properties of tetraethoxysilane (TEOS) and an infrared study of its thermal decomposition. *Le Journal de Physique IV* **03**, C3-75-C73-82 (1993).

131. Kassaee MH, Sholl DS, Nair S. Preparation and Gas Adsorption Characteristics of Zeolite MFI Crystals with Organic-Functionalized Interiors. *J. Phys. Chem. C* **115**, 19640-19646 (2011).

132. Zhang R, *et al.* Surface polarization enhancement: high catalytic performance of Cu/CuOx/C nanocomposites derived from Cu-BTC for CO oxidation. *J. Mater. Chem. A* **4**, 8412-8420 (2016).

133. Katz MJ, *et al.* A facile synthesis of UiO-66, UiO-67 and their derivatives. *Chem. Commun.* **49**, 9449-9451 (2013).

134. Sanil ES, *et al.* Size and morphological control of a metal–organic framework Cu-BTC by variation of solvent and modulator. *J. Porous Mater.* **22**, 171-178 (2014).

135. Tovar TM, *et al.* Diffusion of CO_2 in Large Crystals of Cu-BTC MOF. *J. Am. Chem. Soc.* (2016).

136. Hu Z, Faucher S, Zhuo Y, Sun Y, Wang S, Zhao D. Combination of Optimization and Metalated-Ligand Exchange: An Effective Approach to Functionalize UiO-66(Zr) MOFs for CO_2 Separation. *Chemistry* **21**, 17246-17255 (2015).

137. Hu Z, Nalaparaju A, Peng Y, Jiang J, Zhao D. Modulated Hydrothermal Synthesis of UiO-66(Hf)-Type Metal-Organic Frameworks for Optimal Carbon Dioxide Separation. *Inorg. Chem.* **55**, 1134-1141 (2016).

138. Ruthven DM. *Principles of adsorption and adsorption process*. John Wiley & Sons. Inc. (1984).

139. Zhang W, *et al.* Impact of Synthesis Parameters on the Formation of Defects in HKUST-1. *European Journal of Inorg. Chem.* **2017**, 925-931 (2017).

140. Cavka SJ, Olsbye U, Guillou N, Lamberti C, Bordiga S. A New Zirconium Inorganic Building Brick Forming Metal Organic Frameworks with Exceptional Stability. *J. Am. Chem. Soc.***130**, 13850–13851 (2008).

141. Dhainaut J, *et al.* Systematic study of the impact of MOF densification into tablets on textural and mechanical properties. *CrystEngComm*, (2017).

142. Dhainaut J, *et al.* Synthesis of FAU and EMT-type zeolites using structure-directing agents specifically designed by molecular modelling. *Microporous Mesoporous Mater.* **174**, 117-125 (2013).

143. Peralta D, *et al.* Comparison of the behavior of metal-organic frameworks and zeolites for hydrocarbon separations. *J. Am. Chem. Soc.* **134**, 8115-8126 (2012).

144. Mason JA, Sumida K, Herm ZR, Krishna R, Long JR. Evaluating metal–organic frameworks for post-combustion carbon dioxide capture via temperature swing adsorption. *Energy Environ. Sci.* **4**, 3030 (2011).

145. Alaerts L, *et al.* Selective adsorption and separation of xylene isomers and ethylbenzene with the microporous vanadium(IV) terephthalate MIL-47. *Angew. Chem.* **46**, 4293-4297 (2007).

146. Krishna R, Smit B, Calero S. Entropy effects during sorption of alkanes in zeolites. *Chemical Society reviews* **31**, 185-194 (2002).

147. Caroline F. Mellot AKC. Energetics and Structures of Fluoro- and Chlorofluorocarbons in Zeolites: Force Field Development and Monte Carlo Simulations. *J. Phys. Chem. B* **103**, 3864-3868 (1999).

148. Michael F. Ciraolo JCH, Brian H. Toby, and Clare P. Grey. Combined X-ray and Neutron Powder Refinement and NMR Study of Hydrochlorofluorocarbon HCFC-124a (CF2HCF2Cl) Binding on NaX. *J. Phys. Chem. B* **105**, 12330-12337 (2001).

149. Daems PL, Mathivier A, Denayer JFM, Baron GV.Size and packing related adsorption effects in the liquid phase adsorption of aromatics and alkenes on FAU type zeolites. *Stud. Surf. Sci. Catal*, **158**.

150. Krishna R. Se.parating mixtures by exploiting molecular packing effects in microporous materials. *Phys. Chem. Chem. Phys.* **17**, 39-59 (2015).

151. Shiflett MB, Corbin DR, and Yokozeki A. Comparison of the Sorption of Trifluoromethane (R-23) on Zeolites and in an Ionic Liquid. *Adsorp. Sci. Technol.* **31**, (2013).

152. Lee WR, *et al.* Exceptional CO_2 working capacity in a heterodiamine-grafted metal-organic framework. *Chem. Sci.* **6**, 3697-3705 (2015).

153. Berger AH, Bhown AS. Comparing physisorption and chemisorption solid sorbents for use separating CO_2 from flue gas using temperature swing adsorption. *Energy Procedia* **4**, 562-567 (2011).